Non-Perturbative Features of Quantum Evolution and their Implications on Linear Response Theory

Thesis submitted in partial fulfillment
of the requirements for the degree of
"DOCTOR OF PHILOSOPHY"

by

Alexander Stotland

Submitted to the Senate of Ben-Gurion University
of the Negev

January 12, 2010

Beer-Sheva

Non-Perturbative Features of Quantum Evolution and their Implications on Linear Response Theory

Thesis submitted in partial fulfillment
of the requirements for the degree of
"DOCTOR OF PHILOSOPHY"

by

Alexander Stotland

Submitted to the Senate of Ben-Gurion University
of the Negev

Approved by the adviser

Approved by the Dean of the Kreitman School of Advanced Graduate Studies

January 12, 2010

Beer-Sheva

This work was carried out under the supervision of

Prof. Doron Cohen

In the Department of Physics

Faculty of Natural Sciences

Abstract

Consider a system described by a time-dependent Hamiltonian $\mathcal{H}(Q, P, X(t))$. For such system energy E is not a constant of motion, but rather the driving induces spreading of energy. One can ask how the energy distribution $p_t(E)$ depends on time. In general this function will be different for classical and quantum-mechanical systems. This distribution can be characterized by its moments. Quantum-classical correspondence (QCC) means that the classical energy distribution moments are similar to the quantum-mechanical ones. The question is under what conditions QCC holds and what its limitations are. The well-known type of QCC is the Bohr QCC, which states that if the wavepackets are Gaussian and the potentials are smooth, then the moments are the same for short times. However, the wavepackets are not always Gaussian or the potentials smooth. Moreover, we cannot trust QCC for long times. How is the QCC issue related to the theory of response? Whereas we expect the QCC to hold for *short* times, in the theory of response we are interested in the behavior of the system for *long* times. We start by studying the diffractive energy spreading and its semi-classical limit. We consider driven systems where the driving induces transitions in energy space: (1) particles pulsed by a step potential; (2) particles in a box with a moving wall; (3) particles in a ring driven by an electromotive-force. In all these cases the route towards quantum-classical correspondence is highly non-trivial. All these problems share the same feature: in the classical description the energy absorption is associated with abrupt jumps $\delta E_{\rm cl}$ in phase space. These jumps are reflected in quantum dynamics as a strong diffraction effect, which is the worst case for Bohr's QCC. Some insight is gained by observing that the dynamics in energy space, where n is the level index, is essentially the same as that of Bloch electrons in a tight binding model, where n is the site index. The mean level spacing is like a constant electric field and the driving induces long range hopping $\propto 1/(n-m)$. In all these cases the restricted QCC (for the first two moments of the energy distribution) is preserved, whereas the detailed QCC (for the higher moments) is destroyed.

Within the Linear Response Theory (LRT) the energy absorption of a quantum system is determined by the correlation function of the perturbation term in the Hamiltonian. Within a very restrictive framework of assumptions one can argue that there is

a very good QCC for the correlation functions, and hence one expects *restricted* QCC in the energy absorption process. In practice, it is of much interest to explore the limitation of LRT and to obtain a more general theory for response.

"Atom-optics" billiard systems and closed mesoscopic systems provide the ideal paradigm for testing the manifestation of quantum-mechanical effects in the mesoscopic realm. In this dissertation we show that the calculation of the heating rate of cold atoms in vibrating traps and the calculation of the conductance of mesoscopic disordered rings require a theory that goes beyond the Kubo linear response formulation. The analysis of transitions between energy levels shows similarities with a percolation problem in energy space, assuming that the strong "quantum chaos" conditions do not hold in the first problem and "mesoscopic" circumstances exist in the second one. We also show how the texture and the sparsity of the perturbation matrix, as determined by the geometry of the trap or the strength of the disorder in the ring, dictate the result. We apply the semi-linear response theory (SLRT) to obtain the absorption coefficient of a driven system using a resistor network calculation: Each unperturbed energy level of a particle in a vibrating trap, or of an electron in a mesoscopic ring, is regarded as a node (n) of the network; The transition rates (w_{mn}) between the nodes are regarded as the elements of a random matrix that describes the network. If the size-distribution of the connecting elements is wide (e.g. log-normal-like rather than Gaussian-like) the result for the absorption coefficient differs enormously from the conventional Kubo prediction of linear response theory. We use an improved random matrix model which captures the essential ingredients of the problems and leads to a generalized variable range hopping (VRH) scheme for the analysis. In particular, we apply this approach to obtain practical approximations for the conductance of mesoscopic rings. In this context Mott's picture of diffusion and localization is revisited.

This thesis is submitted as a collection of the following journal articles (attached in the Chapter 3):

1. A. Stotland, A.A. Pomeransky, E. Bachmat, D. Cohen,
   The information entropy of quantum mechanical states,
   Europhysics Letters **67**, 700 (2004)

2. A. Stotland and D. Cohen,
   Diffractive energy spreading and its semiclassical limit,
   J. Phys. A **39**, 10703 (2006)

3. A. Stotland, R. Budoyo, T. Peer, T. Kottos and D. Cohen,
   The mesoscopic conductance of disordered rings, its random matrix theory, and the generalized variable range hopping picture,
   J. Phys. A **41**, 262001 (2008) (Fast Track Communication),
   selected for Editor's Choice FTC

4. A. Stotland, D. Cohen and N. Davidson,
   Semi-linear response for the heating rate of cold atoms in vibrating traps,
   Europhysics Letters **86**, 10004 (2009)

5. A. Stotland, T. Kottos and D. Cohen,
   Random-matrix modeling of semi-linear response, the generalized variable range hopping picture, and the conductance of mesoscopic rings,
   A. Stotland, T. Kottos and D. Cohen, Phys. Rev. B **81**, 115464 (2010)

Contents

Chapter 1

Introduction

In this work we are interested in driven systems which are described by a Hamiltonian $\mathcal{H}(X(t))$, where the parameter $X(t)$ is time-dependent. For these systems the energy E is not a constant of motion. Rather, the driving induces spreading in energy space. In this dissertation we shall be interested in the rate of the energy absorption of such systems. The standard tool to calculate that is the linear response theory (LRT) [1, 2] in which the energy absorption is determined by the correlation function of the perturbation term of the Hamiltonian. The common perception is that the leading result for the response of a driven system should be the same classically and quantum-mechanically. For example, such is the case if one calculates the conductance of a diffusive ring [3]: the leading order result is just the Drude expressions, and on top there are weak localization corrections. In practice, it is of much interest to explore the limitations of LRT and to obtain a more general theory for response.

The theory for the response of closed isolated driven quantized chaotic mesoscopic systems is far from being trivial, even if the interactions between the particles are neglected. In the case of a generic quantized chaotic systems two energy scales are involved: the mean level spacing $\Delta \propto \hbar^d$, where $d = 2, 3$ is the dimensionality of the system, and the semiclassical energy scale $\hbar/\tau_{cl}$. It is implied (see the mini-review of Ref. [4]) that there are generically three regimes depending on the rate $\dot{X}$ of the driving: The adiabatic (Landau Zener) regime; The Fermi-golden-rule (FGR, Kubo) regime; The semiclassical (non-perturbative) regime [4, 5, 6]. Most of the literature in mesoscopic physics is dedicated to the study of the dynamics in either the adiabatic or the FGR regimes.

We consider [P2] driven systems that look simple at the first glance, where the driving induces transitions in energy space: (1) particles pulsed by a step potential; (2) particles in a box with a moving wall; (3) particles in a ring driven by an electromotive-force. In all these cases we will show that the route towards quantum-classical correspondence is highly non-trivial. All these problems share the same feature: in the classical description the energy absorption is associated with abrupt jumps $\delta E_{\rm cl}$ in phase space, and the semiclassical dynamics implies diffractive energy spreading. In the "moving wall" problem there are only two regimes: the adiabatic regime and the semiclassical regime. The EMF-driven ring is a prototype problem in mesoscopic physics. It is richer than the "moving wall" problem because a small scatterer introduces a very small energy scale, the level splitting, and hence we have three regimes rather than two: adiabatic, diabatic and semiclassical. We will also demonstrate how to reduce the "EMF driven ring" problem to the Bloch oscillations problem.

We would like to explore the limitations of LRT and go beyond this theory. For this purpose, we present two "practical" models: (1) a disordered mesoscopic EMF-driven multimode ring [P3, P5] and (2) cold atoms in a vibrating trap [P4]. These models were studied in different physical contexts in the past and can be realized experimentally (see Sections 1.3 and 1.4). In both problems we calculate the rate of energy absorption. We explain that in typical circumstances the regime of validity of LRT is very limited, and one has to apply the semi-linear response theory (SLRT) [7] in order to calculate the conductance in the first problem and the diffusion coefficient in the second one. We also explain the random matrix modeling of SLRT and introduce the generalized variable range hopping picture.

In the rest of the chapter we discuss briefly the LRT and its applicability to finite systems and how the LRT is different from the SLRT. We describe some known results for the conductance studies of mesoscopic rings and for the heating rate of cold atoms in vibrating traps. In the end we present the existent knowledge and the history of the "moving wall" problem and Bloch electrons in a constant electric field.

Note. All the problems studied in this thesis are essentially one-body problems, and therefore the one-body language is employed. However, all our calculations and results here can also be formulated in the many-body context. An extensive discussion of one-

body vs. many-body correlators, their symmetry and the relation to diagrammatics is presented in [8].

1.1 Linear response theory

Let us consider a driven system with a Hamiltonian $\mathcal{H}(R(t))$, where R is some control parameter and $\dot{R}$ is the rate of the (noisy) low-frequency driving. In this case there are diffusion in energy space with a coefficient D and energy absorption $\dot{E}$. If the driving is weak enough, the Hamiltonian can be linearized

$$\mathcal{H}(R(t)) \approx \mathcal{H}_0 + f(t)V \tag{1.1}$$

where R_0 is a constant and

$$\mathcal{H}_0 = \mathcal{H}(R_0), \quad f(t) = R(t) - R_0, \quad V = \frac{\partial \mathcal{H}}{\partial R} \tag{1.2}$$

In the energy basis of $\mathcal{H}_0$ it reads

$$\mathcal{H} = \{E_n\} + f(t)\{V_{nm}\} \tag{1.3}$$

where E_n are the energies of the unperturbed system, and $V_{nm} = \left\langle n \left| \frac{d\mathcal{H}}{dR} \right| m \right\rangle$ are the elements of the perturbation matrix. For example, in the case of a particle in a box with a vibrating wall (located at $R(t)$) the force on the particle is induced by the moving wall and the "small parameter" of the linearizion in Eq. (1.1) is the RMS of the velocity $\dot{R}$ of the wall. In the case of the EMF driven ring there is applied magnetic flux $\Phi(t)$ and the "small parameter" is the RMS of the voltage $\dot{\Phi}$.

In order to calculate the diffusion coefficient within the framework of the linear response theory (LRT) the Kubo formula is used [1, 2]. Here we use the notations of [9, 10].

$$D = G \times \overline{\dot{R}^2} = \int \tilde{C}(\omega)\tilde{S}(\omega)d\omega \tag{1.4}$$

where $\tilde{C}(\omega)$ is the Fourier Transform (FT) of the time auto-correlation function

$$\tilde{C}(\omega) = \text{FT } \langle V(t)V(0)\rangle \tag{1.5}$$

and $\tilde{S}(\omega)$ is the power spectrum of the noisy low frequency driving

$$\tilde{S}(\omega) = \text{FT } \langle \dot{f}(t)\dot{f}(0)\rangle \tag{1.6}$$

The dissipation-diffusion theorem [11, 12, 13], which in the canonical case is $\dot{E} = D/T$, allows us to relate between the diffusion coefficient and the rate of energy absorption.

The quantum version of $\tilde{C}(\omega)$ is [13]

$$\tilde{C}(\omega) \;=\; \frac{1}{N}\sum_{nm} |V_{nm}|^2\, 2\pi\delta(\omega - (E_m - E_n)) \tag{1.7}$$

where N is the size of the energy window of interest. This spectral function can be re-interpreted as describing the band profile of the perturbation matrix $\{|V_{nm}|^2\}$. The expression for G (Eq. (1.4)) takes the form [10]

$$G_{\rm LRT} \;=\; \pi\varrho_{\rm E}\,\langle\langle |V_{nm}|^2\rangle\rangle_a \tag{1.8}$$

where $\langle\langle x\rangle\rangle_a = \langle x\rangle$ is the algebraic average over the near diagonal matrix elements in the energy window of interest. The weight of $|V_{nm}|^2$ in this average is determined by the spectral function as $\tilde{S}(E_n - E_m)$, and $\varrho_{\rm E}$ is the density of states (DOS).

A note should be added regarding the applicability of the Kubo approach to finite systems. The application of the LRT (Kubo) formalism to classical chaotic systems was established in [14, 15, 16]. In the "quantum chaos" context the Kubo formalism was questioned Ref. [17, 18] and later the conditions were clarified and established in [5, 6, 13]. The Kubo formula was also applied to diffusive rings in [19].

The assumption of an infinite system with a continuum of states is crucial in the "standard" derivation of Kubo formula [2]. Otherwise, the driving field does not induce transitions. An *isolated* finite system with a truly discrete spectrum does not absorb energy from the given monochromatic field. In order to obtain a finite conductance, the small system has to be (and to some extent is in real situations) coupled to a very large heat bath, or optionally, the driving should be noisy. The latter possibility is assumed in our work.

1.2 Semi-linear response theory

As in the standard derivation of the Kubo formula, also within the framework of the semi-linear response theory (SLRT) [7, 23, 24], the leading mechanism for absorption is assumed to be Fermi golden rule (FGR) transitions. The FGR transition rate is proportional to the squared matrix elements $|V_{nm}|^2$ and to the power spectrum at the frequency

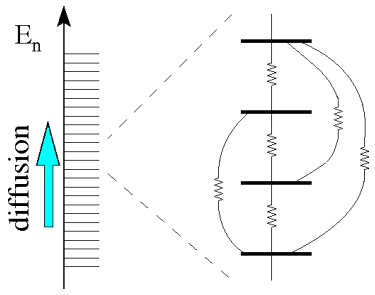

Figure 1.1: Resistor network

$\omega = E_n - E_m$. It is convenient to define the normalized spectral function $\tilde{F}(\omega)$, such that

$$\tilde{S}(\omega) \quad \equiv \quad \mathrm{RMS}(\dot{R})^2 \times \tilde{F}(\omega) \tag{1.9}$$

Contrary to the naive expectation the theory of [23] does not lead to the Kubo formula. This is because the rate of absorption depends crucially on the possibility to make *connected* sequences of transitions. It is implied that both the texture and the sparsity of the $|V_{nm}|^2$ matrix play a major role in the calculation of G. Consequently, SLRT leads to

$$G_{\mathrm{SLRT}} \quad = \quad \pi \varrho_{\mathrm{E}} \, \langle\langle |V_{nm}|^2 \rangle\rangle \tag{1.10}$$

where $\langle\langle ... \rangle\rangle$ is defined using a resistor network calculation. Namely, the energy levels are regarded as the *nodes* of a resistor network, and the FGR transition rates as the *bonds* that connect different nodes (Fig. 1.1).

Following [7] the inverse resistance of a bond is defined as

$$\mathsf{g}_{nm} \quad \equiv \quad 2\varrho_{\mathrm{E}}^{-3} \, \frac{|V_{nm}|^2}{(E_n - E_m)^2} \, \tilde{F}(E_m - E_n) \tag{1.11}$$

and $\langle\langle |V_{nm}|^2 \rangle\rangle$ is defined as the inverse resistivity of the network. Thus the analysis is somewhat similar to a percolation problem in energy space. It is a simple exercise to verify that if all the matrix elements are the same, say $|V_{nm}|^2 = c$, then $\langle\langle |V_{nm}|^2 \rangle\rangle = c$ too. But if the matrix is sparse or textured then typically

$$\langle\langle |V_{nm}|^2 \rangle\rangle_{\mathrm{h}} \ll \langle\langle |V_{nm}|^2 \rangle\rangle \ll \langle\langle |V_{nm}|^2 \rangle\rangle_{\mathrm{a}} \tag{1.12}$$

where the subscript a stands for the algebraic average and h for the harmonic average.

The theory is called SLRT because on the one hand the power spectrum $\tilde{S}(\omega) \mapsto \lambda \tilde{S}(\omega)$ (multiplication by a constant) leads to the diffusion $D \mapsto \lambda D$, but on the other hand

$\tilde{S}(\omega) \mapsto \tilde{S}_1(\omega) + \tilde{S}_2(\omega)$ does not lead to $D \mapsto D_1 + D_2$. This semi-linearity can be tested in an experiment in order to distinguish it from linear response. Opposite to the LRT, an example for SLRT [7] can look like

$$D = \left[\int \mu(\omega) \left[\tilde{S}(\omega) \right]^{-1} d\omega \right]^{-1} \tag{1.13}$$

where $\mu(\omega)$ is a spectral function depending on the system.

1.3 Conductance of mesoscopic rings

The notion of conductance has experienced several transformation in the last century. In the mesoscopic community [2, 25], following Landauer, it is customary nowadays to consider the open geometry that is described in Fig.1.2a, where a device is attached to left and right reservoirs, and the bias is understood as emerging from a chemical potential difference. For a single mode device it is argued that the conductance is essentially the transmission g_{cl}, while for a multimode device ($\mathcal{M}$ modes) with "spinless" electrons it is a sum over the elements g^T_{nm} of the transition matrix (Table 1.1).

We can optionally assume that the chemical potential of the two reservoirs is the *same*, and consider the effect of an electro-motive force (EMF) so that the voltage drop is concentrated across a segment of the device.

The notion of "conductance" reflects an assumption of "linear response" [1]. For an open system the current in a lead is related to the EMF by the Ohm's law $\mathcal{I} = -G_{\text{Landauer}}\dot{\Phi}$ where Φ is the magnetic flux.

It is quite natural to ask what happens if the two leads of the device are detached from the reservoirs, and the system is closed into a ring as in Fig.1.2b. In spite of much interest in closed mesoscopic rings [3, 26, 27, 28, 29, 30, 31, 32] a general straightforward answer to this simple question has not been given yet. Cohen and Etzioni [9] have derived a *classical answer* (i.e. quantum interference ignored) to this question. Different classical conductance formulas are summarized in Table 1.1.

Some people find it inappropriate to define conductance for a closed system because the problem does not possess a stationary solution. Namely, it is clear that without a contact to a thermal bath the driven system is gradually heated up. However, we find

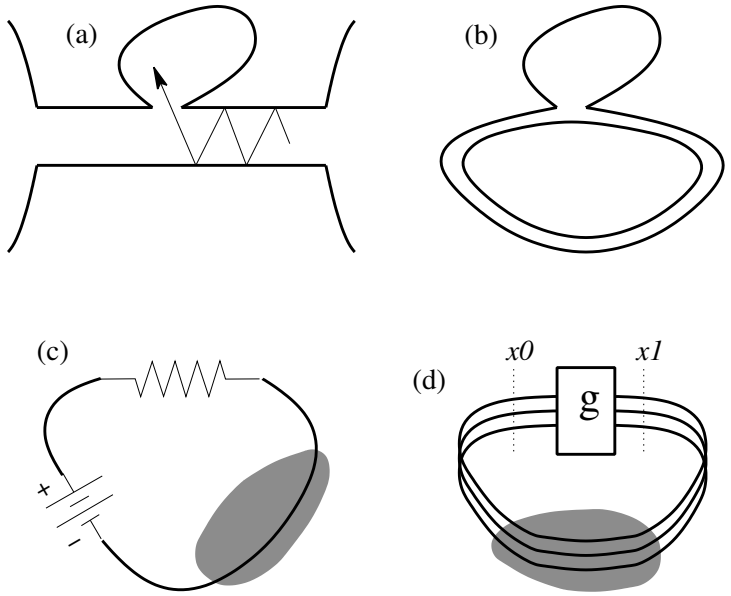

Figure 1.2: Panel (a) displays the standard Landauer (open) geometry of connecting a conductor to a left and a right reservoirs. In this illustration the conductor is a rectangular waveguide to which a cavity is attached. In panel (b) the leads are joined together so as to form a ring. The motion in the ring is assumed to be chaotic due to the scattering in and out of the cavity. Panel (c) is the schematic electrical engineering representation of the system. In panel (d) the system is modeled as a network. The scattering region is described by the transition matrix g_{ab}. In (c) and in (d) we indicate the presence of the environment by the gray shading. In fact (a) can be regarded as a special case of (b) provided it can be assumed that the effect of the environment is to randomize the velocity within the wire region. The current is measured via the section $x = x_1$. The Electro-motive force (EMF) is realized by time dependent Aharonov Bohm flux. The voltage drop can be concentrated anywhere along the ring (say across $x = x_0$). Setting a chemical potential difference in the setup of panel (a) can be regarded as such particular option.

this objection of no relevance. The practical point of view of an electrical engineer is demonstrated in Fig.1.2c. It is clear that at any *moment* the engineer is inclined to characterize the ring by its conductance.

Closed mesoscopic rings provide the ideal paradigm for testing the manifestation of quantum mechanical effects in the mesoscopic realm. The first studies addressed

	Single mode	Multimode
Open	$G = \frac{e^2}{2\pi\hbar} g_{cl}$	$G = \frac{e^2}{2\pi\hbar} \sum_{nm} g^T_{nm}$
Closed	$G = \frac{e^2}{2\pi\hbar} \frac{g_{cl}}{1-g_{cl}}$	$G = \frac{e^2}{2\pi\hbar} \sum_{nm} \left[2g^T(1-g^T+g^R)^{-1}\right]_{nm}$

Table 1.1: The classical conductance formula for open and closed systems. g^T_{nm} and g^R_{nm} are $\mathcal{M} \times \mathcal{M}$ transmission and reflection blocks of the transition matrix.

mainly the Debye regime [33, 34, 35, 36]. Weak localization corrections were studied in [37, 38]. The Kubo formula was also applied to diffusive rings in [19, 20]. Level correlations and localization in energy space were discussed in [21] and also in [22]. For a review see "(Almost) everything you always wanted to know about the conductance of mesoscopic systems" [3]. First measurements of the conductance of closed diffusive rings were reported more than a decade ago [26], while more recently there has been a renewed experimental interest motivated by high precision measurements of individual rings. Measurements of susceptibility of individual closed rings using SQUID is described in [39] and a new micromechanical cantilevers technique for measuring currents in normal metal rings is described in [40]. In a typical experiment a collection of mesoscopic rings is driven by a time dependent magnetic flux which creates an EMF.

For diffusive rings the Kubo formalism leads to the Drude formula [2] for the conductance G. A major challenge in past studies was to calculate the weak localization corrections [37] to the Drude result, taking into account the level statistics and the type of occupation [3]. These corrections are of order Δ/ω_c (where Δ is the mean level spacing and ω_c is the cutoff frequency of the noisy driving), and accordingly do not challenge the leading order Kubo-Drude result. It is just natural to ask what happens to the Drude result if the disorder becomes weak (ballistic case) or strong (Anderson localization case). In the latter case there are two conflicting results for the noise ω_c dependence of G, both following Mott's work [41, 42]. The question is whether to regard the noise as "low frequency driving" or as "temperature". On the one hand, on the basis of the Kubo formula, one expects a crossover from $G \sim \exp(-L/\ell_\infty)$ (where ℓ_∞ is the localization length and L is the length of the system), to the noise dependent result $G \sim \omega_c^2 |\log(\omega_c)|^{d+1}$, where $d = 1$

for quasi one-dimensional (1D) ring. On the other hand, on the basis of the variable range hoping (VRH) picture (for the review see [43, 44]), one expects $G \sim \exp(-(\omega_0/\omega_c)^{1/d+1})$, where ω_0 is a constant. Eventually [10] it has been realized that both the ballistic, the diffusive and the strong localization regimes should be handled on equal footing using the semi-linear response theory (SLRT). The Kubo theory applies in the LRT limit where the driving is very weak, while in mesoscopic circumstances (when the environmental induced relaxation is a *slow* process, compared with the EMF-driven transitions) SLRT leads to a resistor network [45] "hopping" picture in energy space that generalizes the real space hopping picture of Refs. [46, 47]. In our work we present the numerical and the analytical analysis of the application of SLRT to mesoscopic rings.

1.4 Heating rate of cold atoms in vibrating traps

The rate of energy absorption by particles that are confined by vibrating walls was of interest in past studies of nuclear friction [13, 48, 49, 50], where it leads to the damping of the wall motion. More recently it has become of interest in the context of cold atoms physics. In a series of experiments [51, 52, 53] with "atom-optics billiards" some surprising predictions [54, 55] based on linear response theory (LRT) have been verified.

In the past studies the calculation was carried out for a strongly chaotic cavity [13] where it leads to the "wall formula". However, we consider the case where the billiard is fully chaotic but with nearly integrable shape. In such circumstances LRT is *not* applicable (unless the driving is extremely weak so that relaxation dominates). Rather, the analysis that is relevant to the typical experimental conditions should go beyond LRT, and involve a "resistor network" picture of transitions in energy space, somewhat similar to a percolation problem. Consequently, we predict that the rate of energy absorption would be suppressed by orders of magnitude, and provide some analytical estimates supported by a numerical calculation.

1.5 Infinite square-well potential with a moving wall

Because of its simplicity, the problem of a particle in a one-dimensional square well potential with stationary walls is one of the first examples discussed in a beginning course in quantum mechanics. The more complicated situation is where one of the walls is allowed to move. The QM treatment of this problem has a long history ([56, 57, 58]). In [56] the problem is treated by means of a complete set of functions which are exact solutions of the time-dependent Schrodinger equation and comparison is made with a first-order perturbation treatment for a particle initially in the ground state. In [58] the problem is presented as an example of parametric evolution. But we are interested in the time-dependent dynamics of the particle, and in particular transitions between levels in the semi-classical regime [P2].

1.6 Bloch electrons in a constant electric field

The problem of Bloch electrons in a constant electric field has a long history. The Schrodinger equation in one dimension for a Bloch electron (of mass M, charge e) in a electric field E is ([60]):

$$\left[\frac{p^2}{2M} + V(x) + eEx\right]\psi(x) = \epsilon\psi(x) \tag{1.14}$$

where $V(x)$ is the periodic potential and $V(x+a) = V(x)$ with a being the lattice constant. If ϵ is an eigenvalue for a state $\psi(x)$, then $\epsilon + maeE$ is an eigenvalue for the state $W(x - ma)$, where m is any integer. The term $maeE$ leads to what is called Stark ladder. The concept of a Stark ladder was introduced by Wannier in 1960 [59] to describe the energy spectrum of a periodic system in an electric field. Since that time, the Stark ladder has continually been the subject of research and controversy [60, 61, 62, 63, 64, 65, 66, 67, 68, 69]. The very existence of the ladder was initially disputed by Zak [60].

As a part of the controversy Ref. [67] showed that an electron in an arbitrary large lattice is localized by the application of an electric field, and the electron prepared in an electric field dependent Bloch state exercises a periodic motion. But Zak [68] and Leo and MacKinnon [69] showed that the derivation of the result in [67] was incorrect, but not the result itself. Eventually, it has been realized that indeed the electric field

localizes the motion of the electrons, induces a periodic oscillatory motion and this has been confirmed experimentally [70].

Our interest in this problem arises from a possibility to reduce the "EMF driven ring" problem to the Bloch oscillations problem [P2].

Chapter 2

A short summary of the papers

This dissertation comprises 5 published papers [P1, P2, P3, P4, P5] which are attached in the Chapter 3 and summarized briefly in the current chapter. For the details see the relevant papers.

Section 2.1 describes diffractive energy spreading and its semiclassical limit and discusses the quantum-classical correspondence. The paper [P2] is included in Section 3.1.

Section 2.2 explains how the semi-linear response theory (Section 1.2) should be used in order to calculate the conductance of mesoscopic rings (the paper [P3] is included in Section 3.2) and the heating rate of cold atoms in a vibrating trap (the paper [P4] is included in Section 3.3). We introduce an improved sparse random matrix model to capture the essential ingredients of the problems, and show how this model leads to a generalized variable range hopping picture. More details are given in Ref. [P5] included in Section 3.4.

Section 2.3 discusses the information entropy of quantum mechanical states (the paper [P1] is included in Section 3.5). This topic is not related to topics discussed above and attached in this thesis only because it was mentioned in the research proposal.

2.1 Diffractive energy spreading and its semiclassical limit.

We consider a system described by a time-dependent Hamiltonian $\mathcal{H}(Q, P, X(t))$. For such system energy E is not a constant of motion, rather, the driving induces spreading of energy. One can ask how the energy distribution $p_t(E)$ depends on time. In general this function will be different for classical and quantum-mechanical systems. This distribution can be characterized by its moments:

$$\delta E^r = \int p_t(E) E^r dE \tag{2.1}$$

Quantum-classical correspondence (QCC) means that the classical energy distribution moments are similar to the QM ones. The question is under what conditions QCC holds and what its limitations are. The well-known type of QCC is the Bohr QCC, which states that if the wavepackets are Gaussian and the potentials are smooth then the moments are the same for short times. But not always the wavepackets are Gaussian or the potentials are smooth. Moreover, we cannot trust QCC for long times.

The QCC issue is related to the theory of response. Whereas we expect the QCC to hold for *short* times, in the theory of response we are interested in the behavior of the system for *long* times. We can establish a simple operator identity that relates the first two moments ($r = 1, 2$) of the evolving energy distribution to correlation functions of the system. For chaotic systems the correlation persists on short times only. Consequently, if QCC holds for short times, this would imply QCC of the first two moments for long times. This is a variant of the central limit theorem based on the assumption of linear response. Thus we can argue that the long time absorption is determined by the correlation function. For $r > 2$ this statement does not hold!

Incorporating the above we can say that for the first two moments of an energy distribution we expect robust QCC and for the higher moments the QCC is fragile.

If a Gaussian wavepacket is moving in a smooth potential, then its Wigner function evolves in a smooth manner which favours detailed QCC. But we would like to consider the "worst case" for QCC. In [P2] we consider driven systems where the driving induces jumps in energy space:

(i) particles pulsed by a step potential;

(ii) particles in a box with a moving wall;

(iii) particles in a ring driven by an electro-motive-force.

In all these cases the route towards quantum-classical correspondence is highly non-trivial. All these problems share the same feature: in the classical description the energy absorption is associated with abrupt jumps $\delta E_{\rm cl}$ in the phase space (See Figs. 1-3 of [P2]). These jumps are reflected in quantum dynamics as a strong diffraction effect, which is the worst case for Bohr's QCC.

Our main interest is in the non-trivial semi-classical regime where these jumps are much larger than the mean level spacing $\delta E_{\rm cl} \gg \Delta$. We are used to the Fermi golden rule (FGR) picture of transitions $E \longmapsto E +$ "$\hbar\omega$", where ω is the frequency of the driving. However, here we do not have periodic ("AC") driving but rather linear ("DC") driving. Moreover, $\delta E_{\rm cl}$ is an $\hbar$-independent quantity. In order to reconcile the semi-classical picture with the quantum FGR picture we have to assume that the quantum dynamics self-generates a frequency "$\hbar\omega$" $= \delta E_{\rm cl}$.

We solve the first problem analytically and show that the last two problems can be reduced to the problem of Bloch electrons in a tight binding model, which we solve analytically as well. The analogy arises from the following observations: The dynamics in energy space, where n is the level index, is essentially the same as that of Bloch electrons in a tight binding model, where n is the site index. The mean level spacing can be regarded as a constant electric field and the driving induces long range hopping $\sim 1/(n-m)$. In all these cases the restricted QCC ($r = 1, 2$) is preserved, whereas the detailed QCC ($r > 2$) is destroyed.

2.2 Semi-linear response theory.

In [P3, P5, P4] we go on with calculating the response of systems due to an external driving. We discuss the mesoscopic conductance of disordered rings and the heating rate of cold atoms in vibrating traps, their random matrix theory and the generalized variable range hopping picture.

Let us consider a driven chaotic system with Hamiltonian $\mathcal{H}(R(t))$, where R is some control parameter and $\dot{R}$ is the rate of the (noisy) low-frequency driving with a cutoff frequency ω_c. In this case there are diffusion in energy space

$$D = G_{\text{diffusion}} \ \overline{\dot{R}^2} \tag{2.2}$$

and energy absorption

$$\dot{E} = G_{\text{absorption}} \ \overline{\dot{R}^2} \tag{2.3}$$

which are proportional to the RMS (squared) of the rate of the driving within the framework of linear response.

The dissipation-diffusion theorem, which in the canonical case is $\dot{E} = D/T$, allows us to relate between the diffusion coefficient and the rate of energy absorption. For simplicity from now on we use scaled units for G.

In what follows we focus on two systems (Fig. 2.1):

(i) a metallic ring driven by an electro-motive force [P3, P5]. For the calculations we used the Anderson tight binding model, where the lattice size is $L \times M$ with $M \ll L$, L is the length of the ring and M is the number of open modes. The random on-site potential is given by a box distribution of width W.

(ii) cold atoms in a slightly deformed rectangular box that are heated up due to the vibrations of a wall [P4]. The deformation (of strength u) is introduced either by a bump or by deforming a static wall (see Fig. 1 of [P4]).

In the past studies the same type of analysis was also applied for the problem of radiation absorption by metallic grains [7].

In all these problems the Hamiltonian can be written as

$$\mathcal{H}(R(t)) \ \approx \ \mathcal{H}_0 + f(t)V \tag{2.4}$$

where R_0 is a constant and

$$\mathcal{H}_0 = \mathcal{H}(R_0), \quad f(t) = R(t) - R_0, \quad V = \frac{\partial \mathcal{H}}{\partial R} \tag{2.5}$$

In the energy basis of $\mathcal{H}_0$ it reads

$$\mathcal{H} = \{E_n\} + f(t)\{V_{nm}\} \tag{2.6}$$

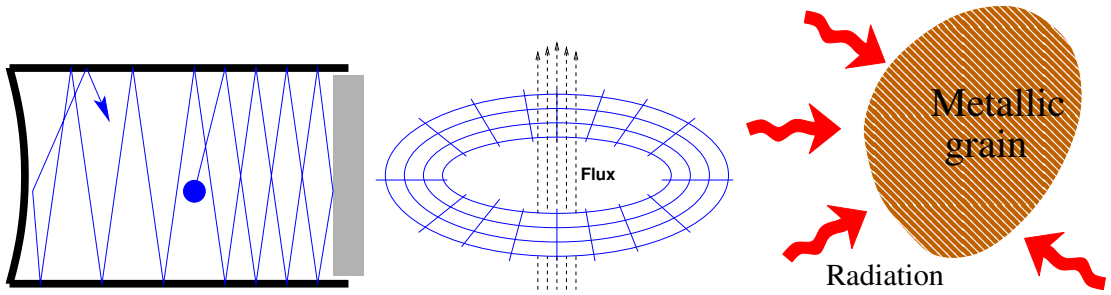

Figure 2.1: Models: (i) 2-D box with a vibrating wall (the solid lines are for the static walls and the shaded line is for the vibrating wall); (ii) Disordered ring driven by EMF; (iii) Radiation absorption by metallic grains

where E_n are the energies of the unperturbed system, and $V_{nm} = \langle n \left| \frac{d\mathcal{H}}{dR} \right| m \rangle$ are the elements of the perturbation matrix. In problem (i) the control parameter R is the flux Φ and we calculate the conductance G as the system is driven by the EMF ($\dot{\Phi}$). In problem (ii) the control parameter R is the location of the moving wall and we calculate the diffusion coefficient G. In both problem the power spectrum of $\dot{R}$ is assumed to have the cutoff frequency ω_c which is small compared with any relevant semiclassical energy scale, but larger compared with the mean level spacing Δ.

In order to calculate the diffusion within the framework of the linear response theory (LRT) the Kubo formula (1.8) is used

$$G_{\rm LRT} \quad = \quad \pi \varrho_{\rm E} \langle\langle |V_{nm}|^2 \rangle\rangle_a \tag{2.7}$$

where $\langle\langle x \rangle\rangle_a = \langle x \rangle$ is the algebraic average over the near diagonal matrix elements, and $\varrho_{\rm E}$ is the density of states (DOS).

However, we show that in the case of a very weak disorder in problem (i) and of a small deformation in problem (ii) the LRT is not applicable, because the rate of absorption depends crucially on the possibility to make *connected* sequences of transitions. Therefore, the semi-linear response theory (SLRT) has to be used to calculate the diffusion coefficient / conductance which leads to (Eq. 1.10)

$$G_{\rm SLRT} \quad = \quad \pi \varrho_{\rm E} \, \langle\langle |V_{nm}|^2 \rangle\rangle \tag{2.8}$$

where the "average" $\langle\langle x \rangle\rangle$ is defined as in Ref. [P5] via a *resistor-network calculation*. Thus the analysis is somewhat similar to a percolation problem in energy space.

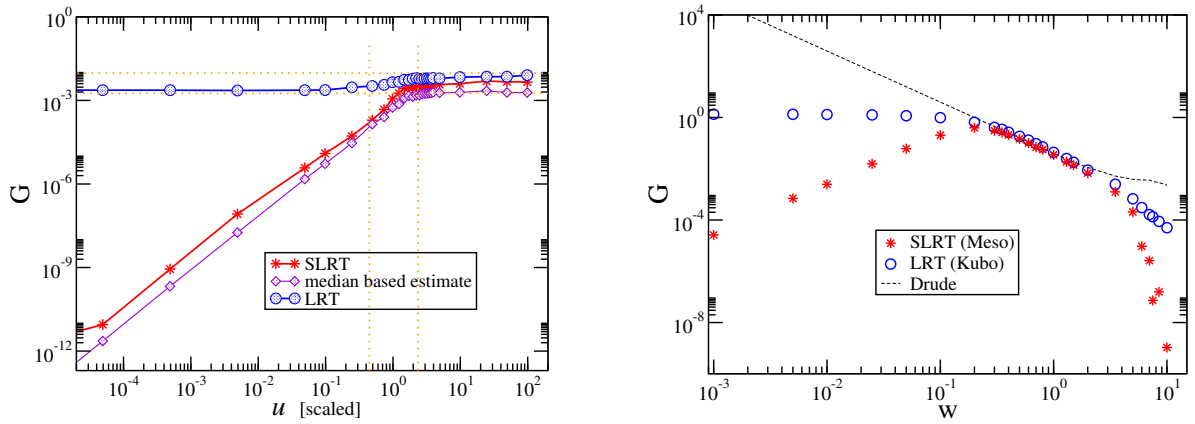

Figure 2.2: LRT vs. SLRT results for *Left panel:* the vibrating trap model (u is the strength of the deformation) and *Right panel:* the disordered ring (W is strength of the disorder).

The results comparing the LRT and the SLRT calculations are presented on Fig. 2.2. The main observation is that for a very weak deformation / disorder the SLRT result is smaller than the LRT result by orders of magnitude. In [P4, P5] we provide the exact conditions that should be satisfied in order to test these results experimentally and supply also some estimated experimental numbers.

The rest of the section is devoted to the brief description of the random matrix modeling of SLRT which leads to a generalized variable hopping picture.

In both discussed problems the Hamiltonian in the $\boldsymbol{n} = (n_x, n_y)$ basis can be written as

$$\mathcal{H} = \mathrm{diag}\{E_{\boldsymbol{n}}\} + u\{U_{\boldsymbol{nm}}\} + f(t)\{V_{\boldsymbol{nm}}\} \tag{2.9}$$

where $\{U_{\boldsymbol{nm}}\}$ describes either the deformation in the vibrating trap problem or the disordered potential in the ring, and u controls its strength. For $u = 0$ different transverse modes are uncoupled in the trap problem and in the limit of very weak disorder the eigenstates are not quantum-ergodic in momentum space in the ring problem. Thus the matrix $\{V_{\boldsymbol{nm}}\}$ is very sparse, i.e. most of its elements are zeros. (In the ring problem this matrix is also sparse in the limit of strong disorder because the eigenstates are not quantum-ergodic in real space). Allowing a small u and diagonalizing the Hamiltonian, we get the form of Eq. (2.6), where the matrix $\{V_{\boldsymbol{nm}}\}$ is still sparse and possibly textured. See representative matrix images on Fig. 2.3.

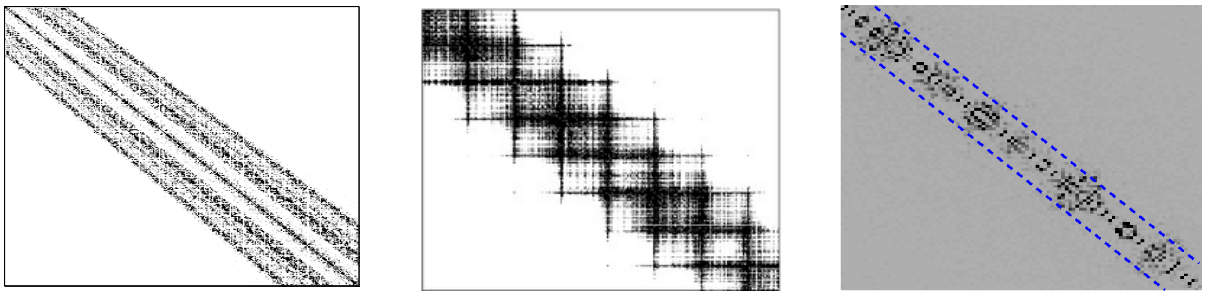

Figure 2.3: Representative perturbation matrices: uniform banded; textured; sparse and textured (from left to right)

The Fourier transform of the correlation function of V in the quantum case is (Eq. 1.7)

$$\tilde{C}(\omega) \equiv \left\langle \left\langle |V_{nm}|^2 \right\rangle \right\rangle_{\text{algebraic}} = \left\langle \sum_n |V_{nn_0}|^2 \; \delta(\omega - (E_n - E_{n_0})) \right\rangle_{\text{algebraic}} \tag{2.10}$$

This correlation function enters the Kubo formula Eq. (1.4), but it reflects neither the sparsity nor the texture! The above way of writing the formula emphasizes the fact that $\tilde{C}(\omega)$ is just the algebraic average of the matrix elements $|V_{nm}|^2$ along the diagonals within the energy window of interest. However, in the case of having sparsity and/or texture the algebraic average is not a "typical" value of the distribution of elements and we need another measure. It turns out that a median (or a geometric average) does reflect the "typical" value. Fig. 2.4 presents a typical histogram in a logarithmic scale. The algebraic average is almost the same for different small deformations but the typical values (the peaks of the distributions) are different by orders of magnitude. The reason is that the algebraic average is dictated by the minority of the large elements of $|V_{nm}|^2$ (which do not change as a function of a small u), whereas the typical values depend on u^2 (see Eq. (13) of [P4] and the discussion before it).

In order to obtain some analytical results the natural guess is to approximate the distribution as a log-normal distribution (in the ring problem we show [P3, P5] that for the strong disorder the distribution is log-box, i.e. it is a box distribution in a logarithmic scale). We introduce different measures to quantify the sparsity of a distribution

$$s = \langle x \rangle^2 / \langle x^2 \rangle \tag{2.11}$$

$$p = \text{Prob}(x > \langle x \rangle) \tag{2.12}$$

$$q = \langle \langle x \rangle \rangle_{\text{median}} / \langle x \rangle \tag{2.13}$$

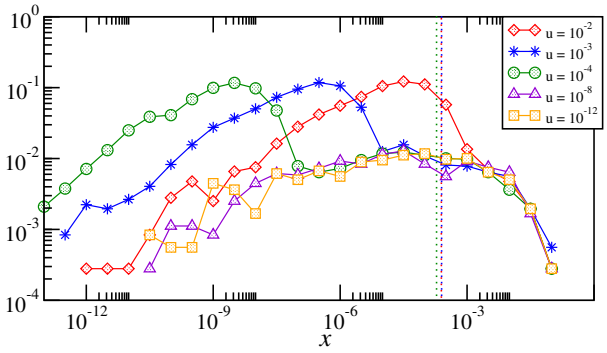

Figure 2.4: A histogram of the perturbation matrix (squared) for different deformations for a vibrating box of unit aspect ratio. The vertical dot lines denote the algebraic average for each distribution.

Small s, p or q mean that the distribution is very wide, and there are many nearly vanishing values. We have derived analytical formulas which express the sparsity as function of the model parameters (for the details see [P4, P5]).

To get the formula for the ratio between the SLRT and the LRT results we used the following generalized Variable Range Hopping (VRH) scheme. Given a hopping range $|E_m - E_n| < \omega$ in the energy, we can look for the typical matrix element x_ω for connected sequences of transitions, which we find by solving the equation

$$\varrho_{\rm E}\omega\,{\rm Prob}\Big(x > x_\omega\Big) \;\sim\; 1 \tag{2.14}$$

where the probability distribution is known (log-normal, log-box). Then the generalized VRH estimate is

$$G_{\rm SLRT} \quad = \quad \int x_\omega \tilde{F}(\omega) d\omega \tag{2.15}$$

where $\tilde{F}(\omega)$ is the normalized power spectrum of $\dot{R}$ defined via the Eq. (1.9). Using this scheme we found that for the log-box distribution assuming an exponential bandprofile the SLRT suppression factor $g_{\rm SLRT} = G_{\rm SLRT}/G_{\rm LRT}$ is

$$g_{\rm SLRT} \quad \sim \quad \frac{1}{\tilde{p}} \;\exp\left[-2\left(\frac{1}{\tilde{p}\;b}\right)^{1/2}\right] \tag{2.16}$$

where $p \approx -\tilde{p}\ln\tilde{p}$ and $b = \varrho_{\rm E}\omega_c$ is the dimensionless bandwidth. For the log-normal distribution the VRH calculation gives the result

$$g_{\rm SLRT} \quad \sim \quad q \;\exp\left[\left({\rm factor} \times \ln\left(\frac{1}{q}\right)\ln\left(b\right)\right)^{1/2}\right] \tag{2.17}$$

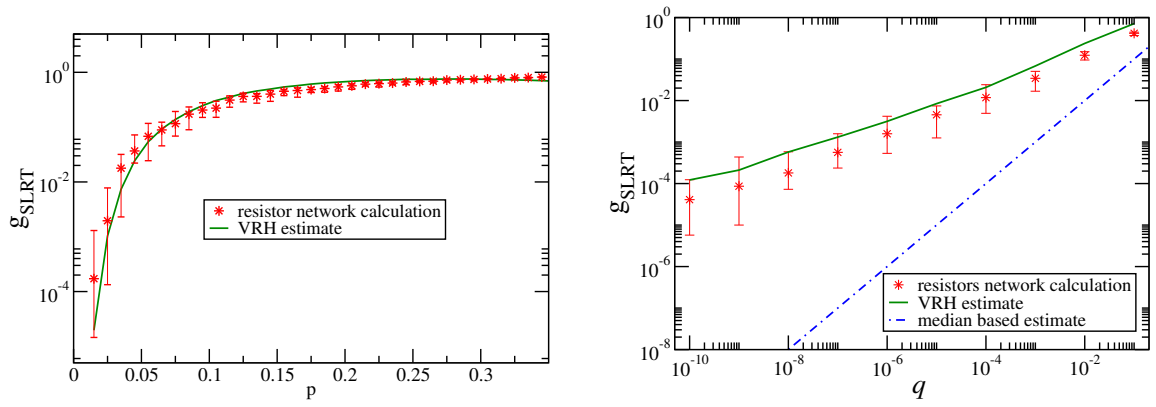

Figure 2.5: The SLRT suppression factor $g_{\rm SLRT}$ versus the sparsity parameter for (a) log-box distribution with exponential power spectrum; (b) log-normal distribution with rectangular power spectrum. The resistor network and the VRH calculation were done for 100 realizations of 256×256 matrices with $b = 10$. In the log-normal case the VRH result is contrasted with the naive geometric mean estimation.

where the factor is determined by the bandprofile (it is 2 for an exponential bandprofile and 4 for a rectangular bandprofile). See Fig. 2.5 for the comparison between the numerical resistor network calculation and the analytical estimate.

In section 9 of [P5] we investigate the RMT statistics in the Anderson regime of the disordered ring problem and show that size distribution of the velocity matrix elements $|v_{mn}|$ that reside inside a band of width ω is within

$$\frac{v_{\rm E}}{\mathcal{M}} \times \left[\frac{L}{\ell_\xi} {\rm e}^{-L/\ell_\xi}, \qquad 1\right] \qquad \text{for } |\omega| > \Delta_\xi \tag{2.18}$$

$$\frac{v_{\rm E}}{\mathcal{M}} \times \left[\frac{L}{\ell_\xi} {\rm e}^{-L/\ell_\xi}, \quad \frac{\omega}{\Delta_\xi} \log\left(\frac{\Delta_\xi}{\omega}\right)\right] \qquad \text{for } |\omega| < \Delta_\xi \tag{2.19}$$

where $\Delta_\xi = \pi v_{\rm E}/\mathcal{M}\ell_\xi$ is the the local level spacing and ℓ_ξ is the localization length. If we ignore the Mott resonant states, then a log-box distribution is implied.

In order to appreciate the similarities and the differences between SLRT and the conventional Hopping calculation, we cast the latter into the SLRT language. Eq. (4.4) of Ref [46] for the DC Hopping conductance due to phonon induced transitions is

$$G_{\rm Ohm} \;=\; \frac{1}{\mathcal{N}} \left[\left[\frac{e^2}{T}(1-f(E_n))f(E_m)w_{mn}^\gamma\right]\right]_\parallel \tag{2.20}$$

The notation $[[...]]_\parallel$ implies that the resistance of the network is calculated between states at the same energy $E \sim E_{\rm E}$, that reside in opposite sides of the sample. Due to the Fermi

occupation factor, the network contains effectively $\mathcal{N} = \varrho_{\rm E} T$ nodes. The division by $\mathcal{N}$ is required because we have defined the [[...]] as inverse-resistivity and not as inverse-resistance of the network.

The occupation factor $(1-f(E_n))f(E_m)/T$ gives $\mathcal{O}(1)$ weight only to the $\mathcal{N}$ levels that reside within a window of width T. If we ignore the relaxation effects and regard the fluctuating environment as a noise source that induces transitions $w^\gamma_{mn} \propto \exp(|E_m - E_n|/T)$, we still should get the same result for G, even if we omit the occupation factor. This point of view allows to bridge between the noisy driving problem that we consider and the phonon-induced hopping in the prevailing literature.

The Einstein relation $G_{\rm Ohm} = (e/L)^2 \varrho_{\rm E} \mathcal{D}$ relates the conductance and diffusion in real space. We deduce that

$$\mathcal{D} \;=\; \left(\frac{L}{\mathcal{N}}\right)^2 [[w^\gamma_{mn}]]_\parallel \tag{2.21}$$

This should be compared with the SLRT expression for the noise induced energy diffusion

$$\mathcal{D}_{\rm E} \;=\; \left(\frac{1}{\varrho_{\rm E}}\right)^2 [[w^\gamma_{mn}]]_\perp \tag{2.22}$$

Here the resistance of the network is calculated between states that reside far away in energy. The SLRT result for $\mathcal{D}_{\rm E}$ and the hopping implied result for $\mathcal{D}$ are both simple and manifestly equivalent: The diffusion coefficient equals the transition rate $[[w^\gamma_{mn}]]$ times the *step* squared. In the SLRT calculation the step in energy space is $1/\varrho_{\rm E}$, while in the standard real space analysis the step is $L/\mathcal{N}$. Optimization of the hopping with respect to the distance ω in energy is equivalent to optimization with respect to the distance r in space.

For the further details see [P5] where we also clarify the relation between SLRT and the traditional VRH calculation (Sec. 10), question the possibility to get VRH from proper LRT analysis (Sec. 11) and contrast VRH with non-thermal hopping due to noisy source (Sec. 12).

2.3 The information entropy of quantum mechanical states

The information entropy of quantum mechanical states is discussed in [P1]. It is not related to topics discussed above and attached in this thesis only because it was mentioned in the research proposal.

It is well known that a Shannon based definition of information entropy leads in the classical case to the Boltzmann entropy. It is tempting to regard the Von Neumann entropy as the corresponding quantum mechanical definition. But the latter is problematic from quantum information point of view. Consequently,

- we introduce a new definition of entropy that reflects the inherent uncertainty of quantum mechanical states
- we derive an explicit expression for it and discuss some of its general properties
- we distinguish between the minimum uncertainty entropy of pure states $S_0(N)$ and the excess statistical entropy of mixtures $F(p_1, p_2, ..., p_N)$

$$S[\rho] = S_0(N) + F(p_1, p_2, ..., p_N) \neq -\sum_r p_r \ln p_r \tag{2.23}$$

Lately K. Zyczkowski (private communication) has pointed out that similar analysis had been introduced earlier in [71].

Chapter 3

The published papers

3.1 Diffractive energy spreading and its semiclassical limit

The content of this section is available as

- a journal article: A. Stotland and D. Cohen, J. Phys. A **39**, 10703 (2006)
- a preprint: arXiv:cond-mat/0605591

INSTITUTE OF PHYSICS PUBLISHING JOURNAL OF PHYSICS A: MATHEMATICAL AND GENERAL

J. Phys. A: Math. Gen. **39** (2006) 10703–10721 doi:10.1088/0305-4470/39/34/008

Diffractive energy spreading and its semiclassical limit

Alexander Stotland and Doron Cohen

Department of Physics, Ben-Gurion University, Beer-Sheva 84005, Israel

Received 24 May 2006, in final form 17 July 2006
Published 9 August 2006
Online at stacks.iop.org/JPhysA/39/10703

Abstract

We consider driven systems where the driving induces jumps in energy space: (1) particles pulsed by a step potential; (2) particles in a box with a moving wall; (3) particles in a ring driven by an electro-motive-force. In all these cases, the route towards quantum-classical correspondence is highly non-trivial. Some insight is gained by observing that the dynamics in energy space, where n is the level index, is essentially the same as that of Bloch electrons in a tight binding model, where n is the site index. The mean level spacing is like a constant electric field and the driving induces long range hopping $\propto 1/(n-m)$.

PACS numbers: 03.65.−w, 03.65.Sq, 05.45.Mt

(Some figures in this article are in colour only in the electronic version)

1. Introduction

Consider a system which is described by a Hamiltonian $\mathcal{H}(X(t))$, where the parameter $X(t)$ is time dependent. For such a system the energy E is not a constant of the motion. Rather, the driving induces spreading in energy space. Assuming that the system is prepared at $t = 0$ in a microcanonical state, one wonders how the energy distribution $\rho_t(E)$ looks like at a later time. In particular, one may wonder whether the quantum $\rho_t(E)$ is similar to the corresponding classical distribution. In the 'quantum chaos' literature it is customary to distinguish between a classical time scale $\tau_{\rm cl}$ and a quantum breaktime t^*. The latter goes to infinity in the '$\hbar \to 0$' limit. A prototype model is the 'quantum kicked rotator' [1] where the energy spreading is diffusive up to t^*, while for larger times one observes saturation due to a dynamical localization effect.

In this work, we analyse much simpler systems where the breaktime t^*, if exists, is much larger than any physically relevant time scale. In fact, one may assume that the time t of the evolution is comparable with the classical (short) time scale. In such circumstances, one naively would expect quantum to classical correspondence (QCC). But in fact the theory is much more complicated [2]. One has to distinguish between

- detailed QCC and
- restricted QCC.

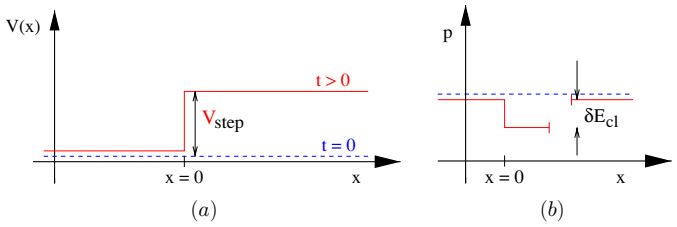

Figure 1. (*a*) Left panel: picture of the potential. Before $t = 0$ the potential is zero (dashed line). After $t = 0$ the potential is the step function (solid line). (*b*) Right panel: phase space picture. Before $t = 0$ there is no potential and the momentum is constant (dashed line). The piece of the distribution that has passed $x = 0$ after $t = 0$ is boosted with $\delta E_{\rm cl} = -V_{\rm step}$.

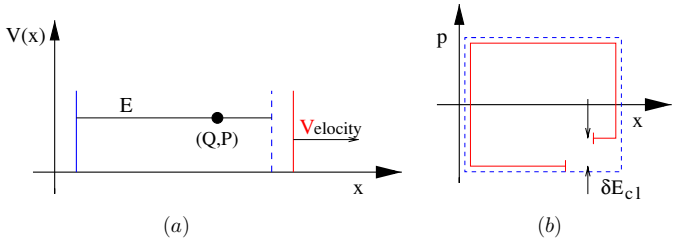

Figure 2. (*a*) Left panel: potential well. The right wall is moving with a constant velocity $V_{\rm wall}$. (*b*) Right panel: phase space picture. If the wall were not moving, the distribution would evolve along the dashed line. If $V_{\rm wall}$ is non-zero, an energy jump $\delta E_{\rm cl} = -2mv_{\rm E}V_{\rm wall}$ is associated with the collision, and one obtains the distribution which is illustrated by the solid line.

Detailed QCC means that all the moments $r = 1, 2, 3, \ldots$ of the quantum mechanical distribution $\rho_t(E)$ are similar to the classical result, while restricted QCC refers only to the $r = 1, 2$ moments. It turns out that the latter are very robust, while the higher moments ($r > 2$) might be much larger in the quantum case. Our first challenge would be to find and to analyse the *worst case* for QCC, for which all the $r > 2$ moments are classically finite but quantum mechanically divergent. We would like to see whether in such circumstances restricted QCC for $r = 1, 2$ survives.

For completeness of this introduction, we summarize in appendix A the reason for the robustness of restricted QCC. Our interest in QCC is motivated by the wish to develop a better understanding of driven systems. We would like to explore examples where QCC is far from obvious even for short times. In what follows, we address four problems that in first sight look unrelated:

(1) Particles that are pulsed by a step potential (figure 1).
(2) Particles in a box with a moving wall (figure 2).
(3) Particles in an electro-motive-force (EMF) driven ring (figure 3).
(4) Wavepacket dynamics of Bloch electrons in a constant electric field.

In fact, we are going to see that problems (1)–(3) share a common feature: in the classical description the energy absorption is associated with abrupt *jumps* in phase space. These jumps are reflected in the quantum dynamics as a strong *diffraction* effect. This diffraction, which takes place in energy space, is the worst case for Bohr's QCC. It turns out that problem (1) can be solved exactly, while problems (2) and (3) reduce essentially to problem (4). Namely, the

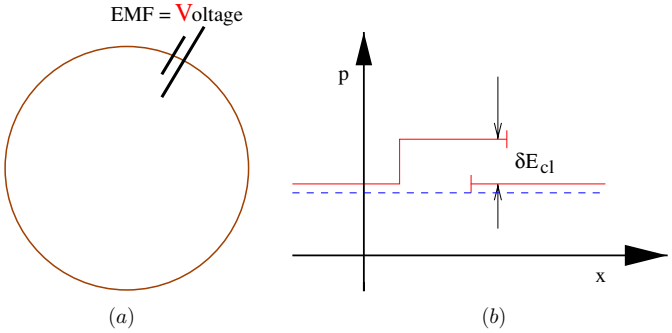

Figure 3. (*a*) Left panel: ring with EMF. (*b*) Right panel: phase space picture. Without the EMF the momentum is a constant of the motion (dashed line). Else an energy jump $\delta E_{\rm cl} = eV_{\rm EMF}$ is associated with each crossing of the EMF step. The emerging phase space distribution is illustrated by the solid line.

dynamics in energy space, where n is the level index, is essentially the same as that of Bloch electrons in a tight binding model, where n is the site index. The mean level spacing is like a constant electric field and the driving induces long range hopping $\propto 1/(n-m)$. This tight binding problem has an exact solution. The objectives of the present work are as follows:

- To highlight the route towards QCC in the case of diffractive energy spreading.
- To provide solutions and numerical demonstrations to the prototype problems.
- To shed new light of the EMF-driven ring problem.
- To illuminate the limitations of linear response theory in the mesoscopic context.

The paper is structured accordingly.

A few words are in order regarding the literature. The quantum treatment of the 'moving wall' problem has started with [3, 4] that were aimed in finding the steady-state solutions for an expanding well. The interest in this model has further evolved within the study of the Fermi acceleration problem [5] where the wall is oscillating. Recently, the non-trivial features of the parametric [6] and of the time-dependent wavepacket dynamics [7] were illuminated. In the latter publication, a satisfactory mathematical treatment of the non-stationary dynamics has not been introduced. Also the problem of Bloch electrons in a constant electric field has a long history. The concept of a Stark ladder was introduced by Wannier [8] to describe the energy spectrum of a periodic system in an electric field. Since that time it has become the subject of controversy [9–19]. Eventually, it has been realized that the electric field localizes the motion of the electrons and induces a periodic oscillatory motion.

2. Energy jumps in phase space

If a Gaussian wavepacket is moving in a smooth potential, then its Wigner function evolves in a smooth manner which favours detailed QCC. But we would like to consider the 'worst case' for QCC. Let us assume that the particle is prepared with some initial momentum p. This means in practice a very extended wavepacket with a very small dispersion in momentum. We turn on at $t = 0$ a step of height $V_{\rm step}$. After a short time t, we observe that the classical phase space distribution is torn into three pieces (see figure 1): phase space points that remain on the left side of the step; phase space points that have crossed the step from left to right and

phase space points that were all the time in the right side of the step. The jump in the kinetic energy of those points that have crossed the step is

$$\delta E_{\rm cl} = -V_{\rm step}. \tag{1}$$

Classically we have in phase space points that move with the original kinetic energy, and another set of points that have gone through an abrupt change of kinetic energy. Thus, the energy distribution consists of two delta peaks. We would like to know what is the corresponding energy distribution in the quantum mechanical case.

A similar phase space picture emerges in the analysis of the 'moving wall' problem. As illustrated in figure 2, we have a particle of mass m and energy E bouncing back and forth inside a one-dimensional box. One wall of the box is displaced with a velocity $V_{\rm wall}$, which is assumed to be much smaller compared with the velocity $v_{\rm E} = (2E/m)^{1/2}$ of the bouncing particle. Consider an initial microcanonical distribution. After a short time t, some of the phase space points collide with the wall which is moving with velocity $V_{\rm wall}$. Consequently, their velocity undergoes a change $v \mapsto -v + 2V_{\rm wall}$, and accordingly the energy jump is

$$\delta E_{\rm cl} = -2m v_{\rm E} V_{\rm wall}. \tag{2}$$

Thus, after a short time the energy distribution consists of two delta peaks: one corresponds to those phase space points that did not collide with the moving wall and the other corresponds to those phase space points that did collide with the moving wall. We ask what is the corresponding quantum result. Namely, how the probability is distributed among the energy levels in the quantum mechanical case. It is implicit that we are going to work in the adiabatic (wall location dependent) basis, else the question is mathematically ill defined.

Possibly the most interesting and experimentally relevant model is that of a one-dimensional EMF-driven ring (figure 3). The classical analysis for this problem is very simple: each time that the particle crosses the EMF step its energy changes by

$$\delta E_{\rm cl} = eV_{\rm EMF}. \tag{3}$$

So also here we have energy jumps. Surprisingly, this problem is interesting even if we do not add a scatterer.

3. Beyond the Fermi golden rule, the semiclassical regime

Both in the case of the 'moving wall' and in the case of the driven ring we have after a short time a finite probability to find the system with a different energy. So, we may say that there is some finite probability to make a transition

$$E \longmapsto E + \delta E_{\rm cl}. \tag{4}$$

Going to the quantum mechanical problem, we may wonder whether or how we get from the Schrödinger equation such transitions. We are used to the Fermi golden rule picture of transitions

$$E \longmapsto E + \text{`}\hbar\omega\text{'} \tag{5}$$

where ω is the frequency of the driving. But here we do not have periodic ('ac') driving but rather linear ('dc') driving. Moreover, $\delta E_{\rm cl}$ is an $\hbar$-independent quantity. It turns out that indeed there exists a regime where the dynamics is classical like (figure 4). This semiclassical regime is defined by the obvious condition

$$\delta E_{\rm cl} \gg \Delta \tag{6}$$

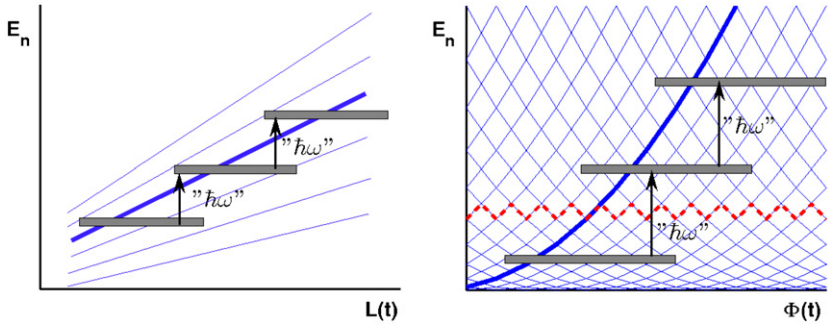

Figure 4. (*a*) Left panel: the energy levels of a one-dimensional box as a function of its width $L(t)$. For the purpose of comparison with other figures $L(t)$ is decreasing as we go to the right (the box becomes smaller) so the levels are going up. The solid line illustrates adiabatic dynamics, while the 'jumps' illustrate semiclassical dynamics. (*b*) Right panel: the energy levels of a one-dimensional ring as a function of the Aharonov–Bohm flux. The solid line illustrates diabatic dynamics, while the 'jumps' illustrate semiclassical dynamics. The dashed line illustrates adiabatic dynamics.

where Δ is the level spacing. In the case of the 'moving wall' problem this condition can be written as

$$V_{\text{wall}} \gg \frac{\hbar}{mL} \tag{7}$$

where L is the size of the box. It is easily verified that this condition is just the opposite of the adiabatic condition. The case of the EMF-driven ring is somewhat richer. The condition that defines the semiclassical regime becomes

$$V_{\text{EMF}} \gg \frac{\hbar v_{\text{E}}}{L} \tag{8}$$

where L is the length of the ring. It is easily verified that this condition is just the opposite of the diabaticity condition. The diabatic regime is defined as that where transitions between energy levels of a 'free' ring can be neglected. If there is a small scatterer inside the ring, a stronger condition than diabaticity is required in order to maintain adiabaticity:

$$V_{\text{EMF}} \ll (1-g)\frac{\hbar v_{\text{E}}}{L} \tag{9}$$

where $g \sim 1$ is the transmission of the scatterer. The adiabatic regime is defined as that where transitions between the actual energy levels of the ring can be neglected. This is the regime where the Landau–Zener mechanism of transitions at avoided crossings [20, 21] becomes significant. The three regimes in the EMF-driven ring problem are illustrated in the diagram of figure 5.

Our main interest is in the non-trivial semiclassical regime as defined by equation (6). In order to reconcile our semiclassical intuition with the quantum Fermi Golden rule picture, we have to assume that the quantum dynamics self-generates a frequency '$\hbar\omega$' $= \delta E_{\text{cl}}$. Indeed, it has been argued in [7] that the non-perturbative mixing of levels on the small energy scales generate this frequency, while the re-normalized transitions on the large (coarse grained) energy scales are FGR like. However, an actual mathematical analysis of the dynamics has not been introduced and was left as an open problem. In section 7 we shall argue that these FGR-like energy jumps can be reinterpreted as unidirectional Bloch oscillations (figure 6).

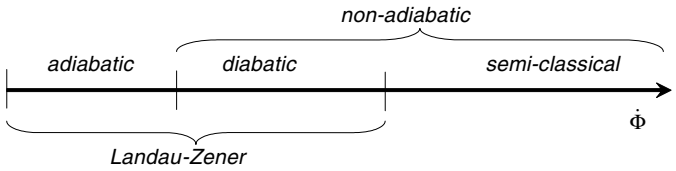

Figure 5. The three regimes in the EMF-driven ring problem. See the text.

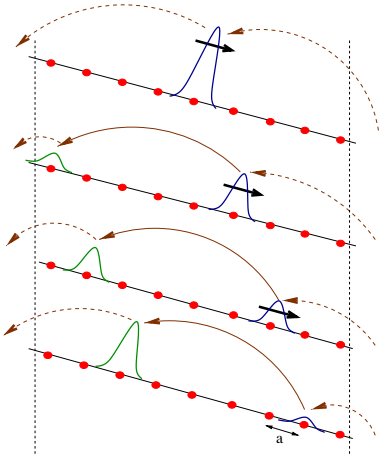

Figure 6. The unidirectional oscillations of Bloch electrons with $\propto 1/(n-m)$ hopping: as the wavepaket slides to the right it shrinks, while being re-injected on the left, where it re-emerges. This should be contrasted with conventional bi-directional oscillations of Bloch electrons with nearest neighbour hopping.

4. Particle pulsed by a step

The simplest example for a semiclassical energy jump is provided by the 'step problem'. The time-dependent Hamiltonian is

$$\mathcal{H} = \frac{p^2}{2m} + \begin{cases} 0 & t < 0 \\ V_{\text{step}} & t \geqslant 0. \end{cases} \tag{10}$$

For this Hamiltonian 'energy space' is in fact 'momentum space', so it is more natural to refer to 'momentum jumps'. Obviously, we can translate any small change in momentum to energy units via $\delta E = v_{\text{E}}\delta p$, where $v_{\text{E}} = (2E/m)^{1/2}$ is the velocity of the particle in the energy range of interest.

The phase space dynamics after kicking an initial momentum state p_0 at $t = 0$ is illustrated in figure 1(*b*). It is clear that the emerging momentum distribution is

$$\rho_t(p) = \left[1 - \frac{v_{\text{E}}t}{L}\right]\delta(p - p_0) + \frac{v_{\text{E}}t}{L}\delta(p - (p_0 + \delta p_{\text{cl}})) \tag{11}$$

where $\delta p_{\text{cl}} = -V_{\text{step}}/v_{\text{E}}$ and L is the spatial extent of the wavepacket. From here on we set $L = 1$ as implied by the standard density normalization of the momentum state $\mathrm{e}^{\mathrm{i}p_0 x}$. It is implicit in the following analysis that we assume a very extended wavepacket ($v_{\text{E}}t \ll L$).

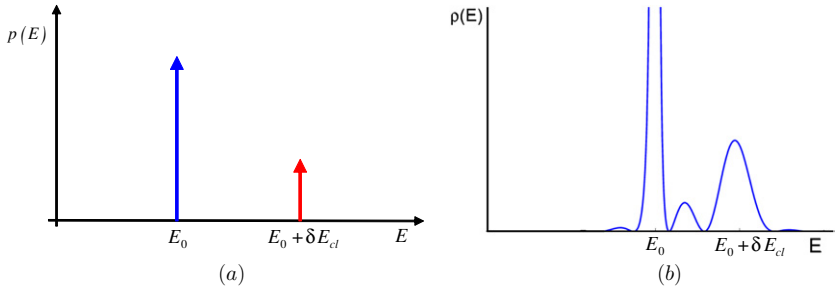

Figure 7. (*a*) Left panel: the classical energy distribution, equation (11), some time after a step potential is turned on. In this illustration $V_{\rm step} > 0$. (*b*) Right panel: the corresponding quantum mechanical energy distribution calculated with equation (13).

The emerging momentum distribution can be characterized by its moments with respect to $p = p_0$. Namely,

$$\langle (p - p_0)^r \rangle = \delta p_{\rm cl}^r \times v_{\rm E} t \qquad r = 1, 2, 3, 4, \ldots. \tag{12}$$

All the moments are finite and grow linearly with time. Below we are going to derive the quantum result. Omitting the trivial $\delta(p - p_0)$ term, and the back-reflection term, the final result for the forward scattering is

$$\rho_t(p) = |\langle p|\mathcal{U}|p_0\rangle|^2 = \frac{\delta p_{\rm cl}^2}{(p - p_0)^2} v_{\rm E}^2 t^2 \,{\rm sinc}^2\left[\frac{1}{2}\left(p - (p_0 + \delta p_{\rm cl})\right) v_{\rm E} t\right] \tag{13}$$

for which

$$\langle (p - p_0)^r \rangle = \begin{cases} \delta p_{\rm cl} \times v_{\rm E} t - \sin(\delta p_{\rm cl} v_{\rm E} t) & \text{for } r = 1 \\ \delta p_{\rm cl}^2 \times v_{\rm E} t & \text{for } r = 2 \\ \infty & \text{for } r > 2. \end{cases} \tag{14}$$

Let us compare the energy distribution in the classical and quantum-mechanical cases (figure 7). As the time t becomes much larger than $\hbar / V_{\rm step}$, the semiclassical peak is resolved. But we never get detailed QCC, because all the high ($r > 2$) moments of the distribution diverge.

It should be appreciated that the power law tails that we get here for the energy distribution are the 'worst case' that can be expected. They emerge because the phase space distribution is torn in the momentum direction. In space representation this reflects a discontinuity in the derivative of the wavefunction. This explains why the tails go like $1/p^4$. We are going to encounter the same type of power law tails also in the other examples.

4.1. Derivation of the quantum result

The rest of this section is devoted for the derivation of the quantum result and can be skipped in first reading. The momentum states are denoted as $|p\rangle$. In order to simplify the calculation we approximate the dispersion relation, within the energy window of interest, as linear $E = v_{\rm E} k$. This implies that back-reflection is neglected. Once the step is turned on, $|p\rangle$ are no longer the stationary states. The new stationary states are

$$|k\rangle \longmapsto \Theta(-x)\, {\rm e}^{{\rm i}kx} + \Theta(x)\, {\rm e}^{{\rm i}(k+u)x} \tag{15}$$

where we use the notation $u = \delta p_{\rm cl}$. Note that these form a complete orthonormal set in the sense $\langle k_1|k_2\rangle = 2\pi\delta(k_1 - k_2)$. The transformation matrix from the old to the new basis is

$$\langle p|k\rangle = \int_{-\infty}^{0} \mathrm{e}^{-\mathrm{i}(p-k)x}\,\mathrm{d}x + \int_{0}^{\infty} \mathrm{e}^{-\mathrm{i}(p-k-u)x}\,\mathrm{d}x \tag{16}$$

$$= \pi\delta(p-k) + \frac{\mathrm{i}}{p-k} + \pi\delta(p-k-u) - \frac{\mathrm{i}}{p-k-u}. \tag{17}$$

Before we go on with the calculation we note that the following elementary integral can be found in any mathematical handbook:

$$\int_{-\infty}^{\infty} \frac{\mathrm{d}k}{2\pi} \frac{1}{(k-p_2)(k-p_1)} \mathrm{e}^{\mathrm{i}kt} = \frac{\mathrm{i}}{2(p_2-p_1)} (\mathrm{e}^{\mathrm{i}p_2 t} - \mathrm{e}^{\mathrm{i}p_1 t}) \qquad p_2 \neq p_1, \quad t > 0.$$

We note that the result on the RHS if finite for $p_2 = p_1$ while in fact it should diverge. This suggests that there is a missing delta term $C\,\mathrm{e}^{\mathrm{i}p_2 t}\delta(p_2 - p_1)$ where C is a constant. In order to find this constant we have regularized this Fourier integral:

$$\lim_{\delta\to 0} \int_{-\infty}^{\infty} \frac{\mathrm{d}k}{2\pi} \frac{k-p_2}{(k-p_2)^2+\delta^2} \frac{k-p_1}{(k-p_1)^2+\delta^2} \mathrm{e}^{\mathrm{i}kt}$$
$$= \frac{\mathrm{i}}{2(p_2-p_1)} (\mathrm{e}^{\mathrm{i}p_2 t} - \mathrm{e}^{\mathrm{i}p_1 t}) + \frac{\pi}{2}\,\mathrm{e}^{\mathrm{i}p_2 t}\delta(p_2 - p_1) \qquad t > 0.$$

With the above we can calculate the matrix elements of the evolution operator:

$$\langle p|\mathcal{U}|p_0\rangle = \sum_k \mathrm{e}^{-\mathrm{i}E_k t} \langle p|k\rangle\langle k|p_0\rangle = \frac{1}{2\pi}\int_{-\infty}^{\infty} \mathrm{e}^{-\mathrm{i}v_{\rm E}kt}\,\langle p|k\rangle\,\langle k|p_0\rangle\,\mathrm{d}k$$
$$= \pi\delta(p-p_0)(\mathrm{e}^{\mathrm{i}v_{\rm E}pt} + \mathrm{e}^{\mathrm{i}v_{\rm E}(p+u)t}) + \frac{\mathrm{i}u}{(p-p_0)(p-p_0-u)}(\mathrm{e}^{\mathrm{i}v_{\rm E}(p_0+u)t} - \mathrm{e}^{\mathrm{i}v_{\rm E}pt}). \tag{18}$$

We have $\langle p|\mathcal{U}(t=0)|p_0\rangle = 2\pi\delta(p-p_0)$ as required. The interesting part of this expression is the second terms which is non-vanishing for $p \neq p_0$. Taking its absolute value and squaring we get after some algebra equation (13).

5. Particle in a box with a moving wall

5.1. The Schrödinger equation

We consider a particle in an infinite well. The left wall is assumed to be fixed at $x = x_0$, while the right wall at $x = X(t)$ is moving with constant velocity $\dot{X} = V_{\rm wall}$. The size of the box is $L(t) = X(t) - x_0$. Classically, the dynamics is very simple: each time that the particle hits the moving wall its energy jumps by $\delta E_{\rm cl} = 2mvV_{\rm wall}$. In the quantum mechanical case, we work in the adiabatic basis. The adiabatic energy levels and the eigenstates for a given value of L are

$$E_n = \frac{1}{2m}\left(\frac{\pi\hbar}{L}n\right)^2 \tag{19}$$

$$\Psi^{(n)}(x) = (-1)^n\sqrt{\frac{2}{L}}\sin\left(\frac{\pi n}{L}x\right) \tag{20}$$

We use the standard prescription in order to write the Schrödinger equation in the adiabatic basis. Using the notations of [22], the equation is written as

$$\frac{\mathrm{d}a_n}{\mathrm{d}t} = -\frac{\mathrm{i}}{\hbar}E_n a_n + \mathrm{i}\dot{X}\sum_m A_{nm}a_m \tag{21}$$

where

$$A_{nm} = \mathrm{i}\left\langle \Psi^{(n)} \middle| \frac{\partial}{\partial X}\Psi^{(m)} \right\rangle. \tag{22}$$

Hence, the Schrödinger equation for the problem in the adiabatic basis is [3, 6]

$$\frac{\mathrm{d}a_n}{\mathrm{d}t} = -\frac{\mathrm{i}}{\hbar}E_n a_n - \frac{V_{\mathrm{wall}}}{L}\sum_{m(\neq n)}\frac{2nm}{n^2-m^2}a_m \tag{23}$$

5.2. The generated dynamics

Let us assume that the initial preparation is $a_n(0) = \delta_{nm}$. The mean level spacing for the 1D box is $\Delta = \pi\hbar v_{\mathrm{E}}/L$. If $\delta E_{\mathrm{cl}} \ll \Delta$ one finds out, by inspection of equation (23), that the dynamics is adiabatic, meaning that $a_n(t) \sim \delta_{nm}$. On the other hand, if $\delta E_{\mathrm{cl}} \gg \Delta$, one expects to find a semiclassical transition $E \mapsto E + \delta E_{\mathrm{cl}}$.

How can we explain the $E \mapsto E + \delta E_{\mathrm{cl}}$ transition from quantum-mechanical point of view? For this purpose we can adopt the core-tail picture of [23]: the 'core' consists of the levels that are mixed non-perturbatively; the 'tail' is formed by first-order transitions from the core. Originally this picture has been applied to analyse the energy spreading in 'quantum chaos' driven systems. Here, the (non-chaotic) moving wall problem allows a much simpler application [7]. The analysis is carried out in two steps which are summarized below.

The first step in the 'core-tail' picture is to analyse the *parametric evolution* which is associated with equation (23). This means to solve equation (23) without the first term on the RHS. (This is the so-called sudden limit). Obviously, the resultant $\tilde{a}_n(t)$ is a function of $\delta X = V_{\mathrm{wall}}t$, while V_{wall} by itself makes no difference. The solution depends only on the endpoints $x(0)$ and $x(t)$. By careful inspection of equation (23), one observes that a level is mixed with the nearby level whenever the wall is displaced a distance $\lambda_{\mathrm{E}}/2$, where $\lambda_{\mathrm{E}} = 2\pi\hbar/(mv_{\mathrm{E}})$ is the de Broglie wavelength. The time scale which is associated with this effect is obviously

$$\tau_{\mathrm{qm}} = \frac{\lambda_{\mathrm{E}}/2}{V_{\mathrm{wall}}}. \tag{24}$$

The second step is to analyse the actual time evolution. This means to take into account the effect of the first term on the RHS of equation (23) and to understand how the resultant $a_n(t)$ differs from $\tilde{a}_n(t)$. One observes that the 'parametric' mixing of nearby levels modulates the transition amplitude. The modulation frequency is

$$\text{`}\omega\text{'} = \frac{2\pi}{\tau_{\mathrm{qm}}}. \tag{25}$$

Once combined with the FGR equation (25) it leads to the anticipated semiclassical result equation (5). It is not difficult to argue that the period of this semiclassical transition is

$$\tau_{\mathrm{cl}} = \frac{2L}{v_{\mathrm{E}}} \tag{26}$$

which is the time to make one round between the walls of the well. Since we are dealing with a simple 1D system this coincides with the Heisenberg time:

$$t_{\mathrm{H}} = \frac{2\pi\hbar}{\Delta} = \tau_{\mathrm{cl}}. \tag{27}$$

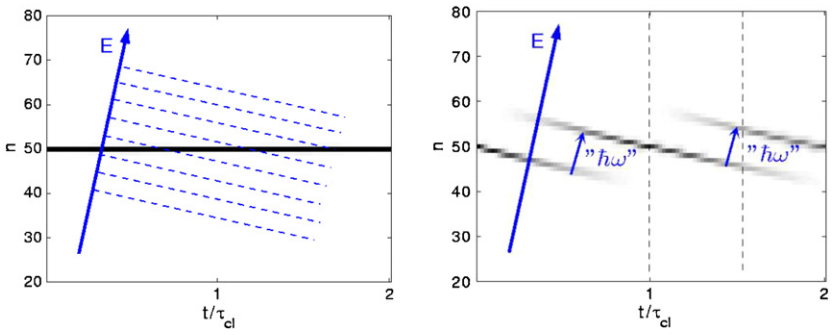

(a) (b)

Figure 8. Density plots of the probability distribution as a function of time for the moving wall problem. (*a*) Left panel: adiabatic regime. The probability stays at the same level. In order to clarify the connection with figure 4(*a*) we have added an E axis. The constant energy dashed lines are for guiding the eye. The populated adiabatic level goes up in energy which implies that the particle is steadily increasing its energy. (*b*) Right panel: semiclassical regime. The probability jumps in energy space. Note that with respect to the E axis we have the steps of figure 4(*a*). The parameters of these simulations were $L = m = \hbar = 1$ and $V_{\rm wall} = 0.1\pi$ for (*a*) and $V_{\rm wall} = 5\pi$ for (*b*). Note that for $n = 50$ the classical period is $\tau_{\rm cl} = 0.0127$. The vertical dashed lines indicate two representative times $t = \tau_{\rm cl}$ and $t = 1.5\tau_{\rm cl}$.

The ratio $\tau_{\rm cl}/\tau_{\rm qm}$ determines the number of nearby level transitions per period. Obviously, the semiclassical condition equation (7) requires this ratio to be much larger than unity. The disadvantage of the above heuristic picture is that it does not lead to a satisfactory quantitative results. Therefore, in later sections we discuss an optional route of analysis via a reduction to a tight binding model.

5.3. Numerical simulation

The solution of equation (23) becomes very simple if we make the approximation $L(t) \approx L_0$. This holds as long as the wall displacement is small. We have verified that the associated numerical error is very small. Using units such that $L_0 = m = \hbar = 1$ we define a diagonal matrix $\boldsymbol{E} = \mathrm{diag}\{\pi^2 n^2/2\}$ and a non-diagonal matrix, $\boldsymbol{W} = \{-\mathrm{i}2\alpha nm/(n^2 - m^2)\}$ with zeros along the diagonal, and where $\alpha = V_{\rm wall}/L$. The evolution matrix in the adiabatic basis is obtained by exponentiation:

$$\boldsymbol{U}(t) = \exp[-\mathrm{i}t\,(\boldsymbol{E} + \boldsymbol{W})]. \tag{28}$$

Figure 8 illustrates the time dependence of probability distribution $|a_n(t)|^2$ for a particle initially prepared at $n_0 = 50$. Figure 8(*a*) displays the solution in the adiabatic regime: the particle stays at the same level. Figure 8(*b*) displays the solution in the semiclassical regime: at each moment the particle partially stays at the same energy and partially makes classical-like transition to the next energy strip. Figure 9 highlights the energy splitting of the wavepacket during the transition.

If we want to avoid the $L(t) \approx L_0$ approximation, the price is a time-dependent $\boldsymbol{E}$ and $\boldsymbol{W}$ matrices. Then the calculation should be done in small $\mathrm{d}t$ time steps:

$$\boldsymbol{U}(t) = \prod_{t'=\mathrm{d}t}^{t} \exp[-\mathrm{i}\,\mathrm{d}t\;\boldsymbol{W}(t')]\exp[-\mathrm{i}\,\mathrm{d}t\;\boldsymbol{E}(t')]. \tag{29}$$

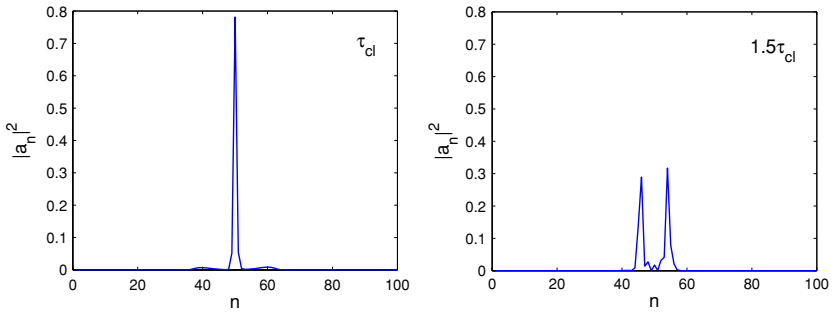

Figure 9. Plots of the probability distribution $|a_n|^2$ at the two representative times that were indicated by the vertical dashed lines in the previous figure. In the classical limit, the energy distribution consists of delta peaks instead of broadened peaks, in complete analogy with figure 7.

The state of the system is described by a truncated column vector $\boldsymbol{a} = \{a_n\}$ of length N. Optionally, it is possible to represent the state of the system in the Fourier-transformed basis. The elements A_k of the Fourier-transformed vector are labelled by $k = (2\pi/N)\tilde{n}$, where $\tilde{n}$ mod(N) is an integer. The practical implementation of equation (29) is greatly simplified if $\boldsymbol{W}_{nm}$ is a function of the difference $n - m$. In such a case $\boldsymbol{W}$ is transformed into a diagonal matrix $\tilde{\boldsymbol{W}}$. Consequently, one can use the standard fast Fourier transform (FFT) algorithm in order to propagate a given state vector. Namely,

$$\boldsymbol{a}(t) = \prod_{t'=\mathrm{d}t}^{t} \mathrm{FFT}^{-1} \exp[-\mathrm{i}\mathrm{d}t\, \tilde{\boldsymbol{W}}(t')]\mathrm{FFT} \exp[-\mathrm{i}\mathrm{d}t\, \boldsymbol{E}(t')]\boldsymbol{a}(0) \tag{30}$$

where both $\boldsymbol{E}$ and $\tilde{\boldsymbol{W}}$ are diagonal. In the moving wall problem $\boldsymbol{W}_{nm}$ is mainly proportional to $1/(n - m)$, so the FFT method is applicable if we restrict the energy range of interest. In the next section, we shall consider the EMF-driven ring problem, leading to a very similar evolution equation, where the FFT method is strictly applicable.

6. Particle in an EMF-driven ring

6.1. The Schrödinger equation

We consider a 1D ring driven by an EMF (figure 3). The EMF is induced by a time-dependent flux which is described by the vector potential

$$A(x, t) = \Phi(t)\delta(x - x_0). \tag{31}$$

This means that the electric field is

$$\mathcal{E}(x) = V_{\mathrm{EMF}}\delta(x - x_0) \tag{32}$$

where $V_{\mathrm{EMF}} = -\dot{\Phi} = \mathrm{const}$. The Hamiltonian that generates the dynamics is

$$\mathcal{H}(\Phi(t)) = \frac{1}{2m}\left(\hat{p} - \frac{e}{c}A(\hat{x}, t)\right)^2 \tag{33}$$

with periodic boundary conditions over x. The length of the ring is L.

Classically, the dynamics is very simple: each time that the particle crosses $x = x_0$ its energy jumps by $\delta E_{\mathrm{cl}} = eV_{\mathrm{EMF}}$. In the quantum mechanical case, it is convenient to work in

the so-called diabatic basis. The diabatic energy levels for a given value of Φ are

$$E_n = \frac{1}{2m}\left(\frac{2\pi\hbar}{L}\right)^2\left(n - \frac{\Phi}{\Phi_0}\right)^2 \tag{34}$$

where $\Phi_0 = 2\pi\hbar c/e$, see figure 4. The Schrödinger equation that describes the time evolution in the diabatic basis is found using the same procedure as in the case of the moving wall. We have to find A_{nm} as defined in equation (22) where now $X = \Phi$. The only extra difficulty is in finding the eigenstates $\Psi^{(n)}$ of equation (33) because $A(x)$ depends on x. The calculation becomes much simpler if we realize that they are related by a gauge transformation to the eigenstates $\tilde{\Psi}^{(n)}$ of a much simpler Hamiltonian:

$$\tilde{\mathcal{H}} = \frac{1}{2m}\left(p - \frac{e\Phi}{cL}\right)^2. \tag{35}$$

Namely,

$$\Psi^{(n)}(x) = \exp\left(\frac{\mathrm{i}e}{\hbar c}\Lambda(x)\right)\tilde{\Psi}^{(n)}(x) \tag{36}$$

$$= \exp\left(\frac{\mathrm{i}e}{\hbar c}\Lambda(x)\right) \times \frac{1}{\sqrt{L}}\exp\left(\mathrm{i}\frac{2\pi n}{L}x\right) \tag{37}$$

$$= \frac{1}{\sqrt{L}}\exp\left(\mathrm{i}\frac{2\pi}{L}\left(\frac{\Phi}{\Phi_0} + n\right)x\right) \tag{38}$$

where in the last line we set $x_0 = 0$ and the gauge function is

$$\Lambda(x) = \frac{\Phi}{L}x. \tag{39}$$

Using the above result we get

$$A_{nm} = -\frac{\mathrm{i}}{\Phi_0}\frac{1}{n-m} \tag{40}$$

and accordingly

$$\frac{\mathrm{d}a_n}{\mathrm{d}t} = -\frac{\mathrm{i}}{\hbar}E_n a_n + \frac{V_{\mathrm{EMF}}}{\Phi_0}\sum_{m(\neq n)}\frac{1}{n-m}a_m. \tag{41}$$

6.2. The generated dynamics

The dynamics of an EMF-driven ring is very similar to the dynamics in the moving wall problem. This is obvious from the phase space picture and also by the inspection of the equation for $a_n(t)$. Also the 'core-tail' heuristic picture of section 5.2 is easily adapted. The parametric scale that signifies mixing of nearby levels is now $\delta X = \Phi_0$ instead $\delta X = \lambda_{\mathrm{E}}/2$ leading to the quantum time scale

$$\tau_{\mathrm{qm}} = \frac{\Phi_0}{V_{\mathrm{EMF}}}. \tag{42}$$

The classical period is

$$\tau_{\mathrm{cl}} = \frac{L}{v_{\mathrm{E}}} \tag{43}$$

and the semiclassical condition can be written as $\tau_{\mathrm{qm}} \ll \tau_{\mathrm{cl}}$.

Since the energies are time dependent we have to use equation (29) for the calculation of the time evolutions. Furthermore, $\boldsymbol{W}$ is diagonal in the momentum representation,

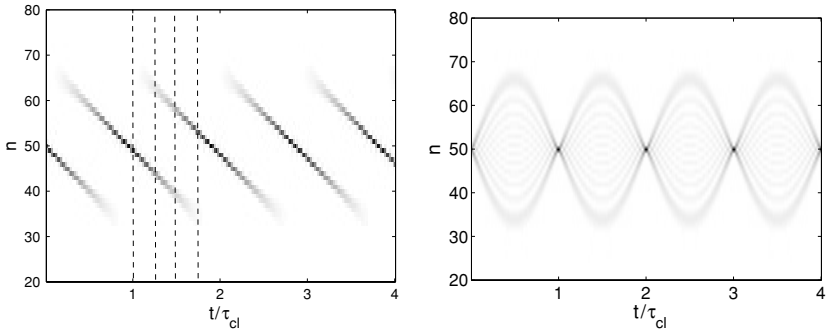

Figure 10. (*a*) Density plots of the probability distribution as a function of time for the EMF-driven ring problem. See the caption of figure 8 for presentation details. The parameters are $L = m = \hbar = e = 1$ with $V_{\mathrm{EMF}} = 588\,840$. Note that for $n = 50$ the classical period is $\tau_{\mathrm{cl}} = 0.000\,21$. This is approximately the same as solving the wavepacket dynamics for Bloch electron in electric field, equation (44), with $\alpha = 93\,717$ and $\varepsilon = 31\,416$. (*b*) Wavepacket dynamics for Bloch electron in electric field with near-neighbour hopping. The parameters are $m = \hbar = e = 1$ with $\alpha = 14\,139$ and $\varepsilon = 3141.6$.

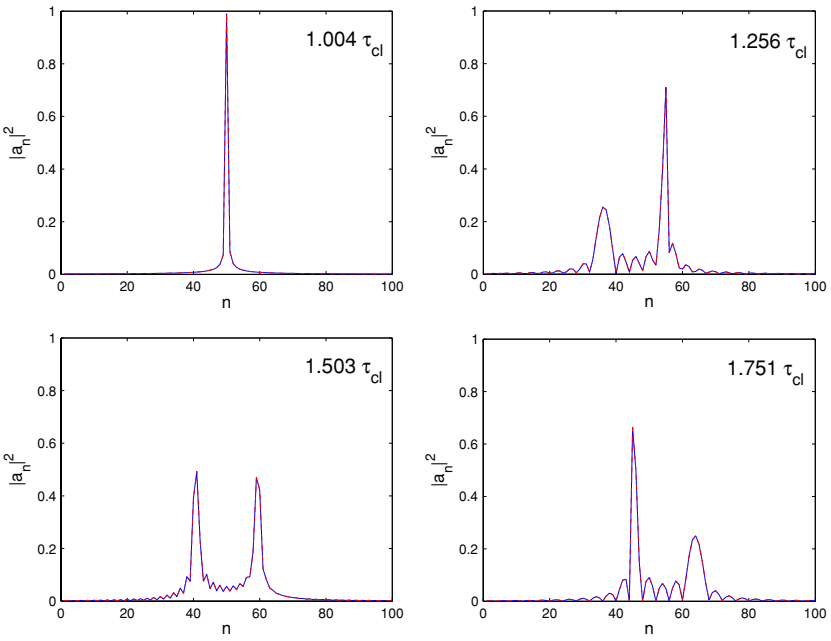

Figure 11. Plots of the probability distribution $|a_n|^2$ at representative times (as indicated). The solid lines are the solution of equation (44) for Bloch electrons, while the dotted lines are the exact numerical solutions for the EMF-driven ring, taking into account the quadratic (rather than linear) dependence of the eigenenergies on Φ.

and therefore we can use the FFT method, equation (30), with $\tilde{\boldsymbol{W}} = \mathrm{diag}\{-\alpha(k - \pi)\}$, where $k = (2\pi/N)\tilde{n}$ is defined $\mathrm{mod}(2\pi)$. The results of the simulations are presented in figures 10(*a*) and 11. We shall further discuss these results in the next sections.

7. Bloch electrons in a constant electric field (I)

If we focus our interest in small energy interval, then in both cases (moving wall, driven ring) the Schrödinger equation in the adiabatic basis is approximately the same as that of an electron in a tight binding model, where n is re-interpreted as the site index:

$$\frac{\mathrm{d}a_n}{\mathrm{d}t} = -\mathrm{i}E_n a_n + \alpha \sum_{m(\neq n)} \frac{1}{n-m} a_m \tag{44}$$

with $E_n = \varepsilon n$. We use from here on $\hbar = 1$ units. The scaled rate of the driving α is re-interpreted as the hopping amplitude between sites, while the levels spacing ε is re-interpreted as an electric field. Assuming that the electron is initially at the site n_0, we would like to find out what is the probability distribution

$$\rho_t(n) = |a_n(t)|^2. \tag{45}$$

It is obvious that the adiabatic regime $\alpha \ll \varepsilon$ corresponds to a large electric field that localizes the electron at its original site. In the other extreme ($\alpha \gg \varepsilon$), if the effect of ε could have been ignored, we would observe unbounded Bloch ballistic motion. The effect of finite ε is to turn this motion into Bloch oscillations. We shall find below that the electron performs periodic motion which we illustrate in figure 6: while the wavepaket drifts with the electric field to the right, it shrinks and disappears, and at the same time re-emerges on the left. If we run the simulation as a movie, it looks as if the motion is from left to right. Still it is bounded in space due to this 're-injection' mechanism.

First of all we solve the equation for $\varepsilon = 0$. The Hamiltonian is diagonal in the momentum basis k and therefore the general solution is

$$a_n(t) = \sum_k A_k \, \mathrm{e}^{\mathrm{i}(kn-\omega_k t)} = \int_0^{2\pi} \frac{\mathrm{d}k}{2\pi} A_k \, \mathrm{e}^{\mathrm{i}(kn-\omega_k t)}. \tag{46}$$

The dispersion relation is found by transforming the Hamiltonian to the k basis:

$$\omega_k = \mathrm{i}\alpha \sum_{n(\neq m)} \frac{\mathrm{e}^{-\mathrm{i}k(n-m)}}{n-m} = \alpha[\pi - k]. \tag{47}$$

If we place at $t = 0$ an electron at site n_0, then $a_n = \delta_{n,n_0}$, and hence $A_k = \mathrm{e}^{-\mathrm{i}kn_0}$. Then, we get

$$a_n(t) = \frac{\sin \pi\alpha t}{\pi(\alpha t + n - n_0)}. \tag{48}$$

Turning to the general case with $\varepsilon \neq 0$ we substitute $a_n(t) = c_n(t) \, \mathrm{e}^{-\mathrm{i}E_n t}$ and get the equation

$$\frac{\mathrm{d}c_n}{\mathrm{d}t} = \alpha \sum_{m(\neq n)} \frac{\mathrm{e}^{\mathrm{i}(n-m)\varepsilon t}}{n-m} c_m. \tag{49}$$

This more complicated equation is still diagonal in the k basis:

$$\frac{\mathrm{d}C_k}{\mathrm{d}t} = -\mathrm{i}\omega_k(t) C_k \tag{50}$$

where

$$\omega_k(t) = \alpha[\pi - \mathrm{mod}(k + \varepsilon t, 2\pi)] \tag{51}$$

and its solutions is

$$C_k(t) = C_k(t=0)\exp\left[-\mathrm{i}\int_0^t \omega_k(t')\,\mathrm{d}t'\right]$$
$$= \begin{cases} \exp\left(-\mathrm{i}kn_0 + \mathrm{i}\alpha\left((k-\pi)t + \dfrac{\varepsilon t^2}{2}\right)\right) & \text{for } \varepsilon > 0 \text{ and } 0 < k < \bar{k} \\ \exp\left(-\mathrm{i}kn_0 + \mathrm{i}\alpha\left((k-3\pi)t + \dfrac{\varepsilon t^2}{2} + \dfrac{2\pi(2\pi-k)}{\varepsilon}\right)\right) & \text{for } \varepsilon > 0 \text{ and } \bar{k} < k < 2\pi \\ \exp\left(-\mathrm{i}kn_0 + \mathrm{i}\alpha\left((k-\pi)t + \dfrac{\varepsilon t^2}{2} + \dfrac{2\pi k}{\epsilon}\right)\right) & \text{for } \varepsilon < 0 \text{ and } 0 < k < \bar{k} \\ \exp\left(-\mathrm{i}kn_0 + \mathrm{i}\alpha\left((k+\pi)t + \dfrac{\varepsilon t^2}{2}\right)\right) & \text{for } \varepsilon < 0 \text{ and } \bar{k} < k < 2\pi \end{cases}$$

which is valid for $0 < t < 2\pi/|\varepsilon|$ and should be continued periodically in time. We have used the notation $\bar{k} = -\varepsilon t \bmod(2\pi)$. Now we can go back to position representation:

$$c_n(t) = \int_0^{\bar{k}(t)} \frac{\mathrm{d}k}{2\pi} C_k\,\mathrm{e}^{\mathrm{i}kn} + \int_{\bar{k}(t)}^{2\pi} \frac{\mathrm{d}k}{2\pi} C_k\,\mathrm{e}^{\mathrm{i}kn}. \tag{52}$$

Taking the absolute value and squaring we get the following result for the probability distributions:

$$\rho_t(n) = \left(2\frac{\alpha}{\varepsilon}\right)^2 \frac{\sin^2\left(\frac{1}{2}\varepsilon t\left(n - n_0 + \alpha\left(t - \frac{2\pi}{|\varepsilon|}\right)\right)\right)}{(n - n_0 + \alpha t)^2\left(n - n_0 + \alpha\left(t - \frac{2\pi}{|\varepsilon|}\right)\right)^2}. \tag{53}$$

The above formula is valid for $0 < t < 2\pi/|\varepsilon|$ and it should be continued periodically in time. Figures 6 and 10(*a*) illustrate the dynamics both schematically and numerically. In the next section we further discuss the nature of this dynamics.

8. Bloch electrons in a constant electric field (II)

In order to appreciate the significance of the $\propto 1/(n-m)$ hopping we again solve the problem of Bloch electrons in a constant electric field, but this time with the 'conventional' nearest neighbour hopping:

$$\frac{\mathrm{d}a_n}{\mathrm{d}t} = -\mathrm{i}E_n a_n + \frac{\alpha}{2}[a_{n+1} - a_{n-1}] \tag{54}$$

with $E_n = \varepsilon n$. The initial preparation at $t = 0$ is $a_n = \delta_{n,n_0}$. We substitute $a_n = \mathrm{e}^{-\mathrm{i}E_n t}c_n$ and get

$$\frac{\mathrm{d}c_n}{\mathrm{d}t} = \frac{\alpha}{2}(\mathrm{e}^{-\mathrm{i}\varepsilon t}c_{n+1} - \mathrm{e}^{\mathrm{i}\varepsilon t}c_{n-1}). \tag{55}$$

This equation becomes diagonal in the k basis:

$$\frac{\mathrm{d}C_k}{\mathrm{d}t} = -\mathrm{i}\omega_k(t)C_k \tag{56}$$

where

$$\omega_k(t) = \alpha\sin(\varepsilon t + k). \tag{57}$$

Its solutions is

$$C_k(t) = C_k(t=0) \times \exp\left[-\mathrm{i}\int_0^t \omega_k(t')\,\mathrm{d}t'\right]. \tag{58}$$

Solving the above integral and making the inverse Fourier transform we obtain

$$c_n(t) = J_{n-n_0}\left(\frac{2\alpha}{\varepsilon}\sin\left(\frac{1}{2}\varepsilon t\right)\right) \tag{59}$$

where $J(\,)$ is the Bessel function of the first kind. Taking the absolute value and squaring we get the probability distribution:

$$\rho_t(n) = \left|J_{n-n_0}\left(\frac{2\alpha}{\varepsilon}\sin\left(\frac{1}{2}\varepsilon t\right)\right)\right|^2. \tag{60}$$

Figure 10(*b*) illustrates the dynamics. As in the previous problems we can distinguish between two time scales. One is related to the diagonal part of the Hamiltonian, and the other one to the hopping term. Keeping the same notation as in previous sections these are

$$\tau_{\rm cl} = 2\pi/\varepsilon \tag{61}$$

$$\tau_{\rm qm} = 1/\alpha. \tag{62}$$

The nature of the dynamics in the case of $\propto 1/(n-m)$ hopping and in the case of near-neighbour hopping is quite different, as it can be appreciated by comparing figures 10(*a*) and (*b*). This is related to the additional symmetries in the latter case. In order to explain this point let us use the notation $\boldsymbol{U}(\alpha, \varepsilon)$ that emphasizes that the evolution depends on two parameters, the first one is associated with the kinetic term $\boldsymbol{W} = w(\hat{p})$ and the other one with the potential term $\boldsymbol{E} = \epsilon(\hat{x})$. For clarity we use $\hat{x}$ for the position coordinate and $\hat{p}$ for the quasi-momentum. In both cases, we have the anti-unitary symmetry $(x, p) \mapsto (x, -p)$ that maps $\boldsymbol{E}$ to $\boldsymbol{E}$ and $\boldsymbol{W}$ to $-\boldsymbol{W}$. Consequently, $\boldsymbol{U}(\alpha; \varepsilon)$ is mapped to $\boldsymbol{U}(\alpha; -\varepsilon)$. This implies that the spreading does not depend on the direction of the electric field. This is a peculiarity of tight binding models. The conventional time reversal symmetry, for which the kinetic term $\boldsymbol{W}$ is left invariant, is $(x, p) \mapsto (x, \pi - p)$. This symmetry characterizes the near-neighbour hopping, but not the $\propto 1/(n-m)$ hopping. This symmetry implies that the spreading looks the same if we reverse the signs of both α and ε, which is like reversing the time. If we combine the two symmetries we deduce that the dynamics, in the case of the near-neighbour hopping, should be indifferent to the sign of α. Note that the combined symmetry that leads to this conclusion is the unitary mapping $(x, p) \mapsto (x, p + \pi)$. Thus, in both cases ($\propto 1/(n-m)$ hopping and near-neighbour hopping) we have generalized Bloch oscillations, but in the former case they are unidirectional (figure 6), while in the latter case they are bi-directional.

9. Discussion

Within Linear response theory (LRT) the energy absorption of a quantum system is determined by the correlation function of the perturbation term. In general, one can argue that there is a very good QCC for the correlation functions, and hence one expects *restricted* QCC in the energy absorption process. The persistence of *restricted* QCC in the $t \to \infty$ limit requires the additional assumption of having a coarse-grained Markovian-like behaviour for long times. Depending on the context one should further assume that the environment supplies both weak decoherence effect that makes the break time t^* irrelevant and a weak relaxation effect so as to achieve a steady state. Then it is possible to use the same argumentation as in the derivation of the central limit theorem in order to argue that all the higher moments become Gaussian like.

Thus, the common perception is that the leading result for the response of a driven system should be the same classically and quantum mechanically. For example, such is the case if one

calculates the conductance of a diffusive ring [24]: the leading order result is just the Drude expressions, and on top there are weak localization corrections.

The above reasoning illuminates that the long time response is based on the short time analysis. Moreover, one realizes that the second moment of the evolving energy distribution has a special significance. Still, all the above observations are within a very restrictive framework of assumptions. In practice, it is of much interest to explore the limitations of LRT and to obtain a more general theory for response.

The theory for the response of closed isolated driven quantized chaotic mesoscopic systems is far from being trivial, even if the interactions between the particles are neglected. In the case of a generic quantized chaotic systems two energy scales are involved: the mean level spacing $\Delta \propto \hbar^d$, where $d = 2, 3$ is the dimensionality of the system, and the semiclassical energy scale $\hbar/\tau_{\rm cl}$. It is implied (see the mini-review of [25]) that there are generically three regimes depending on the rate $\dot{X}$ of the driving:

- The adiabatic (Landau–Zener) regime.
- The Fermi-golden-rule (FGR, Kubo) regime.
- The semiclassical (non-perturbative) regime.

Most of the literature in mesoscopic physics is dedicated to the study of the dynamics in either the adiabatic or the FGR regimes. The existence of a non-perturbative regime [25, 26] is not yet fully acknowledged, though it has been established numerically in the RMT context [27].

Driven one-dimensional systems are non-generic because typically the semiclassical energy scale coincides with the mean level spacing. In other words, the Heisenberg time $t_H = 2\pi\hbar/\Delta$ is the same as the classical time $\tau_{\rm cl}$ rather than being much larger. Indeed, we have seen that in the 'moving wall' problem we have just two regimes: the adiabatic regime and the semiclassical regime.

The EMF-driven ring is a prototype problem in mesoscopic physics. It is richer than the 'moving wall' problem because a small scatterer introduces a very small energy scale, the level splitting, and hence we have three regimes rather than two: adiabatic, diabatic and semiclassical.

The semiclassical regime in the study of EMF-driven rings has not been explored so far. One important observation is that contrary to LRT the gauge of the vector potential *does matter*. Most of past studies assume that the vector potential is $A(x,t) = \Phi(t)/L$. It is true that in LRT the same result for the conductance is obtained with $\tilde{A}(x,t) = \Phi(t)\delta(x - x_0)$. If we try to go from $\tilde{A}(x,t)$ to $A(x,t)$ using a gauge transformation, the 'price' is a modified $V(x)$ that features a linear ramp with a step-like drop at $x = x_0$. This modification of $V(x)$ can be neglected only in the LRT regime. The semiclassical condition of equation (6) is just that opposite of this LRT requirement.

The semiclassical dynamics implies diffractive energy spreading. The mixing of levels in the small energy scales induces jumps in energy space. The realization that this diffractive energy spreading can be re-interpreted using a tight binding Bloch model follows in spirit the celebrated reduction [1] of dynamical localization in periodically kicked systems to a tight binding Anderson problem. An interesting feature is the hopping that goes like $\propto 1/(n - m)$. This hopping leads to a unidirectional rather than bi-directional Bloch oscillations, as implied by the semiclassical reasoning.

Acknowledgments

We thank Tsachy Holovinger for preparing the first version of the 'moving wall' simulation. AS thanks V Goland for fruitful discussions that helped solving the 'Bloch electrons' problem.

The research was supported by the Israel Science Foundation (grant no 11/02) and by a grant from the DIP, the Deutsch–Israelische Projektkooperation.

Appendix. The robustness of restricted QCC

The simplest way to illuminate the robustness of the second moment is by adopting a heuristic phase space picture language. Given two operators $\hat{A} = A(\hat{x}, \hat{p})$ and $\hat{B} = B(\hat{x}, \hat{p})$, with Wigner–Weyl representation $A_{\rm WW}(x, p)$ and $B_{\rm WW}(x, p)$ we have the exact identity

$$\text{trace}(\hat{A}\hat{B}) = \int \frac{\mathrm{d}x\,\mathrm{d}p}{2\pi} A_{\rm WW}(x, p) B_{\rm WW}(x, p). \tag{A.1}$$

If we can justify the replacement of $A_{\rm WW}(x, p)$ by $A(x, p)$ and $B_{\rm WW}(x, p)$ by $B(x, p)$ then we get QCC. The rule of the thumb is that in order to justify such an approximation the phase space contours of $A(x, p)$ and $B(x, p)$ should be significantly different. Otherwise the transverse structure of the Wigner–Weyl functions should be taken into account. This reasoning can be regarded as a phase space version of the stationary phase approximation.

Let $\hat{A} = [H(\hat{x}, \hat{p})]^r$ be the rth power of the Hamiltonian $\mathcal{H} = H(\hat{x}, \hat{p})$ and let be $\hat{B} = \rho(H_0(\hat{x}, \hat{p}))$ a stationary preparation with the Hamiltonian $\mathcal{H}_0 = H_0(\hat{x}, \hat{p})$. In such a case $\text{trace}(\hat{A}\hat{B})$ is the rth moment $\langle \mathcal{H}^r \rangle$ of the energy. If $H = H_0 + \lambda V$, and λ is not large enough, then we do not have detailed QCC. This is discussed thoroughly in [28]. But at the same time, irrespective of λ, restricted QCC is robust. The reason is that for the first two moments we have the identities

$$\langle \mathcal{H} \rangle = \langle \mathcal{H}_0 \rangle + \langle \hat{V} \rangle \tag{A.2}$$

$$\langle \mathcal{H}^2 \rangle = \langle \mathcal{H}_0^2 \rangle + 2\langle \mathcal{H}_0 \rangle \langle \hat{V} \rangle + \langle \hat{V}^2 \rangle. \tag{A.3}$$

Thus the calculation of $\text{trace}(\hat{A}\hat{B})$ with $\hat{A} = [H(\hat{x}, \hat{p})]^r$ reduces to the calculation of $\text{trace}(\hat{A}\hat{B})$ with $\hat{A} = [V(\hat{x}, \hat{p})]^r$. We assume that V and H are not related in any special way. It follows that we have robust QCC for all the moments of V, and consequently also for the first two moments of H, irrespective of λ.

In order to generalize the above reasoning to time-dependent Hamiltonians, it is convenient to adopt the Heisenberg picture. Given that the system is prepared in a stationary state at $t = 0$, one can prove that

$$\langle \mathcal{H}(t)^2 \rangle_0 - \langle \mathcal{H}(0)^2 \rangle_0 = \langle (\mathcal{H}(t) - \mathcal{H}(0))^2 \rangle_0 \tag{A.4}$$

where $\mathcal{H}(t)$ is the Hamiltonian $\mathcal{H}(X(t))$ in the *Heisenberg picture*. Such relation cannot be generalized to higher moments because of lack of commutativity. Using

$$\frac{\mathrm{d}\mathcal{H}}{\mathrm{d}t} = \frac{\partial \mathcal{H}}{\partial t} = \dot{X}\hat{V}(t) \tag{A.5}$$

where $V \equiv \partial\mathcal{H}/\partial X$, we can express $\langle (\mathcal{H}(t) - \mathcal{H}(0))^r \rangle_0$ as an integral over the correlation functions of the perturbation $V(t)$. The QCC for these correlation functions is robust, and hence the QCC for the second moment is also robust.

References

[1] Fishman S, Grempel D R and Prange R E 1982 *Phys. Rev. Lett.* **49** 509
Grempel D R, Prange R E and Fishman S 1984 *Phys. Rev.* A **29** 1639
[2] Cohen D and Kottos T 2003 *J. Phys. A: Math. Gen.* **36** 10151
[3] Doescher S W and Rice M H 1969 *Am. J. Phys.* **37** 1246

[4] Makovski A J and Demebinski S T 1986 *Phys. Rev. Lett.* **56** 290
[5] Jos J V and Cordery R 1986 *Phys. Rev. Lett.* **56** 290293
[6] Cohen D, Barnett A and Heller E J 2001 *Phys. Rev.* E **63** 46207
[7] Cohen D 2002 *Phys. Rev.* E **65** 026218 (section VIII)
[8] Wannier G H 1960 *Phys. Rev.* **117** 432
[9] Zak J 1968 *Phys. Rev. Lett.* **20** 1477
[10] Zak J 1968 *Phys. Rev.* **168** 686
[11] Rabinovitch A and Zak J 1972 *Phys. Lett.* A **40** 189
[12] Rabinovitch A 1977 *Phys. Lett.* A **59** 475
[13] Emin D and Hart C F 1987 *Phys. Rev.* B **36** 7353
[14] Hart C F 1988 *Phys. Rev.* B **38** 2158
[15] Hart C F and Emin D 1988 *Phys. Rev.* B **37** 6100
[16] Mendez E E, Agullo-Rueda F and Hong J M 1988 *Phys. Rev. Lett.* **60** 2426
[17] Zak J 1991 *Phys. Rev.* B **43** 4519
[18] Leo J and MacKinnon A 1991 *Phys. Rev.* B **43** 5166
[19] Zak J 1996 *J. Phys.: Condens. Matter* **8** 8265
[20] Gefen Y and Thouless D J 1987 *Phys. Rev. Lett.* **59** 1752
[21] Wilkinson M 1988 *J. Phys. A: Math. Gen.* **21** 4021
[22] Cohen D 2003 *Phys. Rev.* B **68** 155303
[23] Cohen D 2000 *Ann. Phys., NY* **283** 175
[24] Kamenev A and Gefen Y 1995 *Int. J. Mod. Phys.* B **9** 751
[25] Cohen D 2002 *Dynamics of Dissipation: Proc. 38th Karpacz Winter School of Theoretical Physics* ed P Garbaczewski and R Olkiewicz (Berlin: Springer) (*Preprint* quant-ph/0403061)
[26] Cohen D 1999 *Phys. Rev. Lett.* **82** 4951
[27] Cohen D and Kottos T 2000 *Phys. Rev. Lett.* **85** 4839
[28] Cohen D and Kottos T 2001 *Phys. Rev.* E **63** 36203

3.2 The mesoscopic conductance of disordered rings, its random matrix theory, and the generalized variable range hopping picture

The content of this section is available as

- a journal article: A. Stotland, R. Budoyo, T. Peer, T. Kottos and D. Cohen, J. Phys. A **41**, 262001 (2008) (Fast Track Communication)

  This paper was selected for the Editor's Choice Fast Track Communication.

- a preprint: arXiv:0712.0439

See Appendix C for the explanation of the numerical analysis used in this work.

IOP FTC
IOP PUBLISHING JOURNAL OF PHYSICS A: MATHEMATICAL AND THEORETICAL

J. Phys. A: Math. Theor. **41** (2008) 262001 (11pp) doi:10.1088/1751-8113/41/26/262001

FAST TRACK COMMUNICATION

The mesoscopic conductance of disordered rings, its random matrix theory and the generalized variable range hopping picture

Alexander Stotland[1], Rangga Budoyo[2], Tal Peer[1], Tsampikos Kottos[2] and Doron Cohen[1]

[1] Department of Physics, Ben-Gurion University, Beer-Sheva 84005, Israel
[2] Department of Physics, Wesleyan University, Middletown, CT 06459, USA

Received 9 April 2008, in final form 14 May 2008
Published 4 June 2008
Online at stacks.iop.org/JPhysA/41/262001

Abstract
The calculation of the conductance of disordered rings requires a theory that goes beyond the Kubo–Drude formulation. Assuming 'mesoscopic' circumstances the analysis of the electro-driven transitions shows similarities with a percolation problem in energy space. We argue that the texture and the sparsity of the perturbation matrix dictate the value of the conductance, and study its dependence on the disorder strength, ranging from the ballistic to the Anderson localization regime. An improved sparse random matrix model is introduced to capture the essential ingredients of the problem, and leads to a generalized variable range hopping picture.

PACS numbers: 71.23.An, 02.10.Yn, 05.45.Mt, 73.23.−b

(Some figures in this article are in colour only in the electronic version)

1. Introduction

Closed mesoscopic rings provide the ideal paradigm for testing the manifestation of quantum mechanical effects in the mesoscopic realm [1–4]. First measurements of the conductance of closed rings have been reported more than a decade ago [5], while more recently there is a renewed experimental interest motivated by high-precision measurements of individual rings [6, 7]. In a typical experiment, a collection of mesoscopic rings is driven by a time-dependent magnetic flux which creates an electro-motive-force (EMF). In what follows, we assume low-frequency dc *noisy* driving ($\omega \sim 0$) with power spectrum

$$\tilde{F}(\omega) = \varepsilon^2 \frac{1}{2\omega_c} \exp\left(-\frac{|\omega|}{\omega_c}\right) \equiv \varepsilon^2 \delta_\Gamma(\omega), \tag{1}$$

where ε is the rms value of the voltage and the cutoff frequency ω_c is small compared with any relevant semiclassical energy scale, but larger compared with the mean level spacing Δ.[3] Optionally, if we had assumed an interaction with a thermal bath, the role of ω_c would have been played by the level broadening or by the temperature [8]. In such a setup one expects the rate of energy absorption to be given by Joule's law $G\varepsilon^2$, where the coefficient G is defined as the 'conductance'.[4]

As in the linear response theory (LRT) analysis, we assume that the coherence time is much longer compared with the ballistic time, but smaller compared with the Heisenberg time $(1/\Delta)$. But our interest is in what we call *mesoscopic circumstances*. Namely, *we assume that the environmental-induced relaxation is a slow process, when compared with the EMF-driven transitions* (this is opposite to the LRT limit $\varepsilon \to 0$). Accordingly, we have to work within the framework of *semi-linear response theory* (SLRT) [9–11]:[5] this theory (see section 5) goes beyond the conventional framework of the Kubo formalism.

For diffusive rings the Kubo formalism leads to the Drude formula for G. A major challenge in past studies was to calculate the weak localization corrections [3] to the Drude result, taking into account the level statistics and the type of occupation [4]. These corrections are of order Δ/ω_c and accordingly do not challenge the leading-order Kubo–Drude result. It is just natural to ask what happens to the Drude result if the disorder becomes weak (ballistic case) or strong (Anderson localization case). In the latter case, there are two conflicting results for the noise ω_c dependence of G, both following Mott's work [12]. The question is whether to regard the noise as 'low-frequency driving' or as 'temperature'. On the one hand, on the basis of the Kubo formula, one expects a crossover from $G \sim \exp(-L/\ell_\infty)$ (where ℓ_∞ is the localization length), to the noise-dependent result $G \sim \omega_c^2|\log(\omega_c)|^{d+1}$, where $d = 1$ for quasi-one-dimensional (1D) ring. On the other hand, on the basis of the variable range hoping (VRH) picture, one expects $G \sim \exp(-(\omega_0/\omega_c)^{1/d+1})$, where ω_0 is a constant. Eventually [8] it has been realized that both the ballistic, the diffusive and the strong localization regimes should be handled on equal footing using SLRT. The Kubo theory applies in the LRT limit $\varepsilon \to 0$, while in mesoscopic circumstances SLRT leads to a resistor network [13] 'hopping' picture in energy space that generalizes the real space hopping picture of [14, 15].

2. Outline

In this communication we analyze, within the framework of SLRT, the dependence of the mesoscopic conductance of a quasi-1D ring on the strength of the disorder. We explain that for both weak and strong disorder the non-ergodicity of the quantum eigenstates implies having *texture* and *sparsity* in the perturbation matrix. Such features imply that the rate of energy absorption is suppressed enormously because the system cannot execute *connected sequences of transitions*. The implied deviations from the Kubo–Drude result are demonstrated numerically in figure 1.

We introduce a novel random matrix theory (RMT) model, with either *log-box* or *log-normal* distributed elements, that captures the essential features of the perturbation matrix. A generalized resistor network analysis for the EMF-driven transitions in energy space leads to

[3] Hence there is no issue of quantum recurrences which would arise for a strictly linear or periodic driving. From here on we use units such that $\hbar = 1$.

[4] The terminology of this paper, and in particular our notion of 'conductance' are the same as in the theoretical review [4] and in the experimental work [5].

[5] The term 'semi-linear response' to describe the outcome of the theory of [9] has been coined in a subsequent work [11], where it has been applied to the analysis of the absorption of low-frequency radiation by metallic grains.

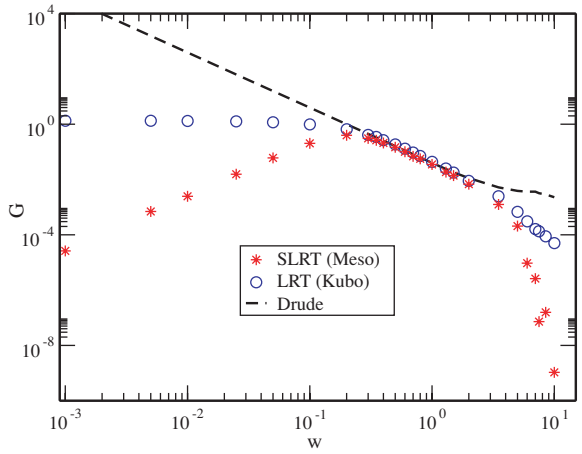

Figure 1. Plot of the scaled conductance $\tilde{G}$ versus W using either the LRT (Kubo) or the SLRT (mesoscopic) recipe, and compared with the Drude-formula-based estimate. The calculation has been carried out for a tight binding Anderson model of size 500×10, transverse hopping amplitude $c = 0.9$ and low driving frequency $\omega_c/\Delta = 7$. The SLRT result departs from the LRT result for both weak disorder (ballistic regime) and strong disorder (strong localization regime).

a generalized VRH picture in the strong disorder limit, while handling on equal footing the opposing limit of very weak disorder.

In the first part of this communication (sections 1–5) we provide the essential details on the model and on the LRT/SLRT calculation, leading to the numerical results in section 6. The second part of this communication leads to the RMT modeling and to the implied generalized VRH picture.

3. Modeling

We consider the disorder quasi-1D ring geometry. The amount of disorder is traditionally characterized by the mean free path ℓ. The semiclassical theory of the conductance leads to the Drude formula[6]

$$G_{\text{Drude}} = \frac{e^2}{2\pi\hbar}\mathcal{M}\frac{\ell}{L}, \tag{2}$$

where L is the length of the ring and $\mathcal{M}$ is the number of open modes (proportional to its cross section). For the numerical calculations we have used the Anderson tight binding model, where the lattice is of size $L \times M$ with $M \ll L$. The longitudinal hopping amplitude per unit time is $c_\parallel = 1$, while in the transverse direction it is numerically convenient to have $c_\perp < 1$, so as to have in the middle of the band a finite energy window with $\mathcal{M} = M$ open modes.

The random on-site potential in the Anderson tight binding model is given by a box distribution of width W. The density of states at the Fermi energy, and the mean free path in

[6] Optionally if the ring is characterized by its transmission g, then ℓ/L is replaced by $g/(1-g)$. See [9, 10] for details. As could be expected the result is in agreement with the Landauer theory [16] provided $g \ll 1$. Indeed, the Landauer formula can be obtained from the Kubo formula, using a semiclassical evaluation of the velocity–velocity correlation function, whenever the contribution of trajectories with a non-zero winding number can be neglected.

the Born approximation, are written as

$$\varrho_{\rm F} \equiv \mathcal{M}\frac{L}{\pi\hbar v_{\rm F}} \equiv \frac{1}{\Delta}; \qquad \ell \sim \left(\frac{v_{\rm F}}{W}\right)^2. \tag{3}$$

The implied definition of $v_{\rm F}$ leads to its identification as the Fermi velocity in the absence of disorder (disregarding a prefactor of order unity). The Anderson localization length for $L = \infty$ sample would be $\ell_\infty = \mathcal{M}\ell$. Accordingly, for a finite sample, depending on the strength of the disorder, one distinguishes between the ballistic regime ($L \ll \ell$), the diffusive regime ($\ell \ll L \ll \ell_\infty$) and the Anderson strong localization regime ($L \gg \ell_\infty$).

4. The LRT calculation

The fluctuation–dissipation version of the Kubo formula expresses the conductance as an integral over the velocity–velocity correlation function:

$$G_{\rm LRT} = \varrho_{\rm F}\left(\frac{e}{L}\right)^2 \times \frac{1}{2}\int_{-\infty}^{\infty} \langle v(t)v(0)\rangle \, {\rm d}t, \tag{4}$$

where v is the velocity in the longitudinal direction. The Drude formula in equation (2) is based on the simplest classical approximation:

$$\langle v(t)v(0)\rangle \approx v_{\rm F}^2 \exp\left[-2\left(\frac{v_{\rm F}}{\ell}\right)|t|\right]. \tag{5}$$

Our objective is to find the conductance of the closed ring in circumstances such that the motion inside the ring is coherent (quantum interferences are not ignored). The calculation involves the quantum version of $\langle v(t)v(0)\rangle$ which can be obtained as the Fourier transform of the spectral function

$$\tilde{C}(\omega) = \frac{1}{N}\sum_{nm} |v_{nm}|^2 2\pi\,\delta_\Gamma(\omega - (E_m - E_n)), \tag{6}$$

where N is the size of the energy window of interest. This spectral function can be re-interpreted as describing the band profile of the perturbation matrix $\{v_{nm}\}$. In particular, the calculation of $\tilde{C}(0) \equiv 2\pi\varrho_{\rm F}\langle\langle |v_{nm}|^2\rangle\rangle_{\rm LRT}$ involves a simple *algebraic* average over the near-diagonal matrix elements at the energy range of interest. Using this notation, the formula for the Kubo conductance takes the form

$$G_{\rm LRT} = \pi\left(\frac{e}{L}\right)^2 \varrho_{\rm F}^2\langle\langle |v_{nm}|^2\rangle\rangle_{\rm LRT}. \tag{7}$$

The $\mathcal{O}(\Delta/\omega_c)$ weak localization corrections to the Drude formula in equation (2) are determined by the interplay of the broadened delta function in equation (6) with the level statistics. See [4]. Equivalently, we may say that the *algebraic* average $\langle\langle\cdots\rangle\rangle_{\rm LRT}$ has some weak sensitivity to the off-diagonal range of the averaging.

5. The SLRT calculation

As in the standard derivation of the Kubo formula, also within the framework of SLRT, the leading mechanism for absorption is assumed to be Fermi-golden-rule (FGR) transitions. These are proportional to the squared matrix elements $|v_{nm}|^2$ of the velocity operator. Still, the theory of [9] does not lead to the Kubo formula. This is because the rate of absorption depends crucially on the possibility to make *connected* sequences of transitions. It is implied that both the texture and the sparsity of the $|v_{nm}|^2$ matrix play a major role in the calculation of

G. SLRT leads to a formula for G that can be cast into the form of equation (7), provided the definition of $\langle\langle \ldots \rangle\rangle$ is modified. Following [11, 10] we regard the energy levels as the nodes of a resistor network. We define

$$\mathsf{g}_{nm} = 2\varrho_{\mathrm{F}}^{-3} \frac{|v_{nm}|^2}{(E_n - E_m)^2} \delta_\Gamma(E_m - E_n). \tag{8}$$

Then it is argued that $\langle\langle |v_{nm}|^2 \rangle\rangle_{\mathrm{SLRT}}$ is the inverse resistivity of the network. It is a simple exercise to verify that if all the matrix elements are the same, say $|v_{nm}|^2 = \sigma^2$, then $\langle\langle |v_{nm}|^2 \rangle\rangle_{\mathrm{SLRT}} = \sigma^2$ too. But if the matrix has texture or sparsity then $\langle\langle |v_{nm}|^2 \rangle\rangle_{\mathrm{SLRT}} \ll \langle\langle |v_{nm}|^2 \rangle\rangle_{\mathrm{LRT}}$.

6. Numerical results

It is natural to define the scaled conductance of the ring as follows:

$$\tilde{G} = \frac{G}{(e^2/2\pi\hbar)\mathcal{M}} = 2\mathcal{M} \times \frac{1}{v_{\mathrm{F}}^2} \langle\langle |v_{nm}|^2 \rangle\rangle. \tag{9}$$

This would be the average transmission per channel, if we had considered the open (Landauer) geometry. But for a closed (ring) geometry, $\tilde{G}$ is determined by the appropriate 'averaging' procedure $\langle\langle \ldots \rangle\rangle_{\mathrm{LRT/SLRT}}$. In the SLRT case, the 'averaging' is in fact a resistor network calculation. If all the near-diagonal elements are comparable in size, then SLRT will give essentially the same result as LRT. More generally, $\langle\langle |v_{nm}|^2 \rangle\rangle_{\mathrm{SLRT}}$ is typically bounded from above by the *algebraic* average, and bounded from below by the *harmonic* average. The latter is defined as $\langle\langle X \rangle\rangle_{\mathrm{h}} = [\langle 1/X \rangle]^{-1}$, and reflects the 'addition of resistors in series'. If the distribution is not too stretched then the *median*, or the *geometric* average or the *mixed* average of [9] might provide a good approximation. But, in general, a proper resistor network calculation is required. The resistor network calculation is sensitive to the texture and the sparsity of the perturbation matrix. By *texture* we mean that the gray-level image of the v_{nm} matrix appears to be scarred by structures, rather than being homogeneous. Looking on the images of the v_{nm} matrices for various values of W, one realizes that both texture and sparsity emerge in the ballistic case, while in the strong localization case one observes only sparsity. We further expand on the quantitative characterization below.

In figure 1 we plot the Drude conductance $\tilde{G}_{\mathrm{Drude}}$ of equation (2), and the Kubo conductance $\tilde{G}_{\mathrm{LRT}}$, together with the mesoscopic conductance $\tilde{G}_{\mathrm{SLRT}}$ versus W. We see that outside of the diffusive regime, for both weak and strong disorder, the SLRT result is extremely small compared with the LRT expectation. This generic behavior is related to the sparsity and the texture of the perturbation matrix, which is implied by the statistical properties of the eigenstates. The statistical analysis is carried out in figure 2, while the RMT perspective is tested in figure 3. The content of figures 2 and 3 is further discussed in the following sections.

In order to determine numerically whether the *texture* is of any importance we simply permute randomly the elements of the v_{nm} matrix along the diagonals, and re-calculate $\tilde{G}$ (see the 'untextured' data points in figure 3). Obviously, by definition, $\tilde{G}_{\mathrm{LRT}}$ is not affected by this numerical maneuver. But it turns out that $\tilde{G}_{\mathrm{SLRT}}$ is somewhat affected by this procedure in the ballistic regime, but still the qualitative results come out the same. Accordingly, we deduce that the main issue is the *sparsity*, and concentrate below on the RMT modeling of this feature.

In the remainder of this paper, we pave an analytical approach to the calculation of the conductance, which will allow us to shed some light on these numerical findings. First, we discuss the familiar diffusive regime where both LRT and SLRT should be in agreement with

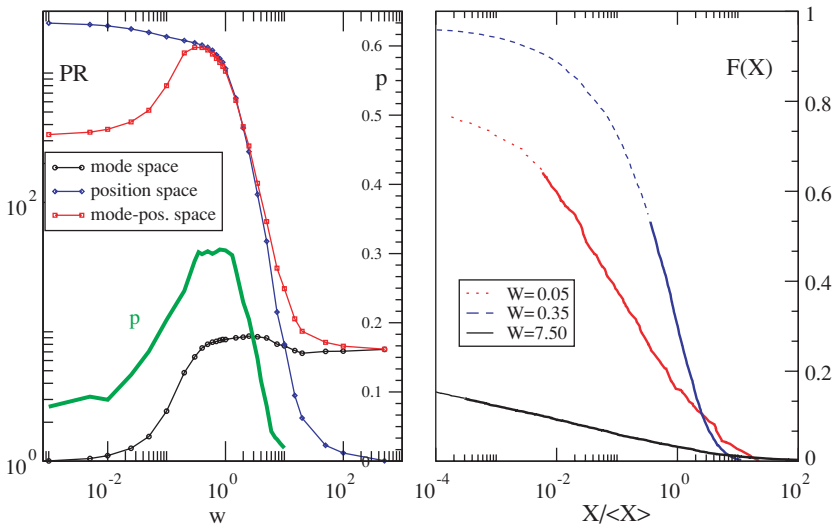

Figure 2. The ergodicity of the eigenstates is characterized by the participation ratio $\mathrm{PR} \equiv [\sum \rho^2]^{-1}$, which is calculated (left panel) in various representations: in position space $\rho_{r_x,r_y} = |\langle r_x, r_y|\Psi\rangle|^2$, in position-mode space $\rho_{r_x,k_y} = |\langle r_x, k_y|\Psi\rangle|^2$, and in mode space $\rho_{k_y} = \sum_{r_x} |\langle r_x, k_y|\Psi\rangle|^2$, where $k_y = [\pi/(\mathcal{M}+1)] \times$ integer. The cumulative distribution $F(X)$ of the in-band matrix elements (right panel) exhibits a log-box distribution in the strong localization regime. Points in the interval $X > \langle\langle X\rangle\rangle_{\mathrm{SLRT}}$, corresponding to non-negligible values, are connected by a thicker line. The extracted sparsity measure (left panel) is $p \equiv F(\langle X\rangle)$.

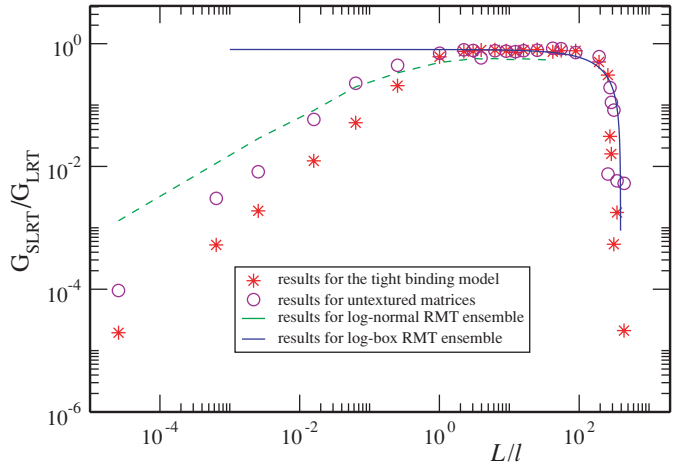

Figure 3. The ratio $G_{\mathrm{SLRT}}/G_{\mathrm{LRT}}$ versus the inverse of $\tilde{G}_{\mathrm{Drude}} = \ell/L$ based on the numerics of figure 1, and compared with artificial RMT modeling using 'sparse' matrices formed of log-normal or log-box distributed elements. We also compare the actual results with 'untextured' results as explained in the text. For weak disorder the agreement is only qualitative indicating that the texture becomes important.

the Drude approximation (the latter should become a good approximation for a big sample). Then we discuss the departure of SLRT from LRT outside of the diffusive regime, which reflects the sparsity of the v_{nm} matrix due to the non-ergodicity of the eigenfunctions.

7. The random wave conjecture

In the diffusive regime, Mott has argued that the eigenstates of the Hamiltonian matrix are ergodic in position space, and look like random waves. Using this assumption one can reconstruct the Drude result. Following Mott[7] we assume that ℓ is the correlation scale of any typical eigenfunction $\Psi(x, y)$. The basic assumption of Mott is that the eigenstates are locally similar to free waves. The total volume L^d is divided into domains of size ℓ^d. Hence we have $(L/\ell)^d$ such domains. Given a domain, the condition to have non-vanishing overlap upon integration is $|\vec{q}_n - \vec{q}_m|\ell < 2\pi$, where $\vec{q}$ is the local wave number within this domain. The probability that $\vec{q}_n$ would coincide with $\vec{q}_m$ is $1/(k_E\ell)^{d-1}$. The contributions of the non-zero overlaps add with random signs hence

$$|v_{nm}| = \left[\frac{1}{(k_E\ell)^{d-1}} \times \left(\frac{L}{\ell}\right)^d\right]^{1/2} \times (\overline{\Psi^2}\ell^d)v_F, \tag{10}$$

where the assuming ergodicity $\overline{\Psi^2} \approx 1/L^d$. From here we get $\tilde{G} \sim \ell/L$, leading to the Drude result. We discuss the limited validity of this result in the following section.

8. The non-ergodicity issue

It is clear that Mott's derivation of the Drude formula on the basis of LRT and the random wave conjecture becomes non-applicable if the eigenfunctions are non-ergodic. This is indeed the case for both weak and strong disorder: a typical eigenfunction does not fill the whole accessible phase space. In the ballistic regime a typical eigenfunction is not ergodic over the open modes in momentum space, while in the strong localization regime it is not ergodic over the ring in real space [17]. Figure 2 demonstrates this point by plotting the participation ratio as a function of the disorder strength. Lack of quantum ergodicity for either weak or strong disorder implies that the perturbation matrix v_{nm} is very textured and/or sparse. For the following analysis, a precise mathematical definition of sparsity is required. In the following sections we shall provide such a definition, but for this purpose we have to shed some light on the size distribution of the matrix elements.

In the strong disorder regime, the observed 'sparsity' is very simple for understanding: eigenstates that are close in energy are typically distant in real space, and therefore have very small overlap. The 'big' matrix elements are contributed by eigenstates that dwell in the same region in real space, and hence sparse in energy space. What we are going to call in the following sections 'sparsity', is merely a reflection of the associated log-box size distribution of the matrix elements (see figure 2(*b*)). The log-box distribution is deduced by a straightforward extension of the above argument. A generic eigenfunction in the localized regime has an exponential shape $\psi(r) \sim \exp(-|r - r_0|/\ell_\infty)$, which is characterized by the localization length ℓ_∞. Consequently, a typical matrix element of $\{|v_{nm}|^2\}$ has the magnitude

$$X \sim \frac{1}{\mathcal{M}^2} v_F^2 \exp\left(-\frac{x}{\ell_\infty}\right), \tag{11}$$

where $x \in [0, L/2]$ has a uniform distribution. The prefactor is most easily derived from the requirement of having $\langle X\rangle \approx (\ell/\mathcal{M}L)v_F^2$ in agreement with the semiclassical result. The latter is deduced from the Fourier transform of the velocity–velocity correlation function (5).

In the weak disorder regime, the explanation of the observed 'sparsity' and textures requires some more effort. For the purpose of this communication we shall be satisfied with

[7] The original argument by Mott is somewhat vague. We thank Holger Schanz for helpful communication concerning a crucial step in the derivation.

a qualitative explanation: if the disorder W were zero, then the mode index (call it n_y) would become a good quantum number. This means that states that are close in energy are not coupled (because they have different n_y). Once W becomes non-zero (but still small) the mixing is described by Wigner Lorentzians (much the same as in the toy model of [9]). Then the ratio between small and large couplings is determined by the different degree of mixing of close versus far modes. Consequently, one observes a wide (but not stretched) distribution for the $\log(X)$ values (see figure 2(*b*)).

9. RMT modeling, beyond the Gaussian assumption

It was the idea of Wigner [18] to model the perturbation matrix of a *complex* system as a (banded) random matrix. Later it has been conjectured by Bohigas [19] that similar modeling may apply to *chaotic* systems. For many purposes it is convenient to assume infinite bandwidth with elements that are taken from a Gaussian distribution, leading to the standard Gaussian Orthogonal or Unitary ensembles (GOE/GUE). But there are obviously physical circumstances in which it is essential to go beyond the Gaussian assumption, and to take into account the implications of having finite bandwidth and/or non-Gaussian distribution of elements [20] and/or sparsity [21] and/or texture.

It should be clear that the default assumption of having a Gaussian distribution of in-band matrix elements is legitimate on practical grounds as long as the matrix elements have *comparable size in absolute value*. But if the eigenfunctions are non-ergodic this assumption becomes problematic, because the elements (in absolute value) might have a wide distribution over many decades in the log scale. In such a case different type of averages may differ by orders of magnitude.

In the following, we regard $\{|v_{nm}|^2\}$ as a random matrix of non-negative numbers $\{X\}$. In general, it might be a banded matrix. If the standard Gaussian assumption applies, then the in-band elements of $\{X\}$ are characterized by the Porter–Thomas distribution. But we are interested in physical circumstances in which many of the in-band elements are vanishingly small. We define this feature as 'sparsity'. In the following section we define p as the fraction of elements that are larger than the average. If we have $p \ll 1$ then we say that the matrix is 'sparse'. We further discuss the definition of p in the following section.

10. Characterization of sparsity

For an artificially generated sparse random matrix $\{X\}$ of non-negative elements, one defines p as the fraction of non-zero elements. Such a definition assumes a bimodal distribution. But in general realistic circumstances we do not have a bimodal distribution. Rather for strong disorder we already had explained that the distribution of the matrix elements $\{|v_{nm}|^2\}$ is log-box. Contemplating a bit on this issue one concludes that the physically generalized definition of the sparsity measure is $p \equiv F(\langle X \rangle)$, where $F(X)$ is the probability to find a value larger than X. We regard a matrix as sparse if $p \ll 1$. Given that $\ln(X)$ is uniformly distributed between $\ln(X_0)$ and $\ln(X_1)$ we define $\tilde{p} \equiv (\ln(X_1/X_0))^{-1}$, and find assuming $X_0 \ll X_1$ that $p \approx -\tilde{p} \ln \tilde{p}$, and $\langle X \rangle \approx \tilde{p} X_1$. Hence for log-box distribution $\langle X \rangle \sim p X_1$, as expected from the standard bimodal case.

In figure 3, we redo the calculation of the conductance with artificial matrices with the same sparsity, i.e. log-box distributed elements with the same p. We observe qualitative agreement for strong disorder. In the other extreme limit of weak disorder there is no agreement, because we have to use a different distribution for the matrix elements: it turns out that also in the

ballistic regime $\log(X)$ has a wide distribution, but it is not stretched as in the case of a log-box distribution (see section 8). In practice, we can describe the X distribution of the matrix elements in the ballistic limit as log-normal[8]. Once we use the appropriate distribution we get a reasonable qualitative agreement. We emphasize that in both cases, of either weak or strong disorder, there is besides the algebraic average $\langle X\rangle$ only *one* additional fitting parameter that characterizes the distribution and hence determines the 'sparsity'. We could of course have generated RMT matrices using the actual distribution (figure 2), but then we would merely re-generate the *untextured* data points.

Given a hopping range $|E_m - E_n| \leqslant \omega$ we can look for the typical matrix element $\overline{X}$ for connected sequences of such transitions, which we find by solving the equation

$$\left(\frac{\omega}{\Delta}\right) \mathrm{F}\left(\overline{X}\right) \sim 1. \tag{12}$$

In particular, for strong disorder we get

$$\overline{X} \approx v_{\mathrm{F}}^2 \exp\left(-\frac{\Delta_\ell}{\omega}\right), \tag{13}$$

where $\Delta_\ell = (L/\ell_\infty)\Delta$ is the local level spacing between eigenstates that are localized in the same region. The same procedure can be applied also in the ballistic regime leading to a simpler variation of (13) where the dependence of $\overline{X}$ on ω predominantly reflects the band profile: it follows from the discussion after equation (6) that v_{nm} is a banded matrix, with a Lorentzian band profile whose width $\sim v_{\mathrm{F}}/\ell$ becomes narrower as the disorder is decreased.

11. Generalized Kubo formula

The definition of the band profile reflects the variation of $\langle X\rangle$ with ω. In complete analogy, we define an effective band profile that reflects the variation of $\overline{X}$ with ω. Namely,

$$\tilde{C}_{\text{qm-LRT}}(\omega) \equiv 2\pi \varrho_{\mathrm{F}} \langle X\rangle, \tag{14}$$

$$\tilde{C}_{\text{qm-SLRT}}(\omega) \equiv 2\pi \varrho_{\mathrm{F}} \overline{X}. \tag{15}$$

The spectral function of equation (6) is a smeared version of the 'bare' spectral function: it is obtained by a convolution $\tilde{C}_{\text{qm-LRT}}(\omega) \star \delta_\Gamma(\omega)$. Consequently, we get

$$G = \frac{1}{2}\left(\frac{e}{L}\right)^2 \varrho_{\mathrm{F}} \int \tilde{C}_{\mathrm{qm}}(\omega)\delta_\Gamma(\omega)\,\mathrm{d}\omega, \tag{16}$$

where the appropriate LRT/SLRT spectral function should be used. This way of writing allows us to obtain an approximation for the mesoscopic conductance using a Kubo-like calculation: it is just re-writing of the Kubo formula in the LRT case, while being a generalized VRH approximation in the SLRT case.

For strong disorder the above generalized VRH approximation gives an integral over $\exp(-|\omega|/\omega_c)\exp(-\Delta_\ell/|\omega|)$, which is a product of two competing factors: the first has to do with the noise/temperature and the second has to do with the couplings. This integral is handled using the usual VRH phenomenology: the result is determined by the maximum of its integrand, which requires to optimize the range ω of the transition. In the weak disorder regime the VRH integral is not the same as in the strong disorder case, because a log-normal

[8] The default fitting of the $\log(X)$ distribution to a *Gaussian* line shape is merely a practical issue. The 'RMT ideology' is to see whether a 'minimum information' ensemble of random matrices can be used in order to derive reasonable estimates. If we want to further improve our estimates in the ballistic regime it is essential to take into account the texture and not only the deviation from log-normal distribution (see section 6).

rather than log-box distribution is involved. We have verified that the generalized VRH integral gives a qualitatively reasonable approximation to the actual resistor network calculation in both cases. In any case one should keep in mind the well-known reservations that apply to such 'mean field' approach [14, 15].

12. Summary

Within SLRT it is assumed that the transitions between levels are given by the Fermi-golden-rule (FGR), but a resistor network analogy is used in order to calculate the energy absorption rate. The calculation generalizes the variable range hopping picture and treats on equal footing the weak and strong disorder regimes. The essential physics is captured by RMT, provided the perturbation matrix is regarded as a member of the appropriate Gaussian/log-normal/log-box ensemble.

The prevailing results in the literature regarding the conductance of small closed metallic rings (for a review, see [4]) concern mainly the diffusive regime, where in leading order the conductance is given by the Drude formula, and SLRT does not differ much from LRT. In the present communication, multi-mode rings in the non-diffusive regime are considered seriously for the first time. Then it become essential to define the precise assumptions regarding the environment and the driving. It is important to realize that both LRT and SLRT assume Markovian FGR transitions. This is a very realistic assumption that can be justified rigorously if one assumes noisy driving (as in our exposition) or else it is implied by having a noisy environment[9]. Accordingly, it should be clear that LRT and SLRT both share the same small parameter as in the FGR picture, which is the ratio between the rate of the driven transitions and the smallest relevant energy scale that characterizes the band profile (bandwidth/sparsity/texture).

There is only one assumption that distinguishes the SLRT (mesoscopic) circumstances from LRT (Kubo) circumstances. This is related to the implicit role of the environmentally induced relaxation process in the determination of the steady state of the system. Within SLRT one assumes that the FGR rate of the driven transitions ($w_{\rm FGR} \propto \varepsilon^2 \mathsf{g}_{nm}$) is larger compared with the relaxation rate ($\gamma_{\rm rlx}$). The inelastic relaxation effect can be incorporated into the SLRT framework by considering a non-symmetric g_{nm} as implied (say) by detailed balance considerations. If the relaxation is the predominant effect ($w_{\rm FGR} < \gamma$), then we are back in the LRT regime [23] where the Kubo–Drude result applies [9].

One can wonder what happens if the FGR assumption of LRT/SLRT breaks down. Not much is known [24]. Reference [25] has attempted to go beyond the FGR approximation using the Keldish formalism, and has recovered a Markovian picture that leads to a Kubo-like result for the conductance. If the Keldish Markovian picture could be established beyond the diffusive regime [26], it would be possible to extend SLRT into the nonlinear regime.

Acknowledgment

This research was supported by a grant from the USA–Israel Binational Science Foundation (BSF).

[9] The possibility to witness dynamical localization-related corrections [22] that go beyond the FGR picture requires strictly coherent microscopic-like circumstances, such that the dephasing time is much longer compared with the *Heisenberg time*, and the low-frequency driving is required to be strictly periodic over those extremely long periods. Such conditions are possibly not easy to achieve in realistic experimental circumstances once multi-mode rings are concerned.

References

[1] The first studies have addressed mainly the Debye regime: Büttiker M, Imry Y and Landauer R 1983 *Phys. Lett.* A **96** 365
Landauer R and Büttiker M 1985 *Phys. Rev. Lett.* **54** 2049
Büttiker M 1985 *Phys. Rev.* B **32** 1846
Büttiker M 1986 *Ann. New York Acad. Sci.* **480** 194
[2] The Kubo formula is applied to diffusive rings in: Imry Y and Shiren N S 1986 *Phys. Rev.* B **33** 7992
Trivedi N and Browne D A 1988 *Phys. Rev.* B **38** 9581
[3] Weak localization corrections were studied in: Reulet B and Bouchiat H 1994 *Phys. Rev.* B **50** 2259
Kamenev A, Reulet B, Bouchiat H and Gefen Y 1994 *Europhys. Lett.* **28** 391
[4] For a review, see: Kamenev A and Gefen Y 1995 (Almost) everything you always wanted to know about the conductance of mesoscopic systems *Int. J. Mod. Phys.* B **9** 751
[5] Measurements of conductance of closed diffusive rings are described by: Ramin M, Reulet B, Bouchiat H and Mailly D 1995 *Phys. Rev. Lett.* **75** 124
[6] Measurements of susceptibility of individual closed rings using SQUID is described in: Koshnick N C, Bluhm H, Huber M E and Moler K A 2007 *Science* **318** 1440
[7] A new micromechanical cantilevers technique for measuring currents in normal metal rings is described in: Bleszynski-Jayich A C, Shanks W E, Ilic R and Harris J G E 2007 *Preprint* arXiv:0710.5259
[8] Cohen D 2007 *Phys. Rev.* B **75** 125316
[9] Cohen D, Kottos T and Schanz H 2006 *J. Phys. A: Math. Gen.* **39** 11755
[10] Bandopadhyay S, Etzioni Y and Cohen D 2006 *Europhys. Lett.* **76** 739
[11] Wilkinson M, Mehlig B and Cohen D 2006 *Europhys. Lett.* **75** 709
[12] Mott N F 1970 *Phil. Mag.* **22** 7
Mott N F and Davis E A 1971 *Electronic Processes in Non-crystalline Materials* (Oxford: Clarendon)
[13] Miller A and Abrahams E 1960 *Phys. Rev.* **120** 745
[14] Ambegaokar V, Halperin B and Langer J S 1971 *Phys. Rev.* B **4** 2612
[15] Pollak M 1972 *J. Non-Cryst. Solids* **11** 1
[16] For review, see: Stone D and Szafer A http://www.research.ibm.com/journal/rd/323/ibmrd3203I.pdf
[17] Wobst A, Ingold G L, Hanggi P and Weinmann D 2003 *Phys. Rev.* B **68** 085103
[18] Wigner E 1955 *Ann. Math.* **62** 548
Wigner E 1957 *Ann. Math.* **65** 203
[19] Bohigas O 1991 Chaos and quantum physics *Proc. Session LII of the Les-Houches Summer School* ed A Voros and M-J Giannoni (Amsterdam: North-Holland)
[20] For deviation from Gaussian distributions see: Prosen T and Robnik M 1993 *J. Phys. A: Math. Gen.* **26** L319
Austin E J and Wilkinson M 1992 *Europhys. Lett.* **20** 589
Alhassid Y and Levine R D 1986 *Phys. Rev. Lett.* **57** 2879
[21] Fyodorov Y V, Chubykalo O A, Izrailev F M and Casati G 1996 *Phys. Rev. Lett.* **76** 1603
[22] Basko D M, Skvortsov M A and Kravtsov V E 2003 *Phys. Rev. Lett.* **90** 096801
[23] Foieri F, Arrachea L and Sanchez M J 2007 *Phys. Rev. Lett.* **99** 266601
[24] Cohen D and Kottos T 2000 *Phys. Rev. Lett.* **85** 4839
[25] Silva A and Kravtsov V E 2007 *Phys. Rev.* B **76** 165303
[26] Silva A and Cohen D 2007 Private communication

3.3 Semi-linear response for the heating rate of cold atoms in vibrating traps

The content of this section is available as

- a journal article: A. Stotland, D. Cohen and N. Davidson, Europhysics Letters **86**, 10004 (2009)
- a preprint: arXiv:0810.0360

See Appendix C for the explanation of the numerical analysis used in this work.

A Letters Journal Exploring the Frontiers of Physics

April 2009

EPL, **86** (2009) 10004
doi: 10.1209/0295-5075/86/10004

www.epljournal.org

Semilinear response for the heating rate of cold atoms in vibrating traps

A. Stotland[1], D. Cohen[1] and N. Davidson[2]

[1] *Department of Physics, Ben-Gurion University - Beer-Sheva, 84005, Israel*
[2] *Department of Physics of Complex Systems, Weizmann Institute of Science - Rehovot, 76100, Israel*

received 22 December 2008; accepted in final form 9 March 2009
published online 17 April 2009

PACS 03.65.-w – Quantum mechanics

Abstract – The calculation of the heating rate of cold atoms in vibrating traps requires a theory that goes beyond the Kubo linear response formulation. If a strong "quantum chaos" assumption does not hold, the analysis of transitions shows similarities with a percolation problem in energy space. We show how the texture and the sparsity of the perturbation matrix, as determined by the geometry of the system, dictate the result. An improved sparse random matrix model is introduced: it captures the essential ingredients of the problem and leads to a generalized variable range hopping picture.

The rate of energy absorption by particles that are confined by vibrating walls was of interest in past studies of nuclear friction [1–3], where it leads to the damping of the wall motion. More recently, it has become of interest in the context of cold atoms physics. In a series of experiments [4–6] with "atom-optics billiards" some surprising predictions [7] based on linear response theory (LRT) have been verified.

In this study, we consider the case where the billiard is fully chaotic[1], but with nearly integrable shape (fig. 1). We explain that in such circumstances LRT is *not* applicable (unless the driving is extremely weak such that relaxation dominates). Rather, the analysis that is relevant to the typical experimental conditions should go beyond LRT and involve a "resistor network" picture of transitions in energy space, somewhat similar to a percolation problem. Consequently, we predict that the rate of energy absorption would be suppressed by orders of magnitude and provide some analytical estimates that are supported by a numerical calculation.

We assume that an experimentalist has control over the position (R) of a wall element that confines the motion of cold atoms in an optical trap. We consider below the effect of low-frequency, noisy (non-periodic) driving. This means that R is not strictly constant in time, either because of drifts [8] that cannot be eliminated in realistic circumstances, or else deliberately as a way to probe the dynamics of the atoms inside the trap [9]. We assume the usual Markovian picture of FGR transitions between energy levels, which is applicable in typical circumstances (see, *e.g.,* [10]). These transitions lead to diffusion in the energy space. If the atomic cloud is characterized by a temperature T, then the diffusion in energy would lead to heating with the rate $\dot{E} = D/T$ (see footnote [2]) and hence to an increase in the temperature of the cloud.

Naively one expects to observe an LRT behavior. That means to have $D \propto [\mathrm{RMS}(\dot{R})]^2$, and more specifically to have a linear relation between the diffusion coefficient and the power spectrum of the driving,

$$D \equiv G \times \mathrm{RMS}(\dot{R})^2 = \int_0^\infty \tilde{C}(\omega)\tilde{S}(\omega)\,\mathrm{d}\omega, \qquad (1)$$

Here $\tilde{S}(\omega)$ is the power spectrum of $\dot{R}$, and $\tilde{C}(\omega)$ is related to the susceptibility of the system. From the experimentalist's point of view the second equality in eq. (1) can be regarded as providing a practical definition for $\tilde{C}(\omega)$, if the response is indeed linear.

We shall explain in this paper that the applicability of LRT in our problem is very limited, namely LRT would lead to wrong predictions in *typical* experimental circumstances. Rather we are going to use a more refined theory, which we call semilinear response theory (SLRT) [11,12], in order to determine D. The theory is called SLRT because on the one hand the power spectrum $\tilde{S}(\omega) \mapsto \lambda\tilde{S}(\omega)$ leads to $D \mapsto \lambda D$, but on the other hand

[1] Our interest is in systems that are classically chaotic. This means exponential sensitivity to change in initial conditions, without having a mixed phase space.

[2] For a more general version of $\dot{E} = D/T$ that does not assume a Boltzmann-like distribution with a well-defined temperature, see sect. 4 of ref. [3].

$\tilde{S}(\omega) \mapsto \tilde{S}_1(\omega) + \tilde{S}_2(\omega)$ does not lead to $D \mapsto D_1 + D_2$. This semilinearity can be tested in an experiment in order to distinguish it from linear response. Accordingly, in SLRT, the spectral function $\tilde{C}(\omega)$ of eq. (1) becomes ill defined, while the coefficient G is still physically *meaningful*, and can be measured in an actual experiment.

If we assume a small driving amplitude the Hamiltonian matrix can be written as $\mathcal{H} = \{E_n\} + f(t)\{V_{nm}\}$, where

$$V_{nm} = \left\langle n \middle| \frac{\mathrm{d}\mathcal{H}}{\mathrm{d}R} \middle| m \right\rangle \tag{2}$$

is the perturbation matrix. More than 50 years ago, Wigner had proposed to regard the perturbation matrix of a complex system as a random matrix (RMT) whose elements are taken from a Gaussian distribution. Later, Bohigas had conjectured that the same philosophy applies to quantized chaotic systems. For such matrices the validity of LRT can be established on the basis of the FGR picture, and the expression for G is the Kubo formula $G_{\rm LRT} = \pi \varrho_{\rm E} \langle\langle |V_{nm}|^2 \rangle\rangle_a$, where $\langle\langle x \rangle\rangle_a = \langle x \rangle$ is the algebraic average over the near-diagonal matrix elements[3], and $\varrho_{\rm E}$ is the density of states (DOS). In contrast to that, using the Pauli master equation [10] with FGR transition rates between levels, the SLRT analysis leads to

$$G_{\rm SLRT} = \pi \varrho_{\rm E} \langle\langle |V_{nm}|^2 \rangle\rangle, \tag{3}$$

where the "average" $\langle\langle x \rangle\rangle$ is defined as in refs. [11,12] via a *resistor-network calculation* [13]. (For mathematical details see "the SLRT calculation" paragraph below.)

Within the RMT framework an element x of $|V_{nm}|^2$ is regarded as a random variable, and the histogram of all x values is used in order to define an appropriate ensemble. For the sake of later discussion we define, besides the algebraic average $\langle\langle x \rangle\rangle_a$, also the harmonic average as $\langle\langle x \rangle\rangle_h = [\langle 1/x \rangle]^{-1}$ and the geometric average as $\langle\langle x \rangle\rangle_g = \exp[\langle \ln x \rangle]$. The result of the resistor network calculation is labeled as $\langle\langle x \rangle\rangle$ (without subscript).

Our interest is in the circumstances where the strong "quantum chaos" assumption of Wigner fails. This would be the case if the distribution of x is wide in the log scale. If x has (say) a log-normal distribution, then it means that the typical value of x is much smaller compared with the algebraic average. This means that the perturbation matrix V_{nm} is effectively sparse (*a lot of vanishingly small elements*). We can characterize the sparsity by the parameter $q = \langle\langle x \rangle\rangle_g / \langle\langle x \rangle\rangle_a$. We are going to explain that for typical experimental conditions we might encounter sparse matrices for which $q \ll 1$. Then the energy spreading process is similar to a percolation in energy space, and the SLRT formula, eq. (3), replaces the Kubo formula.

[3]The average is taken over all the elements within the energy window of interest as determined by the preparation temperature. The weight of $|V_{nm}|^2$ in this average is determined by the spectral function as $\tilde{S}(E_n - E_m)$.

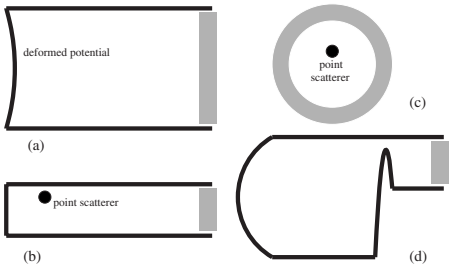

Fig. 1: Model systems: the atoms are held by a potential that may consist of static walls (solid lines), a vibrating wall (shaded lines), and bumps (thick points). The numerics has been done for (b) with a Gaussian bump. We work with two different aspect ratios. For the aspect ratio $AS = 20$, we take $L_x = 200$ and $L_y = 10$. For the aspect ratio $AS = 1$, we take $L_x = 40$ and $L_y = 40$. The position of the Gaussian bump was randomly chosen within the region $[0.4, 0.6]L_x \times [0.4, 0.6]L_y$. The width of the Gaussian is $\sigma_x = \sigma_y = \sigma$. We have assumed noisy driving with $\omega_c = 7\Delta$, where $\Delta = 1/\varrho_{\rm E}$ is the mean level spacing, and the units were such that $\mathsf{M} = 1$.

Outline. – In what follows we present our model system, analyze it within the framework of SLRT, and then introduce an RMT model with log-normal distributed elements, that captures the essential ingredients of the problem. We show that a generalized resistor network analysis for the transitions in energy space leads to a generalized variable range hopping (VRH) picture (the standard VRH picture has been introduced by Mott in [14] and later refined by ref. [15] using the resistor network perspective of ref. [13]). Our RMT-based analytical estimates are verified against numerical calculation. Finally, we discuss the experimental aspect, and in particular define the physical circumstances in which SLRT rather than LRT applies. These two theories give results that can differ by orders of magnitude.

Modeling. – Consider a strictly rectangular billiard whose eigenstates are labeled by $\boldsymbol{n} = (n_x, n_y)$. The perturbation due to the movement of the "vertical" wall does not couple states that have different mode index n_y. Due to this selection rule the perturbation matrix is sparse. If we deform slightly the potential (fig. 1(a)), or introduce a bump (fig. 1(b)), then states with different mode index are mixed. Consequently, the numerous zero elements become finite but still very tiny in magnitude, which means a very wide size distribution featuring a small fraction of large elements. Similar considerations apply for the circular cavity of fig. 1(c), where an off-center scatterer couples radial and angular motion, and which is more suitable for a real experiment (but less convenient for numerical analysis).

Typically, the perturbation matrix is not only *sparse* but also *textured*. This means (see fig. 2) that there are stripes where the matrix elements are larger, and bottlenecks where they are all small. The emergence of texture (*i.e.*, non-random arrangement of the sparse large elements along the diagonals) is most obvious if we

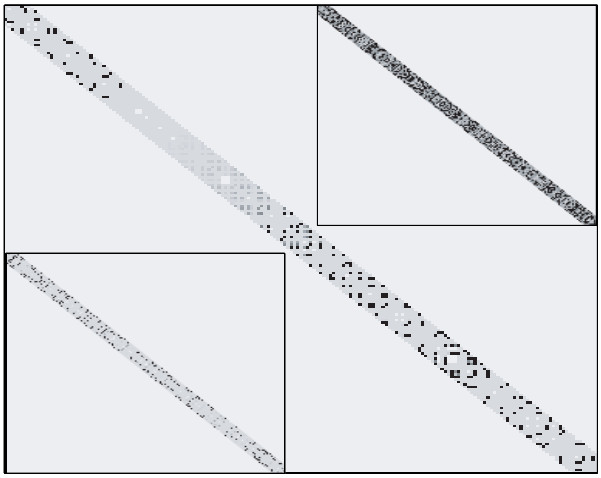

Fig. 2: The image of the perturbation matrix $|V_{nm}|^2$ due to a wall displacement of a rectangular-like cavity that has an aspect ratio $AS = 20$. The potential floor is deformed due to the presence of a $\sigma = 0$ scatterer with $u = 10^{-4}$ (see text). The matrix is both sparse and textured. Lower inset: untextured matrix —the elements along each diagonal are randomly permuted. Upper inset: non-sparse matrix with the same band profile —each element is generated independently from a normal distribution.

consider the geometry of fig. 1(d), where we have a divided cavity with a small weakly connected chamber where the driving is applied. If the chamber were disconnected, then only chamber states with energies E_r would be coupled by the driving. But due to the connecting corridor there is mixing of bulk states with chamber states within energy stripes around E_r. The coupling between two cavity states E_n and E_m is very small outside of the E_r stripes. Consequently, the near-diagonal elements of V_{nm} have wide variation, and hence a wide $\log(x)$ distribution.

Coming back to the geometries of fig. 1(a)–(c), it is somewhat important in the analysis to distinguish between *smooth* deformation that couples only nearby modes, and *diffractive* deformation that mix all the modes simultaneously: Recalling that different modes have different DOS, and that low-DOS modes are sparse within the high-DOS modes, we expect a more prominent manifestation of the texture in the case of a smooth deformation of a cavity that has a large aspect ratio. We later confirm this expectation in the numerical analysis.

The SLRT calculation. – As in the standard derivation of the Kubo formula, also within the framework of SLRT [11,12], the leading mechanism for absorption is assumed to be FGR transitions. The FGR transition rate is proportional to the squared matrix elements $|V_{nm}|^2$, and to the power spectrum at the frequency $\omega = E_n - E_m$. It is convenient to define the normalized spectral function $\tilde{F}(\omega)$, such that

$$\tilde{S}(\omega) \equiv \mathrm{RMS}(\dot{R})^2 \times \tilde{F}(\omega). \tag{4}$$

Contrary to the naive expectation the theory does not lead to the Kubo formula. This is because the rate of absorption depends crucially on the possibility to make *connected* sequences of transitions. It is implied that both the texture and the sparsity of the $|V_{nm}|^2$ matrix play a major role in the calculation of G. Consequently, SLRT leads to eq. (3), where $\langle\langle \ldots \rangle\rangle$ is defined using a resistor network calculation. Namely, the energy levels are regarded as the *nodes* of a resistor network, and the FGR transition rates as the *bonds* that connect different nodes. Following [12] the inverse resistance of a bond is defined as

$$\mathsf{g}_{nm} \equiv 2\varrho_{\mathrm{E}}^{-3} \frac{|V_{nm}|^2}{(E_n - E_m)^2} \tilde{F}(E_m - E_n) \tag{5}$$

and $\langle\langle |V_{nm}|^2 \rangle\rangle$ is defined as the inverse resistivity of the network. It is a simple exercise to verify that if all the matrix elements are the same, say $|V_{nm}|^2 = c$, then $\langle\langle |V_{nm}|^2 \rangle\rangle = c$ too. But if the matrix is sparse or textured then typically

$$\langle\langle |V_{nm}|^2 \rangle\rangle_h \ll \langle\langle |V_{nm}|^2 \rangle\rangle \ll \langle\langle |V_{nm}|^2 \rangle\rangle_a. \tag{6}$$

In the case of sparse matrices this is a mathematically strict inequality, and we can use a generalized VRH scheme that we describe below in order to get an estimate for $\langle\langle x \rangle\rangle$. If the *element-size* distribution of $\log(x)$ is not too stretched, then a reasonable approximation is $\langle\langle x \rangle\rangle \approx \langle\langle x \rangle\rangle_g$, simply because the geometric mean is the *typical* (median) value for the size of the elements. However, if $|V_{nm}|^2$ has either a very stretched element-size distribution, or if it has texture, then our VRH analysis below show that the geometric average becomes merely an improved *lower bound* for the actual result.

Analysis. – We consider a particle of mass M in a two-dimensional box of length L_x and width L_y, such that $0 < x < L_x$ and $0 < y < L_y$ (see fig. 1(b)). With the driving the length of the box becomes $R = L_x + f(t)$. The Hamiltonian is

$$\mathcal{H} = \mathrm{diag}\{E_{\boldsymbol{n}}\} + u\{U_{\boldsymbol{nm}}\} + f(t)\{V_{\boldsymbol{nm}}\}, \tag{7}$$

where $\boldsymbol{n} = (n_x, n_y)$ is a composite index that labels the energy levels $E_{\boldsymbol{n}}$ of a particle in a rectangular box of size $L_x \times L_y$. The deformation is described by a normalized Gaussian potential $U(x, y)$ of width (σ_x, σ_y) positioned at the central region of the box. Its matrix elements are $U_{\boldsymbol{nm}}$, and it is multiplied in the Hamiltonian by a parameter u which signifies the strength of the deformation. Note that the limit $\sigma \to 0$ is well defined and corresponds to an "s-scatterer". The perturbation matrix due to the $f(t)$ displacement of the wall is

$$V_{\boldsymbol{nm}} = -\delta_{n_y,m_y} \times \frac{\pi^2}{\mathsf{M}L_x^3} n_x m_x. \tag{8}$$

The power spectrum of $\dot{f}$ is assumed to be constant within the frequency range $|\omega| < \omega_c$ and zero otherwise. This means that $\tilde{F}(\omega) = 1$ up to this cutoff frequency.

We have also considered (not presented) an exponential line shape $\tilde{F}(\omega) = \exp(-|\omega/\omega_c|)$, leading to qualitatively similar results. After diagonalization of $\{E_{\boldsymbol{n}}\} + u\{U_{\boldsymbol{nm}}\}$, the Hamiltonian takes the form

$$\mathcal{H} = \mathrm{diag}\{E_n\} + f(t)\{V_{nm}\}, \tag{9}$$

where n (not bold) is a running index that counts the energies in ascending order. The DOS remains essentially the same as for $u = 0$, namely

$$\varrho_{\mathrm{E}} = \frac{1}{2\pi}\mathsf{M}L_xL_y. \tag{10}$$

The perturbation matrix $|V_{nm}|^2$ is sparse and textured (see fig. 2). First we discuss the sparsity, and the effect of the texture will be addressed later on.

Considering first zero deformation ($u = 0$) it follows from eq. (8) that the non-zero elements of the perturbation matrix are $|V_{nm}|^2 \approx |\mathsf{M}v_{\mathrm{E}}^2/L_x|^2|$, where $v_{\mathrm{E}} = \sqrt{2E/\mathsf{M}}$. The algebraic average of the near-diagonal elements equals this value (of the large-size elements) multiplied by their percentage p_0. To evaluate p_0 let us consider an energy window $\mathrm{d}E$. The number of near-diagonal elements V_{nm} within the stripe $|E_{n_x,n_y} - E_{m_x,m_y}| < \mathrm{d}\varepsilon$ is $\varrho_{\mathrm{E}}^2\mathrm{d}E\,\mathrm{d}\varepsilon$. It is a straightforward exercise to find out that the number of non-zero elements (*i.e.*, with $n_y = m_y$) is the same number multiplied by $p_0 = [2\pi\mathsf{M}v_{\mathrm{E}}L_y]^{-1}$. Consequently,

$$\langle\langle|V_{nm}|^2\rangle\rangle_a \approx \left[\frac{1}{2\pi\mathsf{M}v_{\mathrm{E}}L_y}\right]\left|\frac{\mathsf{M}v_{\mathrm{E}}^2}{L_x}\right|^2 = \frac{\mathsf{M}v_{\mathrm{E}}^3}{2\pi L_y L_x^2}. \tag{11}$$

Somewhat surprisingly, this result turns out to be the same (disregarding an order unity numerical prefactor) as for a strongly chaotic cavity (see eq. (I3) of ref. [3]), as if there is no sparsity issue. This implies that irrespective of the deformation u, the LRT Kubo result is identical to the 2D version of the wall formula (see sect. 7 of ref. [3]):

$$G_{\mathrm{LRT}} = \frac{4}{3\pi}\frac{\mathsf{M}^2v_{\mathrm{E}}^3}{L_x}. \tag{12}$$

Our interest below is not in G_{LRT} but in G_{SLRT}, which can differ by many orders of magnitudes. For sufficiently small u the large-size matrix elements are not affected, and therefore the algebraic average stays the same. But in the SLRT calculation we care about the small-size matrix elements, that are zero if $u = 0$. Due to the first-order mixing of the levels, the typical overlap $|\langle\boldsymbol{m}|n\rangle|$ between perturbed and unperturbed states is $|uU_{\boldsymbol{nm}}/(E_{\boldsymbol{n}} - E_{\boldsymbol{m}})|$. The typical size of a small V_{nm} element is the multiplication of this overlap (evaluated for nearby levels) by the size of a *non-zero* $V_{\boldsymbol{nm}}$ element. Consequently, the small-size matrix elements are proportional to u^2. The geometric average simply equals their typical size, leading to

$$\langle\langle|V_{nm}|^2\rangle\rangle_g \approx \left(\frac{\mathsf{M}^2v_{\mathrm{E}}^2}{2\pi L_x}\right)^2 \mathrm{e}^{-2\mathsf{M}^2v_{\mathrm{E}}^2(\sigma_x^2+\sigma_y^2)}\ u^2. \tag{13}$$

Motivated by the discussion below eq. (6) a crude estimate for the SLRT result is $G_{\mathrm{SLRT}} \approx q \times G_{\mathrm{LRT}}$, where for small deformation

$$q = \frac{\langle\langle|V_{nm}|^2\rangle\rangle_g}{\langle\langle|V_{nm}|^2\rangle\rangle_a} \ \propto\ u^2, \tag{14}$$

see eqs. (11) and (13). It follows from the above (and see fig. 3) that for small deformations $q \ll 1$, and consequently we expect $G_{\mathrm{SLRT}} \ll G_{\mathrm{LRT}}$. This should be contrasted with the case of strongly deformed box for which all the elements are of the same order of magnitude and q becomes of order unity. Our next task is to further improve the SLRT estimate using a proper resistor network calculation[4].

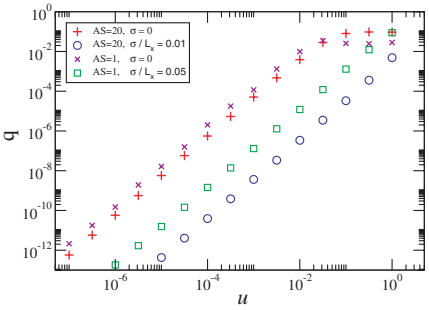

Fig. 3: (Colour on-line) The sparsity parameter q is plotted *vs.* the strength u of the deformation potential for cavities with aspect ratios $AS = 1$ and $AS = 20$. We see that for large aspect ratio q has some sensitivity to σ. As explained in the text $G_{\mathrm{SLRT}}/G_{\mathrm{LRT}}$ is correlated with q, but for large aspect ratio it is even more sensitive to σ due to the emergence of textures, whose presence is not reflected by the value of q.

RMT modeling. – The $|V_{nm}|^2$ matrix looks like a random matrix with some distribution for the size of the elements (see fig. 4). It might also possess some non-trivial texture that we ignore within the RMT framework. The RMT perspective allows us to derive a quantitative theory for G using a generalized VRH estimate. Let us demonstrate the procedure in the case of a homogeneous (neither banded nor textured) random matrix with log-normal distributed elements. The mean and the variance of $\ln(x)$ are trivially related to geometric and the algebraic averages, namely $\langle\ln(x)\rangle = \ln\langle\langle x\rangle\rangle_g$ and $\mathrm{Var}(x) = -2\ln(q)$. Given a hopping range $|E_m - E_n| \leqslant \omega$, we can look for the typical matrix element x_ω for connected sequences of transitions, which we find by solving the equation $\varrho_{\mathrm{E}}\omega\mathrm{F}(x_\omega) \sim 1$, where $\mathrm{F}(x)$ is the probability to find a matrix element larger than x. This gives

$$x_\omega \approx \langle\langle x\rangle\rangle_g \exp\left[2\sqrt{-\ln q^\alpha}\right], \tag{15}$$

where $\alpha = \ln(\varrho_{\mathrm{E}}\omega_c)$. From this equation we deduce the following: For $q \lesssim 1$, meaning that the distribution is not too wide, $x_\omega \approx \langle\langle x\rangle\rangle_g$ as anticipated. But as the matrix gets more sparse ($q \ll 1$), the result deviates from the

[4]For a very small u, an optional route that bypass the resistor network calculation is to analyze the slow ($\propto u^2$) transitions between noise-broadened energy levels.

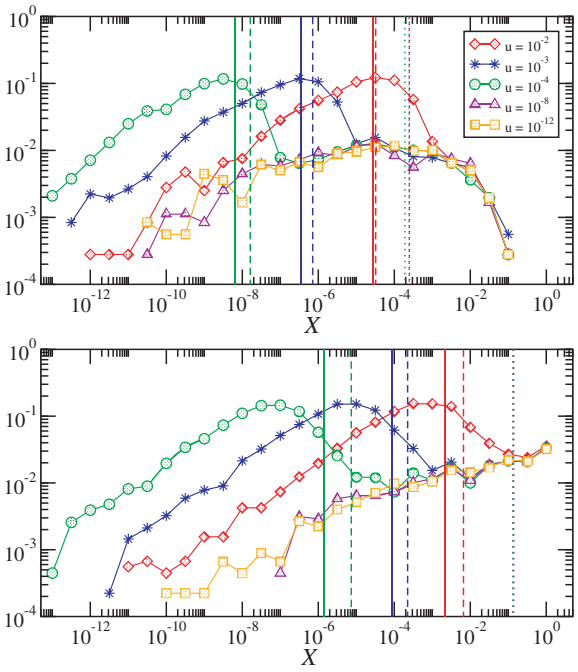

Fig. 4: (Colour on-line) Histograms of matrix elements for different values of u for $AS = 1$ (upper) and $AS = 20$ (lower). Here, we assume a $\sigma = 0$ scatterer. The vertical lines for $u = 10^{-2}, 10^{-3}, 10^{-4}$ indicate the $\langle\langle x\rangle\rangle$ obtained from the LRT algebraic average (three dotted lines that are barely resolved), from the SLRT resistor network calculation (solid lines), and from the untextured calculation (dashed lines). The geometric mean approximately coincides with the peaks, and underestimates the SLRT value for the larger AS where the sparsity is much larger.

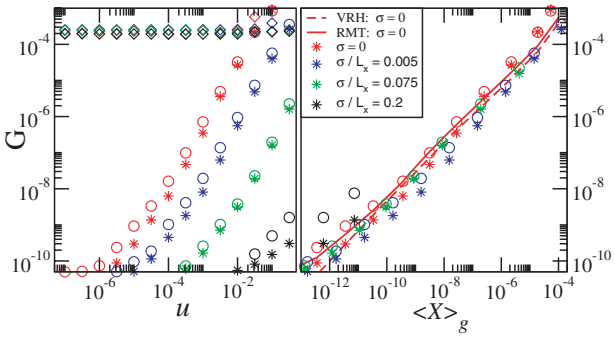

Fig. 5: (Colour on-line) Left panel: the scaled $\tilde{G} \equiv \langle\langle x\rangle\rangle$ in the LRT and in the SLRT case as a function of u for $AS = 1$ and different smoothness of the deformation. The stars are for the physical matrices, while the circles are for their untextured versions (see text). The diamonds are for the LRT case. Right panel: the SLRT result $\langle\langle x\rangle\rangle$ *vs.* the geometric average $\langle\langle x\rangle\rangle_g$. These are compared with RMT-based results, and with the associated analytical estimate of eq. (16). We see that the agreement is very good.

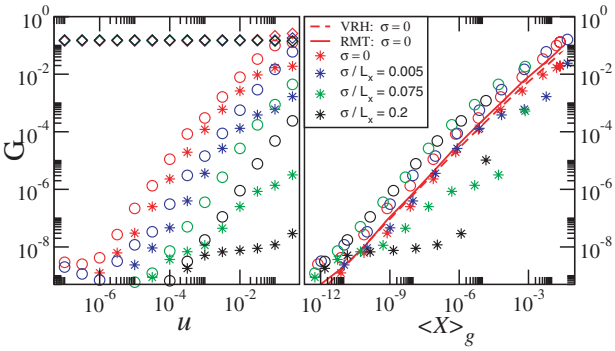

Fig. 6: (Colour on-line) The same set of plots as in fig. 5 but for $AS = 20$. In the right panel, we clearly see the departure of the physical result from the untextured and RMT results, and hence from the analytical estimate of eq. (16).

geometric average, the latter becoming merely a lower bound.

The generalized VRH estimate is based on optimization of the integral $\int x_\omega \, \tilde{F}(\omega) \, \mathrm{d}\omega$. For the rectangular $\tilde{F}(\omega)$, which has been assumed below eq. (8), this optimization is trivial and gives $\approx x_{\omega_c}$, leading to

$$G_{\mathrm{SLRT}} = q \exp\left[2\sqrt{-\ln q^\alpha}\right] \times G_{\mathrm{LRT}}, \qquad (16)$$

where G_{LRT} is given by eq. (12) and q is given by eq. (14). We have also tested the standard VRH that assumes an exponential $\tilde{F}(\omega)$ (not presented).

Numerical results. – The analytical estimates in eqs. (11) and (13) are supported by the histograms of fig. 4. For each choice of the parameters (AS, σ, u), we calculate the *algebraic*, *geometric* and the SLRT resistor network averages of $\{|V_{nm}|^2\}$ (see figs. 5 and 6). We also compare the actual results for G_{SLRT} with those that were obtained from a log-normal RMT ensembles with the same algebraic and geometric averages as that of the physical matrix[5]. As further discussed in the next paragraph one concludes that the agreement of the physical results with the associated VRH estimate eq. (16) is very good whenever the perturbation matrix is not textured, which is in fact the typical case for non-extreme aspect ratios.

In order to figure out whether the result is fully determined by the distribution of the elements or else texture is important we repeat the calculation for *untextured* versions of the *same* matrices. The untextured version of a matrix is obtained by performing a random permutation of its elements along the diagonals. This procedure affects neither the bandprofile nor the $\{|V_{nm}|^2\}$ distribution, but merely removes the texture. In fig. 5 we see that the physical results cannot be distinguished from the untextured results, and hence are in agreement with the RMT and with the associated VRH estimate. On the other hand, in fig. 6, which is for large aspect ratio, we see that the physical results deviate significantly from the untextured result. As the width of the Gaussian potential becomes larger (smoother deformation), the texture becomes more important. These observation are in complete agreement

[5]Since for the log-normal distribution the median equals the geometric average, we used the median in the definition of q for the sake of the numerical stability.

with the expectations that were discussed in the modeling section.

Experiment. – As in [4–6], a collection of $N \sim 10^6$ atoms, say ^{85}Rb atoms ($\mathsf{M} = 1.4 \times 10^{-25}$ kg), are laser cooled to low temperature of $T \sim 10\,\mu$K, such that the the typical thermal velocity is $v_{\rm E} \sim 0.05$ m/s. The atoms are trapped in an optical billiard whose blue-detuned light walls confine the atoms by repulsive optical dipole potential. The motion of the atoms is limited to the billiard plane by a strong perpendicular optical standing wave. The thickness of the billiard walls ($\sim 10\,\mu$m) is much smaller than its linear size ($L \sim 200\,\mu$m). The 2D mean level spacing is $\Delta = \varrho_{\rm E}^{-1} \sim 2.5 \times 10^{-34}$ J, which is 2.4 Hz. One or more of the billiard walls can be vibrated with several kilohertz frequency by modulating the laser intensity. The dimensionless spectral bandwidth of this driving can be set as say $\omega_c/\Delta \sim 1000$, with an amplitude $\sim 10\,\mu$m, such that $\dot{R} \sim 0.015$ m/s. The temperature of the trapped atoms can then be measured as a function of time by the time-of-flight method. The LRT estimate $G_{\rm LRT} \sim 1.3 \times 10^{-51}$ J s/m^2 would lead to heating rate $\dot{E} \sim 2 \times 10^{-27}$ J/s, which is ~ 0.15 mK/s. Considering (say) the geometry of fig. 1(c), the deformation (u) is achieved either by introducing an off-center optical "spot", or by deforming slightly the optical walls (such precise control on the geometry has been demonstrated in previous experiments). Having control over u we can have $q \sim 10^{-5}$ that would imply factor 100 suppression, *i.e.,* an estimated heating rate of few μK/s. Such heating rate can be accurately measured, yielding high sensitivity to the energy diffusion process studied here.

SLRT *vs.* LRT. – Typically the environment introduces in the dynamics an incoherent relaxation effect. If the relaxation rate is strong compared with the rate of the externally driven transitions, then the issue of having "connected sequences of transitions" becomes irrelevant, and the SLRT slowdown of the absorption is not expected. In the latter case, LRT rather than SLRT is applicable. It follows that for finite relaxation rate there is a crossover from LRT to SLRT behavior as a function of the intensity of the driving. In cold atom experiments, the relaxation effect can be controlled, and typically it is negligible. Hence, SLRT rather than LRT behavior should be expected. This implies, as discussed above, a much smaller absorption rate. Furthermore, as discussed at the beginning of this paper, one can verify experimentally the signature of SLRT: namely, the effect of adding independent driving sources is expected to be non-linear with respect to their spectral content.

Conclusions. – In this work, we have introduced a theory for the calculation of the heating rate of cold atoms in vibrating traps. This theory, which treats the diffusion in energy space as a resistor network problem, is required if the cavity is not strongly chaotic and if the relaxation effect is small. The SLRT result, unlike the LRT (Kubo) result, is extremely sensitive to the sparsity and the textures that characterize the perturbation matrix of the driving source. For typical geometries the ratio between them is determined by the sparsity parameter q as in eq. (16), and hence is roughly proportional to the deformation (u^2) of the confining potential. If the cavity has a large aspect ratio, and the deformation of the confining potential is smooth, then the emerging textures in the perturbation matrix of the driving source become important, and then the actual SLRT result becomes even smaller.

By controlling the density of the trapped atoms, or their collisional cross-section (*e.g.,* via the Feshbach resonance), the atomic collision rate can be tuned by many orders of magnitude. Their effect on the dynamics can thus be made either negligible (as assumed above) or significant, thereby serving as an alternative (but formally similar) mechanism for *weak breakdown of integrability*. It follows that heating rate experiments can be used not only to probe the deformation (u) of the confining potential, but also to probe the interactions between the atoms.

* * *

This research was supported by a grant from the USA-Israel Binational Science Foundation (BSF).

REFERENCES

[1] Blocki J., Boneh Y., Nix J. R., Randrup J., Robel M., Sierk A. J. and Swiatecki W. J., *Ann. Phys. (N.Y.)*, **113** (1978) 330.
[2] Koonin S. E., Hatch R. L. and Randrup J., *Nucl. Phys. A*, **283** (1977) 87; Koonin S. E. and Randrup J., *Nucl. Phys. A*, **289** (1977) 475.
[3] Cohen D., *Ann. Phys. (N.Y.)*, **283** (2000) 175, cond-mat/9902168.
[4] Friedman N., Kaplan A., Carasso D. and Davidson N., *Phys. Rev. Lett.*, **86** (2001) 1518.
[5] Kaplan A., Friedman N., Andersen M. F. and Davidson N., *Phys. Rev. Lett.*, **87** (2001) 274101.
[6] Andersen M., Kaplan A., Grunzweig T. and Davidson N., *Phys. Rev. Lett.*, **97** (2006) 104102.
[7] Barnett A., Cohen D. and Heller E. J., *Phys. Rev. Lett.*, **34** (2001) 413.
[8] Savard T. A., Ohara L. M. and Thomas J. E., *Phys. Rev. A*, **56** (1997) R1095.
[9] Friebel S., D'Andrea C., Walz J., Weitz M. and Hansch T. W., *Phys. Rev. A*, **57** (1998) R20.
[10] Louisell W. H., *Quantum Statistical Properties of Radiation* (Wiley, London) 1973.
[11] Cohen D., Kottos T. and Schanz H., *J. Phys. A*, **39** (2006) 11755; Wilkinson M., Mehlig B. and Cohen D., *Europhys. Lett.*, **75** (2006) 709.
[12] Bandopadhyay S., Etzioni Y. and Cohen D., *EPL*, **76** (2006) 739; Stotland A., Budoyo R., Peer T., Kottos T. and Cohen D., *J. Phys. A*, **41** (2008) 262001.
[13] Miller A. and Abrahams E., *Phys. Rev.*, **120** (1960) 745.
[14] Mott N. F., *Philos. Mag.*, **22** (1970) 7.
[15] Ambegaokar V., Halperin B. and Langer J. S., *Phys. Rev. B*, **4** (1971) 2612; Pollak M., *J. Non-Cryst. Solids*, **11** (1972) 1.

3.4 Random-matrix modeling of semi-linear response, the generalized variable range hopping picture, and the conductance of mesoscopic rings

The content of this section is available as

- a journal article: A. Stotland, T. Kottos and D. Cohen,
  Phys. Rev. B **81**, 115464 (2010)
- a preprint: arXiv:0908.3991

See Appendices A, B for the supplementary material and Appendix C for the explanation of the numerical analysis used in this work.

Random-matrix modeling of semilinear response, the generalized variable-range hopping picture, and the conductance of mesoscopic rings

Alexander Stotland,[1] Tsampikos Kottos,[2] and Doron Cohen[1]
[1]*Department of Physics, Ben-Gurion University, Beer-Sheva 84105, Israel*
[2]*Department of Physics, Wesleyan University, Middletown, Connecticut 06459, USA*
(Received 27 August 2009; revised manuscript received 29 October 2009; published 31 March 2010)

Semilinear response theory determines the absorption coefficient of a driven system using a resistor network calculation: each unperturbed energy level of a particle in a vibrating trap, or of an electron in a mesoscopic ring, is regarded as a node (n) of the network; the transition rates (w_{mn}) between the nodes are regarded as the elements of a random matrix that describes the network. If the size distribution of the connecting elements is wide (e.g., log-normal–like rather than Gaussian type) the result for the absorption coefficient differs enormously from the conventional Kubo prediction of linear response theory. We use a generalized variable range hopping scheme for the analysis. In particular, we apply this approach to obtain practical approximations for the conductance of mesoscopic rings. In this context Mott's picture of diffusion and localization is revisited.

DOI: 10.1103/PhysRevB.81.115464 PACS number(s): 03.65.−w, 73.23.−b, 05.45.Mt

I. INTRODUCTION

Semilinear response theory (SLRT) (Ref. 1–3) provides a procedure for the calculation of the absorption coefficient of a driven system, assuming that there are well-defined transition rates w_{mn} between levels E_n that are ordered by energy. In this context it is helpful to regard w_{mn}^{-1} as describing resistors that connect nodes of a network, a point of view that has become popular in the related studies of variable range hopping (VRH).[4–9] In the random matrix theory (RMT) framework w_{mn} is a random matrix whose construction is inspired by analyzing the statistical properties of the Hamiltonian of an actual physical system.[10,11] Three physical applications have been discussed so far: (i) metallic rings driven by electromotive force;[12] (ii) metallic grains driven by low-frequency radiation;[3] and (iii) cold atoms that are heated up due to the vibrations of a wall.[13] It is crucial to observe that depending on the parameters that define the physical model, the matrix w_{mn} might be *banded* and *sparse*.[14,15] Consequently, nontrivial results that go beyond linear response theory (LRT) are obtained.

In order to have a precise mathematical definition of the RMT model, let us write the random matrix as

$$w_{mn} = \boldsymbol{X}_{mn} \times \widetilde{B}(E_m - E_n). \tag{1}$$

In this expression $\widetilde{B}(\omega)$ describes the band profile of the matrix and $\boldsymbol{X}_{mn}$ is a random matrix whose entries x are positive uncorrelated random numbers. If $\log(x)$ is widely distributed over many decades, as in the case of log-normal or log-box distribution, then we say that the matrix is effectively sparse. Sparsity means that the majority of elements are very small compared with the average value.

Irrespective of real-space dimensionality, we regard the index n of the energy levels as labeling the nodes of a one-dimensional (1D) lattice (see Fig. 1) hence the w_{mn} define a 1D resistor network. The inverse resistivity of this network (see Appendix A) is denoted as $w=[[w_{mn}]]$ and has the meaning of diffusion coefficient. In proper units the relation is

$$D_{\mathrm{E}} = \varrho_{\mathrm{E}}^{-2} \times [[w_{mn}]], \tag{2}$$

$$\equiv G\varepsilon^2, \tag{3}$$

where ϱ_{E} is the mean density of states (DOS). The parameter ε represents the RMS amplitude of the driving field: it is the RMS displacement of a wall element if we consider the heating of cold atoms in a trap; it is the RMS voltage if we consider a ring that is driven by an electromotive-force (EMF). We assume here that $w_{mn} \propto \varepsilon^2$, which holds whenever the standard conditions of the Fermi-Golden rule (FGR) are satisfied.

Within the framework of the FGR picture the transitions rates w_{mn} are determined by the matrix elements V_{mn} of the perturbation term in the Hamiltonian. The naive expectation is to obtain the Kubo formula $G=\pi\varrho_{\mathrm{E}}\langle\langle|V_{mn}|^2\rangle\rangle_{\mathrm{a}}$ for the absorption coefficient G. The calculation involves a weighted algebraic average

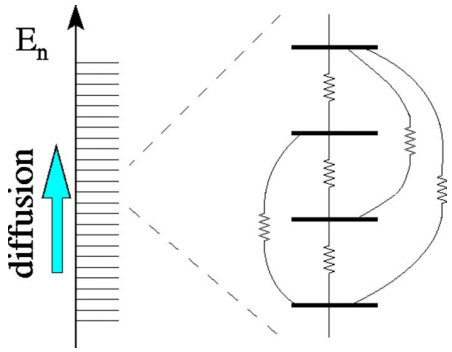

FIG. 1. (Color online) The driving induces transitions between levels E_n of a closed system, leading to diffusion in energy space and, hence, an associated heating. The diffusion coefficient D_{E} can be calculated using a resistor network analogy. Connected sequences of transitions are essential in order to have a nonvanishing result, as in the theory of percolation.

$$\langle\langle |V_{mn}|^2\rangle\rangle_{\rm a} = \int_{-\infty}^{\infty} \langle |V_{mn}|^2\rangle_{\omega} \widetilde{F}(\omega)\frac{d\omega}{2\pi}, \tag{4}$$

where $\widetilde{F}(\omega)$ is a normalized function that describes the spectral content of the driving source and $\langle..\rangle_{\omega}$ is defined as the average value for $(E_m - E_n) \sim \omega$ transitions. A more careful inspection reveals that the Kubo calculation does not apply to the problem as defined above. In order to appreciate the difference we rewrite Eq. (2) as

$$G = \pi \varrho_{\rm E} \langle\langle |V_{mn}|^2\rangle\rangle. \tag{5}$$

The double average notation indicates a *resistor-network* calculation. This SLRT "average" is bounded from above by the algebraic average of Eq. (4) and from below by the corresponding harmonic mean. Later in this paper we adopt a generalized VRH procedure in order to estimate the SLRT average

$$\langle\langle |V_{mn}|^2\rangle\rangle \approx \int_{-\infty}^{\infty} [|V_{mn}|^2]_{\omega} \widetilde{F}(\omega)\frac{d\omega}{2\pi}, \tag{6}$$

where $[..]_{\omega}$ is the typical value for $(E_m - E_n) \sim \omega$ transitions. The notion of typical value will be defined later: it is determined by the size distribution of the matrix elements.

Physically the idea behind SLRT is very simple: in order to have "good" absorption it is essential to have *connected sequences* of transitions. Consequently, if w_{mn} is sparse, the traditional Kubo expression provides gross overestimate because it is based on an algebraic average calculation. Consequently, our interest is to calculate the *ratio* between the SLRT and the LRT conductance, which we define as the SLRT suppression factor

$$g_{\rm SLRT} \equiv \frac{\langle\langle |V_{mn}|^2\rangle\rangle}{\langle\langle |V_{mn}|^2\rangle\rangle_{\rm a}}, \tag{7}$$

where $\langle\langle \ldots \rangle\rangle_{\rm a}$ denotes the usual weighted algebraic average that appears in the Kubo formula. Loosely speaking, if the percentage of *large* in-band elements is $s \ll 1$ then a generalized VRH estimate might lead to a result of the type

$$g_{\rm SLRT} \sim \exp\left(-\frac{\rm const}{s^{\rm power}}\right). \tag{8}$$

A few publications have been devoted to report various partial results that have been obtained using SLRT. The purpose of the present paper is to bridge between SLRT and the traditional literature, to further develop the analytical tools, and to provide elaborated tangible results that hopefully can be tested in actual experiments.

Our main focus concerns the Ohmic conductance $G_{\rm Ohm}$ of small metallic rings, which is related to the G of Eq. (5) via $G_{\rm Ohm} = \varrho_{\rm E} G$, where E is the Fermi energy. Up to a factor, the perturbation matrix consists of the elements v_{mn} of the velocity operator. Accordingly, $G_{\rm Ohm}$ is the LRT or the SLRT average over $|v_{mn}|^2$. Past literature has provided a theory for the conductance in the Debye or adiabatic regimes[16,17] where the FGR picture does not apply. Diffusive rings have been further analyzed[18] in the Kubo regime and later weak-localization corrections have been incorporated[19,20] and verified experimentally.[21–23]

Still neither VRH in real space nor SLRT response in the ballistic regime had been considered in the context of mesoscopic conductance. In Fig. 2 we present some reprocessed numerical results that have been reported in Ref. 12. These numerical results indicate that indeed for both weak and strong disorder the matrix elements of the velocity operator become sparse with $s \ll 1$. As explained in Ref. 12 this is related to the nonergodicity of the eigenstates. In the present paper we would like to present a full analysis of the conductance that starts from the strength of the disorder W as an input. The disorder determines the sparsity s, and then, using RMT modeling and a generalized VRH approximation, leads to some tangible results (Fig. 3) for the SLRT suppression factor $g_{\rm SLRT}$. We also explain how this factor can be measured in an actual laboratory experiment and how *semilinear* response can be distinguished from *linear* response in a way that does not involve any ambiguities.

Outline. Section II motivates the study by introducing the physical model, including subsections that relate to the characterization of metallic rings and their Kubo-Drude conductance. Some more details are given in Appendices B and C. Section III discusses the RMT modeling in general. Section IV briefly reviews the SLRT calculation procedure. Section V elaborates on the generalized VRH approximation. Section VI introduces the analysis of some prototype non-Gaussian ensembles. Some more details are given in Appendices D and E. Section VII discusses the semiclassical theory of the matrix elements that are required for the calculation of the mesoscopic conductance. Section VIII discusses the SLRT calculation in the ballistic regime. Section IX discusses the SLRT calculation in the Anderson localization regime. Section X clarifies the relation between SLRT and the traditional VRH calculation. Section XI questions the possibility to get VRH from proper LRT analysis. Section XII contrasts VRH with nonthermal hopping due to noisy source. Section XIII proposes how to experimentally test SLRT via conductance measurements. Section XIV summarizes the major observations regarding the relation between SLRT, LRT, and VRH.

II. PHYSICAL MODEL

In order to physically motivate the analysis, we consider a particle of mass m in a rectangular box of length $L_x = L$ and width L_y. In one problem, that of Ref. 13, we had assumed Dirichlet boundary conditions and considered the response for vibrations of the wall. In the present paper we assume ring geometry with periodic boundary conditions on L_x and consider the response to EMF. In both cases the Hamiltonian matrix can be written as

$$\mathcal{H} = {\rm diag}\{E_{\boldsymbol{n}}\} + \{U_{\boldsymbol{m},\boldsymbol{n}}\} + f(t)\{V_{\boldsymbol{m},\boldsymbol{n}}\}, \tag{9}$$

where $\boldsymbol{n} = (n_x, n_y)$ labels the unperturbed eigenstates of a clean box/ring, $U(x,y)$ describes the potential floor (either smooth deformation or uncorrelated disorder), and V is the perturbation matrix due to the driving. Given that the energy of the particle is E we define $k_{\rm E} = (2\mathsf{m}E)^{1/2}$ and

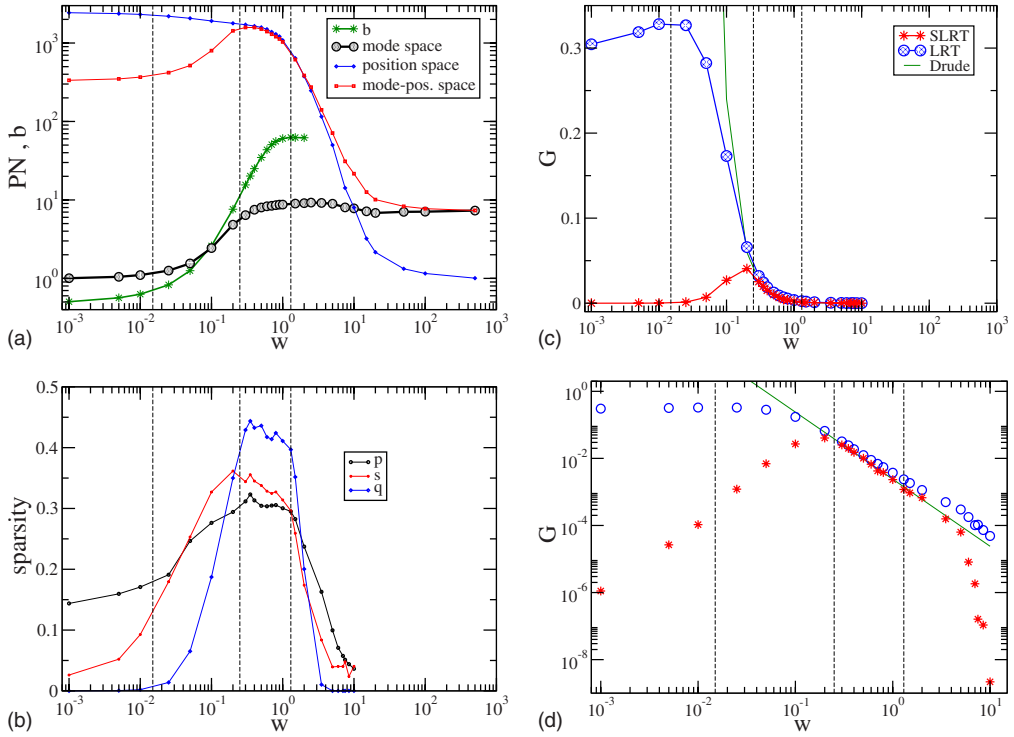

FIG. 2. (Color online) (a) The ergodicity of the eigenstates is characterized by the PN which is calculated in various representations (see Appendix B). The bandwidth b of v_{nm} constitutes another measure for mixing. The clean, ballistic, diffusive, and localization regimes (see Sec. II A) are separated by vertical lines. (b) The sparsity parameters (q, p, and s) that characterize the perturbation matrix v_{nm} are plotted versus the disorder W. (c) The scaled conductance in arbitrary units equals $\langle\langle|v_{mn}|^2\rangle\rangle$. The Drude, the LRT, and the SLRT results are displayed versus the strength of the disorder W. (d) The same plot in the logarithmic scale. We see that in the ballistic regime the SLRT conductance becomes worse as the disorder becomes weaker, in opposition with the Drude expectation.

$v_{\mathrm{E}}=(2E/\mathsf{m})^{1/2}$. The associated number of open modes, i.e., the number of energetically allowed n_y values, is

$$\mathcal{M}=\frac{k_{\mathrm{E}}L_y}{\pi}. \tag{10}$$

The density of states is

$$\varrho_{\mathrm{E}}=\frac{\mathsf{m}}{2\pi}L_xL_y=\mathcal{M}\frac{L}{2v_{\mathrm{E}}}. \tag{11}$$

The static part of the Hamiltonian can be diagonalized and in the new basis the Hamiltonian takes the form

$$\mathcal{H}=\mathrm{diag}\{E_n\}+f(t)\{V_{mn}\}, \tag{12}$$

where E_n are the perturbed energies. The power spectrum $\tilde{S}(\omega)=\varepsilon^2\tilde{F}(\omega)$ of the low-frequency driving $\dot{f}$ is either rectangular with sharp cutoff at some frequency ω_c or exponential

$$\tilde{F}(\omega)=\frac{1}{2\omega_c}\exp\left(-\frac{|\omega|}{\omega_c}\right). \tag{13}$$

We assume that ω_c is small compared with any relevant semiclassical energy scale but larger compared with the mean-level spacing. If the driving is by a thermal source then ω_c can be identified as the *temperature* of the source. This latter point of view is useful in the discussion of the relation between SLRT and VRH.

In the case of an EMF driven ring ε is the RMS of the voltage and the interaction $-f(t)V$ of the particle with the magnetic flux $f(t)$ involves $V=-(e/L)v$, where v is the velocity operator. Hence

$$V_{mn}=\frac{e}{L}v_{mn}=\frac{e}{L}(E_m-E_n)^2r_{mn}, \tag{14}$$

where r is the position operator. Thus an LRT or an SLRT study of the conductance reduces to a study of the statistical properties of the so-called dipole-matrix elements. These statistical properties become nontrivial for either weak or strong disorder and they should be described by a *non-Gaussian ensemble. The following subsections contain some extra details regarding metallic rings and can be skipped in first reading.*

A. Characterization of metallic rings

A metallic ring is characterized by the Fermi velocity v_{E}, the Fermi momentum k_{E}, the length of the ring L, its width $L_\perp$, and the strength of the disorder W. The latter determines the mean-free path ℓ. The Fermi velocity v_{E} can be regarded as providing conversion between "length" and "time" hence we have two dimensionless parameters: the number of open modes $\mathcal{M}\sim(k_{\mathrm{E}}L_\perp)^{d-1}$ and the degree of disorder L/ℓ. For-

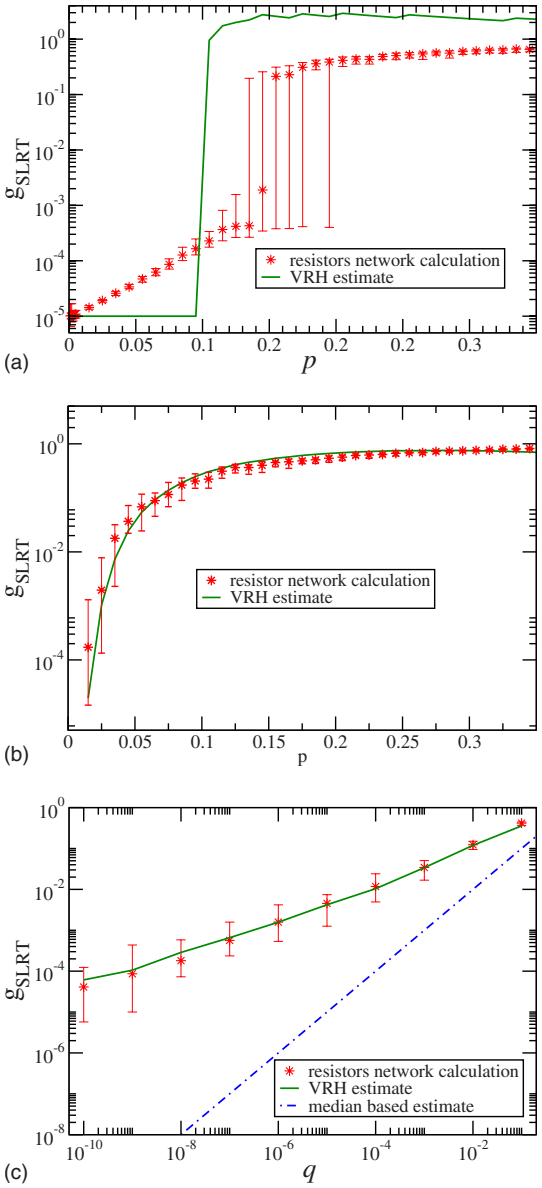

FIG. 3. (Color online) The SLRT suppression factor g_{SLRT} versus the sparsity parameter (p or q) for bimodal distribution with rectangular power spectrum (upper panel); (log-box distribution with exponential power spectrum (middle panel); and log-normal distribution with rectangular power spectrum (lower panel). The resistor network and the VRH calculation were done for 100 realizations of 256×256 matrices with $b=10$. In the bimodal case VRH is not satisfactory. In the log-normal case the VRH result is contrasted with the naive median based estimate.

mally there is a third independent dimensionless parameter $k_{\mathrm{E}}L$ but we assume it to be very large compared with $\mathcal{M}$ and hence it has no significant role in the analysis below. The various regimes in this problem are described below and in the diagram of Fig. 4: (a) clean ring $(L/\ell)<1/\mathcal{M}$, (b) ballistic ring $(L/\ell)<1$, (c) diffusive ring $(L/\ell)>1$, and (d) Anderson regime $(L/\ell)>\mathcal{M}$.

It is a matter of terminology whether to exclude the "clean" case from the ballistic regime and the "Anderson" case from the "diffusive" regime. The time scale which is

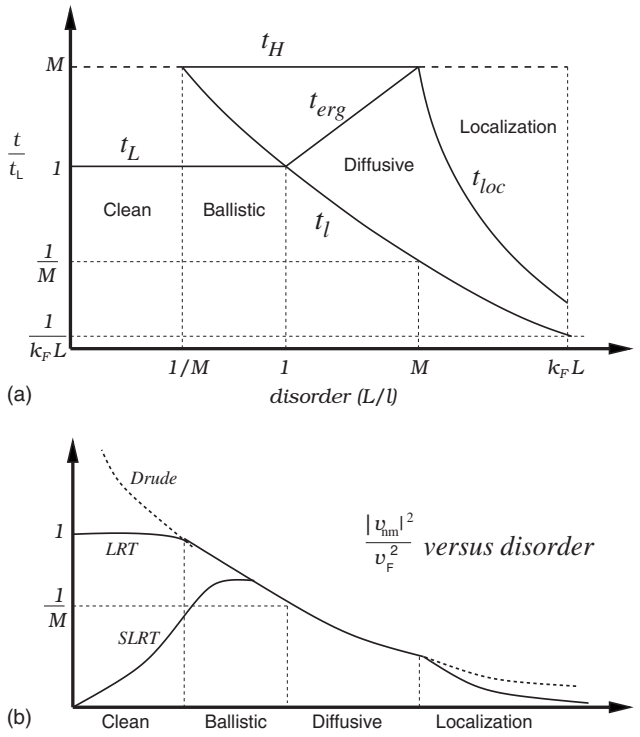

FIG. 4. Upper panel: time scales versus the disorder strength (see Sec.II A). Lower panel: schematic illustration that sketches the dependence of the dc conductance on the strength of the disorder. It should be regarded as a caricature of Fig. 2.

associated with the length of the rings is $t_L=L/v_{\mathrm{E}}$, the time scale which is associated with the scattering is mean-free time $t_\ell=\ell/v_{\mathrm{E}}$, and the time scale which is associated with quantum recurrences is the Heisenberg time $t_{\mathrm{H}}=\mathcal{M}t_L$. If the very strong condition $t_\ell>t_{\mathrm{H}}$ is satisfied then we call it "clean ring" meaning that the disorder does not mix the levels and its effect can be treated using first-order perturbation theory.

More generally we define the ballistic regime by the condition $\ell\gg L$. If the disorder is strong enough then the levels are mixed nonperturbatively leading to genuine semiclassical ballistic behavior with

$$t_L<t_\ell<t_{\mathrm{H}}\quad[\text{Ballistic}]. \tag{15}$$

In the diffusive regime it is meaningful to define the ergodic (Thouless) time via the relation $D_0t\sim L^2$ where $D_0=v_{\mathrm{E}}\ell$, leading to $t_{\mathrm{erg}}=(L/\ell)t_L$. In the strict diffusive regime we have

$$t_\ell<t_{\mathrm{erg}}<t_{\mathrm{H}}\quad[\text{Diffusive}]. \tag{16}$$

If we have (formally) $t_{\mathrm{erg}}>t_{\mathrm{H}}$ then there is no ergodization but rather a strong (Anderson) localization effect shows up. This means that one expects a breaktime t_{loc} that marks a crossover from diffusion to saturation. A standard argumentation (see below) gives the estimate $t_{\mathrm{loc}}=\mathcal{M}^2t_\ell$. One observes that in the Anderson regime

$$t_\ell<t_{\mathrm{loc}}<t_{\mathrm{H}}\quad[\text{Anderson}]. \tag{17}$$

The self-consistent determination of ℓ_ξ originates in old studies of dynamical localization in the quantum kicked rotator problem. Assuming that the localization length is ℓ_ξ, the lo-

cal level spacing is $\Delta_\xi = \pi v_E/\mathcal{M}\ell_\xi$, and hence the breaktime is $t_{\rm loc}=2\pi/\Delta_\xi$. The self-consistency condition is $Dt_{\rm loc}\sim \ell_\xi^2$, leading to

$$\ell_\xi \approx \mathcal{M}\ell. \tag{18}$$

The identification of the Anderson regime is via the requirement $L>\ell_\xi$. Finally we note that the largest meaningful value of disorder is $(L/\ell)=k_E L$, for which ℓ equals the Fermi wavelength.

B. Kubo-Drude conductance

The coefficient G is defined through the expression $D_E=G\varepsilon^2$ for the one-particle diffusion coefficient, where ε is the RMS of the voltage. Taking Eq. (14) into account it follows that

$$G = \pi\varrho_E \times \left(\frac{e}{L}\right)^2 \langle\langle |v_{mn}|^2\rangle\rangle. \tag{19}$$

The Ohmic conductance is defined as the coefficient in the Joule formula $G_{\rm Ohm}\epsilon^2$ for the rate of energy absorption. For an $\mathcal{N}$ particle system at temperature T it is related to G via a general diffusion-dissipation relation

$$G_{\rm Ohm} = \varrho_E \times G \quad [\text{Fermi}], \tag{20}$$

$$G_{\rm Ohm} = (\mathcal{N}/T) \times G \quad [\text{Boltzmann}]. \tag{21}$$

The Boltzmann occupation applies to semiconductors, where $\mathcal{N}/L$ is the density of the particles. For Fermi occupation ϱ_E/L is the density of states at the Fermi energy per unit length of the ring and it is in agreement with the Boltzmann result if we regard $\mathcal{N}=\varrho_E T$ as the effective number of carriers.

In the case of a diffusive ring it makes sense to relate the diffusion in energy to the diffusion in real space. This relation holds in the strict dc limit. Using the Einstein relation $G_{\rm Ohm}=(e/L)^2\varrho_E\mathcal{D}$ we deduce that

$$\mathcal{D} = \pi\varrho_E \times \langle\langle |v_{mn}|^2\rangle\rangle_{\omega_c\sim 0}. \tag{22}$$

It is important to keep in mind that for a disconnected ring $\mathcal{D}=0$ but still we can get from Eq. (22) a nonzero result $G\neq 0$ because the spectral content of the driving may have a finite cut-off frequency ω_c.

The reference case for all our calculations is the Drude result which is obtained for a diffusive ring in the semiclassical approximation (see Appendix C). Assuming a mean-free path ℓ we write the Drude result as

$$G_{\rm Drude} = \frac{e^2}{2\pi\hbar}\mathcal{M}\frac{\ell}{L}, \tag{23}$$

where L is the length of the ring and $\mathcal{M}$ is the number of open modes (proportional to its cross section).

The quantum Kubo calculation gives in leading order the same result as Drude: this is well known and obviously it is also a by-product of the subsequent analysis. One observes that the there is a *maximum* Kubo conductance which is obtained in the limit of a clean ring, i.e., for $\ell/L=\mathcal{M}$. For completeness we note that for a ring with transmission g_0, the following formal identification applies (see Appendix C):

$$\frac{\ell}{L} \Leftrightarrow \frac{g_0}{1-g_0} \quad [<\mathcal{M}]. \tag{24}$$

This makes transparent the relation between the Drude and the Landauer results.

In later sections our interest is to find the SLRT suppression factor $g_{\rm SLRT}$ that determines the ratio $G_{\rm Ohm}/G_{\rm Drude}$. For this purpose we have to find not only the average value of $|v_{mn}|^2$ but also their statistics.

III. RMT MODELING

Regarded as a random matrix V_{mn} is characterized by its band profile and by the size distribution of its elements. The standard RMT modeling due to Wigner assumes either full or banded matrix with elements that are taken out of a Gaussian distribution. But our interest is in circumstances where the size distribution is wide, i.e., the elements of $|V_{mn}|^2$ look like realizations of a random variable x whose logarithmic value $[\log(x)]$ is distributed over several decades.

In practice the $|V_{mn}|^2$ of a physical model does not have an idealized flat band profile. Consequently, we write

$$|V_{mn}|^2 = \boldsymbol{X}_{mn} \times \widetilde{C}(E_m - E_n), \tag{25}$$

where $\widetilde{C}(\omega)$ describes the band profile of the matrix. Numerically the band profile is obtained by averaging separately each diagonal $[(n-m)=\text{const}]$ of the matrix and plotting the result against $\omega=(E_m-E_m)\approx(n-m)\varrho_E^{-1}$.

The question arises, given a matrix A_{mn} that consist of real non-negative elements, how to numerically define its bandwidth b, its sparsity s, and the associated distribution $\rho(x)$ of its in-band elements. For the purpose of this paper it was important to adopt an unambiguous definition of s, which loosely speaking is defined as the percentage of large in-band elements. The suggested procedure below is based on the participation number (PN) concept. The PN of a set $\{x_i\}$ is defined as

$$\text{PN} = \frac{(\sum_i x_i)^2}{\sum_i x_i^2} \tag{26}$$

and reflects the number of the large elements. The procedure to determine s and b goes as follows: (1) we consider a truncated A_{mn} within the energy window of interest. (2) We calculate the band profile by averaging separately the elements over each diagonal. (3) We construct an untextured matrix A^{utx}_{mn} by performing random permutations of the elements along the diagonals. (4) We construct a uniformized matrix A^{unf}_{mn} by replacing each of the elements of a given diagonal by their average. (5) We calculate the participation number of the elements in A_{mn}. This is like counting the number of large elements. (6) We calculate the participation number of the elements in A^{unf}_{mn}. This is like counting the number of in-band elements. (7) The ratio of the numbers that have been calculated in the previous step is defined as

the sparsity s. (8) Likewise the bandwidth b is deduced from the number of in-band elements.

The size distribution $\rho(x)$ refers to the in-band elements. In order to verify that A_{mn} is really like a random matrix we perform the SLRT calculation (see Sec. IV) once on A_{mn} and once on the untextured matrix A^{utx}_{mn}. If the results are significantly different we say that texture, i.e., the nonrandom arrangement of the large elements, is important. The RMT analysis in this paper assumes that texture is not too significant.

In particular, we are interested in the bimodal, log-box, and log-normal ensembles. The *bimodal distribution* is characterized by the probability p of having a large value $x=x_1$, otherwise $x=x_0 \ll x_1$, hence

$$\rho(x) = (1-p)\,\delta(x-x_0) + p\,\delta(x-x_1). \tag{27}$$

In the case of a *log-box distribution* the variable $\ln(x)$ has uniform distribution within $[x_0,x_1]$, hence

$$\rho(x) = \frac{1}{\ln(x_1/x_0)}\frac{1}{x}. \tag{28}$$

In the case of a *log-normal distribution* the variable $\ln(x)$ has a Gaussian distribution with mean $\ln(x_0)$ and standard deviation σ, hence

$$\rho(x) = \frac{1}{\sqrt{2\pi}\sigma}\frac{1}{x}e^{-[\ln(x/x_0)]^2/2\sigma^2}. \tag{29}$$

A random variable can be characterized by the algebraic, geometric and harmonic averages

$$\langle\langle x\rangle\rangle_{\mathrm{a}} = \langle x\rangle, \tag{30}$$

$$\langle\langle x\rangle\rangle_{\mathrm{g}} = \exp[\langle \ln x\rangle], \tag{31}$$

$$\langle\langle x\rangle\rangle_{\mathrm{h}} = [\langle 1/x\rangle]^{-1}. \tag{32}$$

The sparsity of a matrix that consists of uncorrelated realizations can be characterized by a parameter s or optionally by the parameters p and q that are defined as follows:

$$s = \langle x\rangle^2/\langle x^2\rangle, \tag{33}$$

$$p = \mathrm{Prob}(x > \langle x\rangle), \tag{34}$$

$$q = \langle\langle x\rangle\rangle_{\mathrm{median}}/\langle x\rangle. \tag{35}$$

By this definition p is the fraction of the elements that are larger than the algebraic average and q is the ratio between the median and the algebraic average. We regard a matrix as sparse if $s \ll 1$ or equivalently if $p \ll 1$ or $q \ll 1$.

IV. SLRT CALCULATION

As in the standard derivation of the Kubo formula, also within the framework of SLRT, the leading mechanism for absorption is assumed to be FGR transitions. These are proportional to the squared matrix elements $|V_{mn}|^2$. The power spectrum of $\dot{f}(t)$ is $\widetilde{S}(\omega)=\varepsilon^2\widetilde{F}(\omega)$, where ε is the RMS value of the driving amplitude. Consequently, the FGR transition rates are

$$w_{mn} = 2\pi\frac{|V_{mn}|^2}{(E_m-E_n)^2}\widetilde{S}(E_m-E_n). \tag{36}$$

From Eqs. (1), (25), and (36) one deduces the identification

$$\widetilde{B}(\omega) = \frac{2\pi}{\omega^2}\widetilde{C}(\omega)\widetilde{S}(\omega). \tag{37}$$

The inverse resistivity of the network has the meaning of diffusion coefficient and from the definition of G in Eq. (3) we deduce the SLRT *formula* Eq. (5) with

$$\langle\langle |V_{mn}|^2\rangle\rangle \equiv \left[\left[2\varrho_{\mathrm{E}}^{-3}\frac{|V_{mn}|^2}{(E_m-E_n)^2}\widetilde{F}(E_m-E_n)\right]\right]. \tag{38}$$

This should be contrasted with the *Kubo formula* that involves an algebraic instead of SLRT average

$$\langle\langle |V_{mn}|^2\rangle\rangle_{\mathrm{a}} \equiv \left[\varrho_{\mathrm{E}}^{-1}\sum_m |V_{mn}|^2\widetilde{F}(E_m-E_n)\right]_{\mathrm{avr}} \tag{39}$$

with average over the reference state n. The average is done over all the states whose energy E_n is within the energy window of interest. In the metallic context it is an average around the Fermi energy.

It is a simple exercise to verify that if all the matrix elements are the same, say $|V_{mn}|^2=c_0$, then $\langle\langle |V_{mn}|^2\rangle\rangle=c_0$ too. Also it is a simple exercise to verify that the SLRT formula coincides with the Kubo formula if there is no randomness, i.e., if $|V_{mn}|^2$ is a well-defined function of E_m-E_n. But if the matrix is structured or sparse then

$$\langle\langle |V_{mn}|^2\rangle\rangle_{\mathrm{h}} < \langle\langle |V_{mn}|^2\rangle\rangle \ll \langle\langle |V_{mn}|^2\rangle\rangle_{\mathrm{a}}. \tag{40}$$

If only neighboring levels are coupled then "adding resistors in series" (see Appendix A) implies equality of the SLRT average to the harmonic average

$$\langle\langle |V_{mn}|^2\rangle\rangle_{\mathrm{h}} \equiv \left[\varrho_{\mathrm{E}}^{-1}\sum_m \frac{1}{|V_{mn}|^2}\widetilde{F}(E_m-E_n)\right]^{-1}_{\mathrm{avr}}. \tag{41}$$

More generally the harmonic average is a gross underestimate. A generalized VRH scheme that we present in Sec. V provides the following approximation for the SLRT average:

$$\langle\langle |V_{mn}|^2\rangle\rangle \sim [\varrho_{\mathrm{E}}^{-1}[|V_{mn}|^2]_\omega\widetilde{F}(\omega)]_{\max}, \tag{42}$$

where the maximum is calculated with respect to ω. The typical value $|V_{mn}|^2_\omega$ for ω transitions will be defined precisely in Sec. V and it reflects the size distribution of the matrix elements. The VRH integral Eq. (6) is an *ad hoc* refinement of Eq. (42) that better interpolates with the LRT result and therefore it is advantageous for actual numerical analysis. Further analysis (see Sec. VI) indicates that compared with the weighted harmonic average $\langle\langle |V_{mn}|^2\rangle\rangle_{\mathrm{h}}$, of Eq. (41), the corresponding geometric average $\langle\langle |V_{mn}|^2\rangle\rangle_{\mathrm{g}}$ provides in most cases a better lower bound.

V. GENERALIZED VRH APPROXIMATION

A 1D network is characterized by its inverse resistivity $w=[[w_{mn}]]$. Inspired by Ref. 6, the inverse resistivity can be

estimated analytically by finding the maximum threshold such that the elements $w_{mn} > w_0$ form a *connected cluster*. This leads in the present context to a generalized VRH estimate which we explain in the following paragraph.

Given a threshold w and truncating the bandwidth at ω, a sufficient condition for having a connected cluster is to have at least one nonzero element per ω segment

$$\varrho_E \omega \times \text{Prob}[x\tilde{B}(\omega) > w] \quad \text{larger than unity}. \tag{43}$$

We define the typical value x_ω for range ω transitions via the relation

$$\varrho_E \omega \times \text{Prob}(x > x_\omega) \sim 1 \tag{44}$$

and rewrite the condition for having a connected cluster in the following suggestive form:

$$w < x_\omega \tilde{B}(\omega). \tag{45}$$

Thus an underestimate for the diffusion coefficient is $D \sim w\omega^2$ based on hopping rate w with steps ω. The VRH estimate is based on the idea to optimize this underestimate with respect to ω and w, leading to

$$D_E \sim [\omega^2 x_\omega \tilde{B}(\omega)]_{\max}, \tag{46}$$

where the maximum is with respect to the hopping range ω. In the FGR context this leads to Eq. (42) with

$$[|V_{mn}|^2]_\omega \equiv x_\omega \tilde{C}(\omega). \tag{47}$$

VI. SLRT ANALYSIS OF SOME PROTOTYPE NON-GAUSSIAN ENSEMBLES

In this section we derive results for SLRT suppression factor g_{SLRT} for the bimodal, for the log-box, and for the log-normal ensembles. The bimodal distribution is the simplest for pedagogical purpose while the log-box and log-normal ensembles are of greater physical relevance. The main results are summarized below while further details of the calculation are given in Appendices D and E. Figure 3 presents the outcome of numerical analysis that tests the accuracy of the generalized VRH approximation. In later sections we shall see that the presented results are of relevance to the study of conductance in the limits of strong and weak disorders.

The bimodal ensemble. In this case there is a minority of large elements ($x=x_1$) that have percentage $p \ll 1$ and a majority of small elements ($x=x_0 \ll 1$) that have percentage $1-p$. Consequently, the typical value for ω transition has a percolationlike crossover from $x_\omega = x_0$ to $x_\omega = x_1$ at the frequency $\omega = (\varrho_E p)^{-1}$. Therefore

$$g_{\text{SLRT}} \sim \begin{cases} q\tilde{F}(\omega \sim 0) & bp < 1 \\ (1/p)\tilde{F}[1/(\varrho_E p)] & bp > 1, \end{cases} \tag{48}$$

where $b = \varrho_E \omega_c$ is the dimensionless bandwidth and $q \approx x_0/(px_1)$. The first expression reflects the possibility of *majority dominance* of the small elements while the second expression reflects the possibility of *minority dominance* of the large elements. Note that the VRH approximately implicitly assumes that $F(\omega)$ drops (say) exponentially such that $g_{\text{SLRT}} \ll 1$, otherwise the result cannot be trusted.

The log-box ensemble. In this case the probability distribution of $\ln(x)$ is uniform over many decades. Therefore, it is reasonable to assume that the result for g_{SLRT} is *minority dominated*. It is natural to characterize the log-box distribution of Eq. (28) by a parameter $\tilde{p} = [\ln(x_1/x_0)]^{-1}$, and to realize that the percentage of large elements is $p \approx -\tilde{p} \ln \tilde{p}$. Note that the corresponding sparsity parameter is $s \approx 2\tilde{p}$. The typical value for ω transitions is

$$x_\omega \approx \frac{1}{\tilde{p}} \exp\left(-\frac{1}{\tilde{p}\varrho_E \omega}\right) \langle\langle x \rangle\rangle_a \tag{49}$$

and the VRH estimate, assuming an exponential bandprofile gives

$$g_{\text{SLRT}} \sim \frac{1}{\tilde{p}} \exp\left[-2\left(\frac{1}{\tilde{p}b}\right)^{1/2}\right]. \tag{50}$$

Note the similarity, as well as the subtle difference, compared with the bimodal minority dominance expectation.

The log-normal ensemble. In this case the probability distribution of $\ln(x)$ is a Gaussian centered around the median. Therefore, it is reasonable to assume that the result for g_{SLRT} is *majority dominated*. It is natural to characterize the log-normal distribution of Eq. (29) by a parameter q, which is defined as the ratio of the median to the algebraic average. Note that the corresponding sparsity parameter is $s = q^2$. The VRH calculation gives the result

$$g_{\text{SLRT}} \sim q \exp\left\{\left[\text{factor} \times \ln\left(\frac{1}{q}\right)\ln(b)\right]^{1/2}\right\}, \tag{51}$$

where the factor is determined by the band profile (it is 2 for an exponential bandprofile and 4 for a rectangular bandprofile). Note that $g_{\text{SLRT}} \sim q$ is the simplest guess that reflects the majority dominance expectation.

VII. SEMICLASSICAL ESTIMATE OF THE OHMIC CONDUCTANCE

There is a well-established semiclassical procedure to deduce the algebraic average of the matrix elements $|V_{mn}|^2$ that correspond to the energy difference $\omega = E_m - E_n$ from the associated correlation function $\langle V(t)V(0)\rangle$. We would like to apply this procedure in order to estimate the conductance of metallic rings. Hence our interest is in the matrix elements of the velocity operator. The semiclassical estimate is based on the following observation:

$$\langle\langle |v_{mn}|^2 \rangle\rangle_\omega = \frac{1}{2\pi\varrho_E} \text{FT}[\langle v(t)v(0)\rangle], \tag{52}$$

where FT stands for Fourier transform. The velocity-velocity correlation function can be obtained via a time derivative of the time-dependent diffusion coefficient $\mathcal{D}(t)$, which is the time derivative of the spreading $\langle [r(t)-r(0)]^2 \rangle$.

In the Drude "classical" approximation one assumes an exponential decay of the velocity-velocity correlation func-

tion and long-time diffusion $\mathcal{D}_0$ as determined by the mean-free path (see Appendix C). This is satisfactory in the ballistic and diffusive regimes, and leads to a Lorentzian line shape

$$\langle\langle |v_{mn}|^2\rangle\rangle_\omega = \frac{1}{b} v_{\mathrm{E}}^2 \frac{R(\omega)}{1+(t_\ell \omega)^2}, \tag{53}$$

where $b=\mathcal{M}L/\ell$ is the dimensionless bandwidth of the matrix and $R(\omega)=1$.

But in the Anderson regime we know that there is a breaktime t_{loc} that marks the crossover form diffusion to localization and hence for a bulk system formally $\mathcal{D}=0$. Consequently, the FT consideration of Eq. (53) leads to the conclusion that in the limit $\omega \to 0$ the band profile should vanish if the system is infinite. The simplest reasoning[9] leads to the expression

$$R(\omega) = \frac{L}{\ell_\xi} e^{-2L/\ell_\xi} + \frac{1}{1+(t_{\mathrm{loc}}\omega)^{-2}}, \tag{54}$$

where the first term reflects the finite length of the system and it is deduced using Eq. (24). We shall see in Sec. IX, using a different more refined approach, that the second term is almost correct. Namely, the more careful analysis using the Mott's picture predicts that the small frequency dependence is not $[\omega]^2$ but $[\omega \log(\omega)]^2$.

The quantum-mechanical analysis should further take into account (i) the statistics of the levels and (ii) the fluctuations in the size of the matrix elements. The former implies wiggles in $R(\omega)$ for small frequencies while the latter imply that the average size of the matrix elements does not necessarily reflect their typical value. Figure 4 summarizes the dependance of the matrix elements on the disorder.

It should be clear that we always have the sum rule

$$\sum_m |v_{mn}|^2 = v_{\mathrm{E}}^2. \tag{55}$$

In the clean ring limit the sum is dominated by the diagonal or near diagonal element while all the other off-diagonal elements become negligible. Still the estimate Eq. (53) for the other off-diagonal matrix elements remains valid and can be justified using first-order perturbation theory. If the ring is ballistic (but not clean) then the semiclassical estimate Eq. (53) implies that the large elements form a band of width $b>1$. If the matrix is not sparse then the contribution of all the b in-band elements to the sum rule is comparable. But if (say) only a fraction $s \ll 1$ of of elements are contributing then their typical value $|v_{mn}|^2 \sim \langle\langle |v_{mn}|^2\rangle\rangle_\omega / s$ is much larger compared with the average. We shall come back to a more detailed discussion of "sparsity" in the subsequent sections.

In the diffusion regime $R(\omega)$ mainly reflects the level-spacing statistics of the individual levels, which is a "microscopic" effect that leads to small weak-localization corrections that had been studied extensively.[19,20] But in the strong-localization Anderson regime the implication of the breaktime leads to the dramatic conclusion that $R(\omega) \ll 1$ for $\omega \ll \Delta_\xi$, where the local level spacing Δ_ξ is *not* related to the volume-dependent microscopic level spacing $\varrho_{\mathrm{E}}^{-1}$ but to the strength of the disorder.

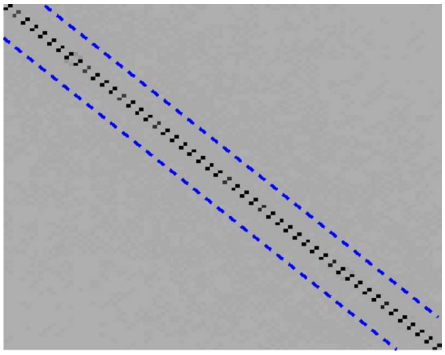

(a)

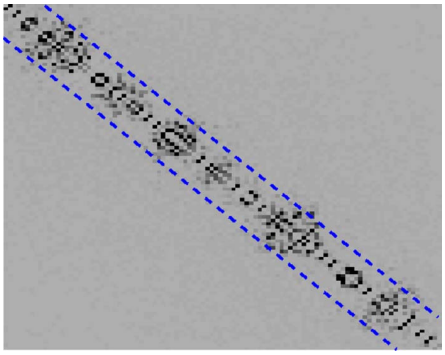

(b)

FIG. 5. (Color online) Images of 100×100 pieces of the perturbation matrix $|v_{nm}|^2$ in the clean ($W=0.001$) and ballistic ($W=0.1$) regimes. The dashed lines correspond to the ballistic bandwidth $\mathcal{M}=10$, which is associated with the time scale t_L.

In the Anderson regime it is evident that $\langle\langle |v_{mn}|^2\rangle\rangle_\omega$ is not the typical value of the matrix elements. Roughly speaking and disregarding the ω dependence

$$|v_{mn}| \sim \frac{v_{\mathrm{E}}}{\mathcal{M}} \exp\left(-\frac{|r|}{\ell_\xi}\right), \tag{56}$$

where $r \in [0, L/2]$ has a uniform distribution, implying a log-box distribution for the size of the elements. Accordingly, the typical value is exponentially small in the length of the ring while the average is determined by the small percentage of large elements and comes out in agreement with the semiclassical estimate. In Sec. IX we further elaborate on the statistical analysis of the sparsity in the Anderson regime using the Mott's picture of localization.

VIII. RMT STATISTICS IN THE BALLISTIC REGIME

For zero disorder $W=0$ each energy level is doubly degenerate in the basis of real eigenfunctions and the couplings are pairwise, i.e., the matrix element between states of different energies is zero. See Fig. 5. Consequently, the EMF cannot induce connected sequences of transitions and the SLRT conductance should be zero. The nonzero elements of the perturbation matrix according to the sum rule [Eq. (55)] are $|v_{nm}|=v_{\mathrm{E}}$. The algebraic average of the near diagonal elements equals this value (of the large size elements) multiplied by their percentage $p_0 \approx 1/2$. Consequently

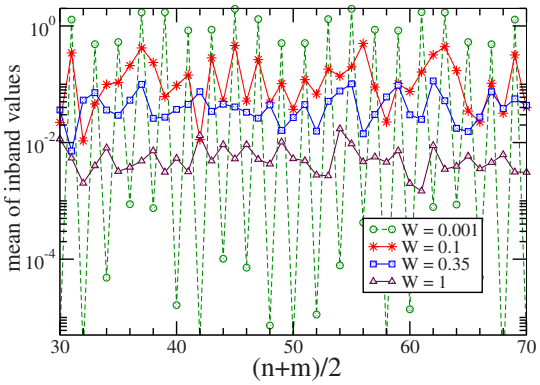

FIG. 6. (Color online) The mean of the in-band values of the $|v_{nm}|^2$ matrix elements as a function of $(n+m)/2$ for different values of disorder. The pronounced modulation in the ballistic regime is an indication for texture.

$$\langle\langle |v_{nm}|^2\rangle\rangle_{\rm a} \approx \frac{1}{2}v_{\rm F}^2. \tag{57}$$

For sufficiently small W these large-size matrix elements are not affected, and therefore, the algebraic average stays the same. Consequently, in the clean-ring limit the Kubo conductance is formally finite and attains the maximal value as discussed with regard to Eq. (23).

In the clean as well as in the whole ballistic regime the algebraic average $\langle\langle |v_{mn}|^2\rangle\rangle_\omega$ does not reflect the sparsity and the textures of the v_{mn}. See Figs. 6 and 7. When we look on the image of v_{mn} the immediate reaction is to be impressed by the *texture* and therefore we discuss it first. Subsequently, we discuss the *sparsity*, which is in fact more significant for the analysis.

The mean DOS of the two-dimensional ring is $\varrho_{\rm E}$. But $L_x \gg L_y$ and, therefore, it is not uniform. As the disorder W is increased, levels start to mix first in the high DOS regions, and only later in the low DOS regions. This is the reason for the appearance of textures. Let us be more detailed about the

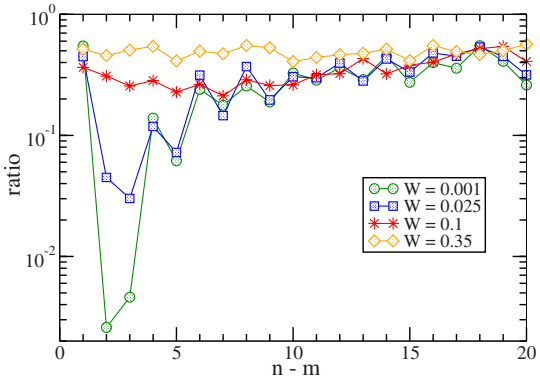

FIG. 7. (Color online) The ratio between the typical value $[|v_{nm}|^2]_\omega$ and the average value $\langle|v_{nm}|^2\rangle_\omega$ that enter into Eqs. (6) and (4), respectively. In this plot the typical value is the median. The horizontal axis is n-m corresponding to the scaled frequency $\varrho_{\rm E}\omega$. Note that both $[|v_{nm}|^2]_\omega$ and $\langle|v_{nm}|^2\rangle_\omega$ when plotted as a function of ω have a Lorentzian line shape.

nonuniformity of the DOS. As a function of the energy E each time that a mode is opened the DOS is boosted. Consequently, $\varrho_{\rm E}$ is modulated. This systematic modulation is associated with the opening of a single additional mode at every threshold energy and, therefore, scales like $1/\mathcal{M}$. On top there is an additional weaker nonsystematic modulation of the DOS because the levels of low-density modes add up to the levels of the high-density modes. It is the latter type of modulation which is reflected in Figs. 5 and 6, where the energy window contains throughout exactly ten open modes.

In the regions where levels are not yet mixed one can estimate the majority of small matrix elements using first-order perturbation theory: Due to the first-order mixing of the levels, the typical overlap $|\langle \boldsymbol{m}|n\rangle|$ between perturbed and unperturbed states is

$$|\langle \boldsymbol{m}|n\rangle| = \left|\frac{U_{\boldsymbol{nm}}}{E_{\boldsymbol{n}} - E_{\boldsymbol{m}}}\right|. \tag{58}$$

The typical size of a small v_{nm} element is the multiplication of this overlap, calculated for $(E_{\boldsymbol{n}}-E_{\boldsymbol{m}}) \sim \varrho {\rm E}^{-1}$, by the size of the nonzero $|v_{\boldsymbol{nm}}|=v_{\rm E}$ element. As *a priori* expected this first order estimate gives a result that agrees with the semiclassical estimate Eq. (53) evaluated for $\omega \sim \varrho_{\rm E}^{-1}$. Thus

$$q \approx \mathcal{M}\frac{L}{\ell} \quad \text{[for white disorder]}. \tag{59}$$

Above some threshold, first-order perturbation theory fails everywhere, meaning that nonperturbative mixing takes place in any energy. Still, due to the modulation of the DOS, the mixing range is wider in the near-thresholds energies and therefore the matrix elements there are *smaller*. So now we have the opposite situation, of *high*-DOS *bottleneck* instead of *low*-DOS *bottleneck*.

One easily observes that the crossover from weak disorder (that features separated mixing regions and low-DOS bottlenecks) to stronger disorder (that features a connected mixing region and high-DOS bottlenecks) is associated with the crossover from the clean to the ballistic regime. The width of the crossover region depends on the nonuniformity of the DOS and therefore diminishes as the number of open modes becomes large.

The above reasoning implies that the texture might be important in the SLRT analysis primarily in the clean ring regime but much less in the genuine ballistic regime. But what about sparsity? Using the FGR in order to determine the energy range over which mixing takes place, we obtain an estimate for the bandwidth of the perturbation matrix

$$b = 2\pi\varrho_{\rm E}^2|U_{nm}|^2 \approx \mathcal{M}\frac{L}{\ell}, \tag{60}$$

which agrees with the semiclassical estimate. But in the ballistic regime $b<\mathcal{M}$. This means that a typical eigenstates cannot occupy all the $\mathcal{M}$ open modes. Rather it has there a participation number $M=b$ smaller than $\mathcal{M}$ (see Fig. 2). Consequently, we deduce that the sparsity of the perturbation matrix is

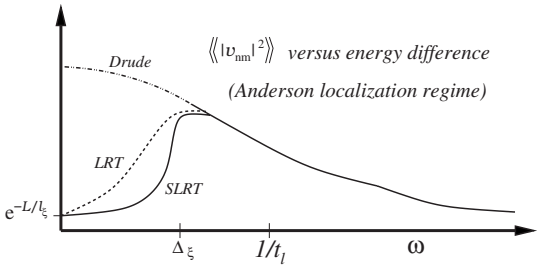

FIG. 8. Schematic plot that illustrates the dependence of the average and the typical values of the matrix elements on the energy separation ω. These are labeled as "LRT" and "SLRT," respectively, and compared with the semiclassical (Drude) expectation. The plot refers to the Anderson regime. For a corresponding numerical illustration in the ballistic regime see Fig. 7.

$$s = \frac{M}{\mathcal{M}} \approx \frac{L}{\ell} \equiv q^2 \quad \text{[for smooth disorder]}, \tag{61}$$

where the identification of s with q^2 is based on the assumption of a log-normal distribution which we further discuss in the next paragraph. Unlike the texture, the sparsity persists via the whole ballistic regime up to the border with the diffusive regime. For this reason we regard the sparsity as the main ingredient in the SLRT analysis.

The discussion of sparsity in the previous paragraph is somewhat meaningless unless one specifies the distribution to which s refers. At this point of the discussion it is essential to distinguish between *white disorder* for which the scattering is isotropic and *smooth disorder* for which only nearby modes are coupled (small scattering angle). The latter applies if the potential floor within the ring has a smooth rather than erratic variation with respect to the Fermi wavelength. Assuming smooth disorder it becomes essential to extend the perturbation theory of Appendix B beyond first order. It makes sense to say that $|v_{mn}| \sim |W|^r$, where the order r is bounded by $\mathcal{M}$. Therefore, $\log(|v_{mn}|)$ has some bounded distribution which can be approximated (say) by a Gaussian. It follows that a log-normal ensemble should be qualitatively appropriate to describe the statistical properties. It follows that $g_{\rm SLRT}$ can be estimated using Eq. (51) with the q of Eq. (61). On the other hand in the case of white disorder $|v_{mn}|$ of the majority elements is given by *first*-order perturbation theory and then one should use Eq. (51) with the q of Eq. (59).

IX. RMT STATISTICS IN THE ANDERSON REGIME

The simplest picture of localization regards the lattice as composed of segments of size ℓ_ξ and assumes that each eigenstate is well localized in one of this segments. Accordingly, non-negligible matrix elements are only between states that reside in the same space segment. We shall refer to this as the "zero-order" picture. Taking into account that the matrix element of the velocity operator are related to those of the position operator by the relation $|v_{mn}|^2 = \omega^2 |r_{mn}|^2$, it follows that $R(\omega) \sim (\omega/\Delta_\xi)^2$ in consistency with the semiclassical reasoning of Sec. VII, which is summarized by Fig. 8.

In order to refine this picture we use the following procedure due to Mott. The zero-order basis is determined by ignoring the possibility of the particle to hop from segment to segment. In order to find the "true" eigenstates we have to take into account the residual interaction. It is reasonable to postulate that if the distance between two zero-order eigenstates is $r = r_n - r_m$ then the residual interaction is

$$\kappa = \Delta_\xi \exp(-|r|/\ell_\xi). \tag{62}$$

The prefactor is the natural educated guess, which is later justified (see below) by requiring consistency with the semiclassical result.

If we have two zero-order eigenstates that do not reside at the same segment but have distance r in space and distance ε in energy then the true eigenstates have energy difference $\omega = \sqrt{\varepsilon^2 + \kappa^2}$ and the dipole-matrix element becomes $|r_{mn}| = (\kappa/\omega) \times (r/2)$ instead of zero. Originally the zero-order eigenstates had a density $(\varrho_{\rm E}/L) d\varepsilon dr$ but now the region $|\varepsilon| < \exp(-|r|/\ell_\xi)$ is depleted and forms a density $d\omega/\Delta_\xi$ of so-called Mott resonant states. If we slice all those states that have energy difference ω then

$$|v_{mn}| \sim \begin{cases} \Delta_\xi r e^{-|r|/\ell_\xi} & \text{off res} \\ |\omega| r_\omega & \text{on res}, \end{cases} \tag{63}$$

where

$$r_\omega = \ell_\xi \log(\Delta_\xi/\omega). \tag{64}$$

This implies that the size distribution of the $|v_{mn}|$ elements that reside inside a band of width ω is within

$$\frac{v_{\rm E}}{\mathcal{M}} \times \left[\frac{L}{\ell_\xi} e^{-L/\ell_\xi},\ 1 \right] \quad \text{for } |\omega| > \Delta_\xi \tag{65}$$

$$\frac{v_{\rm E}}{\mathcal{M}} \times \left[\frac{L}{\ell_\xi} e^{-L/\ell_\xi},\ \frac{\omega}{\Delta_\xi} \log\left(\frac{\Delta_\xi}{\omega} \right) \right] \quad \text{for } |\omega| < \Delta_\xi. \tag{66}$$

Compared with Eq. (54) this is a refinement that takes properly into account the ω dependence of the matrix elements. Disregarding a logarithmic correction it reproduces the semiclassical result Eq. (53).

If we ignore the Mott resonant states, then a log-box distribution is implied. The Mott resonant states form a *box* distribution on top. In a log scale the Mott resonant states contributes a peak of large elements. But this peak does not affect the x_ω calculation. Consequently, for practical purpose we can regard the matrix elements in the SLRT calculation as having a simple log-box distribution as reflected by the crude approximation of Eq. (56). The sparsity of this distribution is characterized by

$$\tilde{p} = \mathcal{M} \frac{\ell}{L} \tag{67}$$

and the SLRT suppression factor is given by Eq. (50).

X. SLRT VS VRH CALCULATION

In order to appreciate the similarities and the differences between SLRT and the conventional Hopping calculation, we

cast the latter into the SLRT language. Equation (4.4) of Ref. 6 for the dc hopping conductance due to phonon-induced transitions is

$$G_{\rm Ohm} = \frac{1}{\mathcal{N}}\left[\left[\frac{e^2}{T}[1-f(E_n)]f(E_m)w^{\gamma}_{mn}\right]\right]_{\parallel}. \tag{68}$$

The notation $[[\ldots]]_{\parallel}$ implies that the resistance of the network is calculated between states at the same energy $E\sim E_{\rm E}$ that reside in opposite sides of the sample. Due to the Fermi occupation factor, the network contains effectively $\mathcal{N}=\varrho_{\rm E}T$ nodes. The division by $\mathcal{N}$ is required because we have defined the $[[\ldots]]$ as inverse resistivity and not as inverse resistance of the network.

The occupation factor $[1-f(E_n)]f(E_m)/T$ gives $\mathcal{O}(1)$ weight only to the $\mathcal{N}$ levels that reside within a window of width T. If we ignore the relaxation effects and regard the fluctuating environment as a noise source that induces transitions $w^{\gamma}_{mn}\propto\exp(|E_m-E_n|/T)$, we still should get the same result for G, even if we omit the occupation factor. This point of view allows to bridge between the noisy driving problem that we consider in this paper and the phonon-induced hopping in the prevailing literature.

The Einstein relation $G_{\rm Ohm}=(e/L)^2\varrho_{\rm E}\mathcal{D}$ relates the conductance and diffusion in real space. We deduce that

$$\mathcal{D} = \left(\frac{L}{\mathcal{N}}\right)^2 [[w^{\gamma}_{mn}]]_{\parallel}. \tag{69}$$

This should be compared with the SLRT expression for the noise-induced energy diffusion

$$\mathcal{D}_{\rm E} = \left(\frac{1}{\varrho_{\rm E}}\right)^2 [[w^{\gamma}_{mn}]]_{\perp}. \tag{70}$$

Here the resistance of the network is calculated between states that reside far away in energy. The SLRT result for $\mathcal{D}_{\rm E}$ and the hopping implied result for $\mathcal{D}$ are both simple and manifestly equivalent: the diffusion coefficient equals the transition rate $\{[w^{\gamma}_{mn}]\}$ times the *step* squared. In the SLRT calculation the step in energy space is $1/\varrho_{\rm E}$ while in the standard real-space analysis the step is $L/\mathcal{N}$. Optimization of the hopping with respect to the distance ω in energy is equivalent to optimization with respect to the distance r in space.

XI. CAN WE GET VRH FROM KUBO?

The analysis that we have introduced in this paper gives the impression that SLRT is essential in order to derive the VRH result. This statement looks to be in contradiction with the prevailing common wisdom and therefore deserves further clarification. In the discussion below we explain that VRH can be obtained from Kubo for an *artificial* toy model but not for the *physical* model that we have analyzed in this paper following Anderson and Mott.

It is instructive to point out that the Kubo formula, Eq. (39), can be rephrased as saying that

$$D = [D_n]_{\rm avr}, \tag{71}$$

where D_n is the diffusion coefficient for a spreading process that start at state n. If we consider an artificial model where the eigenstates are labeled as $n=(i\nu)$ with energies $E_{i\nu}=\epsilon_{\nu}$ and matrix elements $V_{i\nu,j\mu}\sim\exp(-|r_i-r_j|/\ell_{\xi})$, such that

$$w_{i\nu,j\mu} \sim \exp\left[-\frac{|r_i-r_j|}{\ell_{\xi}} - \frac{|\epsilon_{\nu}-\epsilon_{\mu}|}{\omega_c}\right] \tag{72}$$

then all the D_n are the same value. Furthermore, their common value is given by a VRH-like expression which reflects an optimization of the hopping distance. Consequently, the average D is also given by the exactly the same VRH-like expression.

However, in the physical model that we have considered in this paper the D_n in the Anderson regime are typically dominated by one term only and therefore wildly fluctuate. It is then clear that an algebraic average would give a very large result which is dominated by the minority of large elements. In fact our analysis, which merely reproduces Mott's original analysis, shows that up to logarithmic correction the Kubo formula gives $G\propto\omega_c^2$. In order to get VRH we have to perform an SLRT analysis rather than LRT analysis.

In the above discussion one could wonder whether a good strategy for obtaining an SLRT estimate would be to take a harmonic instead of algebraic average over D_n. In fact there are circumstances where such procedure gives a very good result.[1] However, in general, such procedure is expected to underestimate the correct result because it is based on the assumption that the hopping is always with the same optimal step, as in series addition of resistors, without the possibility to bypass in parallel.

XII. VRH VS HOPPING

It is customary to assume that a noisy nonthermal source has a Lorentzian power spectrum

$$\widetilde{F}(\omega) = \frac{1}{\pi}\frac{\omega_c}{\omega^2+\omega_c^2}. \tag{73}$$

Let us consider the Anderson regime and assume that $\omega_c \ll \Delta_{\xi}$. It should be clear that the VRH result is not applicable here. This is because the transport is dominated by $\omega > \Delta_{\xi}$ transitions. In this case SLRT give the same result as Kubo, which we call simple hopping[9]

$$\mathcal{D} \approx \omega_c t_{\rm loc}\mathcal{D}_0 = \frac{(\ell_{\xi})^2}{t_c}, \tag{74}$$

where $t_c=1/\omega_c$. This is as expected from heuristic considerations. It describes a random walk hopping process with steps of size ℓ_{ξ} and time τ_{γ}. This type of result has been highlighted in old studies of the quantum-kicked rotator problem.[24]

XIII. EXPERIMENTAL DEMONSTRATION OF SEMI LINEAR RESPONSE

For a given metallic ring the experimentalist has control over the frequency and on the strength of the driving. These can be adjusted such that FGR transitions are the dominant mechanism for energy absorption. This excludes the adiabatic regime where near-neighbor transitions dominate either

due to Landau-Zener[17] or Debye relaxation mechanism.[16]

Assuming that FGR transitions are the dominant mechanism, this does not automatically imply linear response. The rate of the driven transitions can be smaller or larger compared with the environmental induced rate of transitions and accordingly we expect a crossover from LRT to SLRT.[1]

The simple-minded indication for semilinear response is a drop in the value of the absorption coefficient if the driving is strong enough (see estimates below). What can be measured is the SLRT suppression factor $g_{\rm SLRT}$ and its dependence on the spectral content of the driving.

As observed in Ref. 3, the distinction of semilinear from linear response is not ambiguous. The theory is called SLRT because on the one hand the power spectrum $\widetilde{S}(\omega)\mapsto\lambda\widetilde{S}(\omega)$ leads to $D\mapsto\lambda D$ but on the other hand $\widetilde{S}(\omega)\mapsto\widetilde{S}_1(\omega)+\widetilde{S}_2(\omega)$ does not lead to $D\mapsto D_1+D_2$. This semilinearity can be tested in an experiment in order to distinguish it from linear response.

Let us discuss in more details the experimental conditions that are required in order to observe semilinear response. The problem is characterized by the following parameters:

$$\text{system:}\quad (\omega_0,\omega_c^{\rm sys}), \tag{75}$$

$$\text{driving:}\quad (\omega_c,\varepsilon), \tag{76}$$

$$\text{bath:}\quad (\gamma_\phi,\gamma_{\rm rlx}), \tag{77}$$

where $\omega_c^{\rm sys}$ is the frequency that characterizes the semiclassical motion; $\omega_0=\varrho_{\rm E}^{-1}$ is the frequency corresponding to the mean-level spacing; ω_c and ε are the cut-off frequency and the RMS value of the driving (EMF); and $\gamma_\phi,\gamma_{\rm rlx}$ are the dephasing and the relaxation rates due to the environment.

As already stated we are not interested in adiabatic driving ($\omega_c<\omega_0$) but rather in what we call dc driving. The conditions that have to be satisfied in an SLRT-oriented experiment are

$$\text{dc driving:}\quad \omega_0 \ll \omega_c \ll \omega_c^{\rm sys}, \tag{78}$$

$$\text{FGR condition:}\quad \omega_0 \ll w_\varepsilon \ll \omega_c, \tag{79}$$

$$\text{LRT condition:}\quad w_\varepsilon \ll \gamma, \tag{80}$$

$$\text{SLRT condition:}\quad \gamma \ll w_\varepsilon, \tag{81}$$

where w_ε is the FGR transition rate [Eq. (36)].

There are several experimental methods which could support the theoretical predictions of our paper. The experiment can be based on metallic rings (gold,[25,26] copper,[27] silver[28]), GaAs and other semiconductor heterostructures,[29,30] molecular wires, etc. To estimate the experimental numbers let us consider a semiconductor (GaAs) ring driven by time-dependent magnetic flux

$$\mathcal{M}=5,\quad L=0.1\ \mu\text{m},\quad \ell=50\ \mu\text{m}, \tag{82}$$

$$v_{\rm F}=2.7\times10^5\ \text{m/s}. \tag{83}$$

The long mean-free path is required in order to be deep in the ballistic regime with sparsity

$$q=\mathcal{M}\frac{L}{\ell}\sim 0.01. \tag{84}$$

By Eq. (11) the mean-level spacing is

$$\omega_0=\frac{2v_{\rm F}}{\mathcal{M}L}\approx 1\ \text{meV}. \tag{85}$$

The ballistic time is $t_L=L/v_{\rm F}\approx 3.7\times10^{-13}$ s hence

$$\omega_c^{\rm sys}=\frac{2\pi v_{\rm F}}{L}\approx 11\ \text{meV}, \tag{86}$$

which is $\sim10^{13}$ Hz in frequency units. In order to satisfy the dc driving condition we assume a power spectrum of width $\omega_c\lesssim\omega_c^{\rm sys}$. The EMF is induced by a time-dependent magnetic field $\varepsilon\approx(\omega_c L^2)B$. The FGR rate is estimated using Eq. (36) with $E_n-E_m\sim\omega_0$

$$w_\varepsilon\approx\frac{e^2\mathcal{M}^3L}{\omega_c\ell}\times\varepsilon^2\approx\frac{e^2\mathcal{M}^3L^5\omega_c}{\ell}\times B^2. \tag{87}$$

In order to satisfy the FGR condition the magnetic field should be at least $180G$. The expected crossover between linear to semi-linear response occurs for $w_\varepsilon\sim\gamma$. Assuming, for example, $t_{\rm rlx}\sim2\times10^{-12}$ s we get $\gamma\sim3\omega_0$ leading to

$$B_{\rm SLRT\ threshold}\sim 320G. \tag{88}$$

Under the above conditions we expect that as B is increased there will be crossover from linear to semilinear response with suppression factor $g_{\rm SLRT}\approx0.3$, where we used Eq. (51). The crossover is of course not sharp because w_ε is after all distributed over a wide range. In fact the functional shape of the crossover can be used in order to deduce this distribution.[31] In any case it should be reemphasized that the experimental verification for the nature of the crossover requires merely to test whether the absorption rate depends in a nonlinear way on the spectral content of the driving.

XIV. SUMMARY AND DISCUSSION

Possibly the nicest thing about SLRT is that it consists a natural extension of LRT that places under one roof various results for the conductance in different regimes. It should be clear that in the strict dc limit ($\omega_c\to0$), irrespective of the functional form of the power spectrum, we always get for G a result that formally agrees with the Landauer formula. See the discussion in Sec. II B. In the diffusive regime it becomes equivalent to the Drude formula with small weak localization corrections. But in the other regimes (Anderson and Ballistic), if the low-frequency driving has some arbitrary spectral content, then very different results are obtained (Hopping, VRH, and generalized VRH).

It is interesting that in our "minimal" treatment of the problem there is no need to introduce relaxation due to phonons in order to get a VRH result. Rather, we regard VRH as arising from the competition between the statistical properties of the matrix elements and the power spectrum of a noisy driving field.

The formalism allows to take various limits involving the size of the system (L), the driving frequency (ω_c) and its

intensity (ε), and the rate of the environmentally induced transitions (γ). The order of the limits is very important. In particular: if we take the limit $L\to\infty$ followed by $\varepsilon\to 0$, keeping γ constant, then we get LRT; while if we take $L\to\infty$ followed by $\gamma\to 0$, keeping ε constant, then we get SLRT. Also note that if we keep L constant and take $\omega_c\to 0$ we get the adiabatic limit and not the dc limit of LRT/SLRT.

We have dedicated Sec. XIII to introduce actual estimates that are required in order to observe SLRT in a real experiment. It is important to realize that the experimental procedure allows to distinguish in a nonambiguous way between LRT and SLRT by playing with the spectral content of the driving source. Furthermore, one can test specific predictions for the $g_{\rm SLRT}$ suppression factor, e.g., Eq. (50) with Eq. (67), and Eq. (51) with Eq. (59) or Eq. (61). We note that the explicit incorporation of the environmentally induced transitions into the resistor-network calculation and the subsequent analysis of the resulting SLRT steady state is straightforward.[31]

The SLRT calculation is based on a resistor network picture of transitions between energy levels, for which an RMT framework is very appropriate and effective. In the so called "quantum chaos" context Wigner (in the nuclear context) and later Bohigas (in the mesoscopic context) have motivated the interest in Gaussian ensembles but there are circumstances where non-Gaussian ensembles are appropriate, which lead to novel physics. Indeed we have faced in this paper the analysis of log-normal and log-box ensembles corresponding to the weak and strong disorder limits. We have demonstrated that for such ensembles a large SLRT suppression effect is expected that could not be anticipated within the LRT framework.

ACKNOWLEDGMENTS

We thank Yigal Meir (BGU) and Yuri Galperin (Oslo) for discussions of VRH that have motivated some of the sections in this paper. This research has been supported by a grant from the USA-Israel Binational Science Foundation (BSF).

APPENDIX A: THE RESISTOR NETWORK CALCULATION

In this appendix we explain how the inverse resistivity $G=[[G_{nm}]]$ of a one-dimensional resistor network is calculated. We use the language of electrical engineering for this purpose. In general this relation is semilinear rather than linear, namely, $[[\lambda G]]=\lambda[[G]]$, but $[[A+B]]\neq[[A]]+[[B]]$. The experimental implications of this observation in the SLRT context are discussed in Sec.XIII.

There are a few cases where an analytical expression is available. If only near-neighbor nodes are connected, allowing $G_{n,n+1}=g_n$ to be different from each other, then "addition in series" implies that the inverse resistivity calculated for a chain of length N is

$$G=\left[\frac{1}{N}\sum_{n=1}^{N}\frac{1}{g_n}\right]^{-1}. \tag{A1}$$

If $G_{nm}=g_{n-m}$ is a function of the distance between the nodes n and m then it is a nice exercise to prove that "addition in parallel" implies

$$G=\sum_{r=1}^{\infty} r^2 g_r. \tag{A2}$$

In general an analytical formula for G is not available and we have to apply a numerical procedure. For this purpose we imagine that each node n is connected to a current source I_n. The Kirchhoff equations for the voltages are

$$\sum_m G_{mn}(V_n-V_m)=I_n. \tag{A3}$$

This set of equation can be written in a matrix form

$$\boldsymbol{GV}=\boldsymbol{I}, \tag{A4}$$

where the so-called discrete Laplacian matrix of the network is defined as

$$\boldsymbol{G}_{nm}=\left[\sum_{n'} G_{n'n}\right]\delta_{n,m}-G_{nm}. \tag{A5}$$

This matrix has an eigenvalue zero which is associated with a uniform voltage eigenvector. Therefore, it has a pseudoinverse rather than an inverse and the Kirchhoff equation has a solution if and only if $\Sigma_n I_n=0$. In order to find the resistance between nodes $n_{\rm in}=0$ and $n_{\rm our}=N$, we set $I_0=1$ and $I_N=-1$ and $I_n=0$ otherwise, and solve for V_0 and V_N. The inverse resistivity is $G=[(V_0-V_N)/N]^{-1}$.

APPENDIX B: MODEL DETAILS

In the numerical study we consider the Anderson tight binding model, where the lattice is of size $L\times M$ with $M\ll L$, and lattice constant a. The longitudinal and the transverse hopping amplitudes per unit time are $c_\parallel$ and $c_\perp$, respectively. The random on-site potential in the Anderson tight-binding model is given by a box distribution of width determined by W.

The numerical calculations of Ref. 12 assume $c_\parallel=1$ and $c_\perp=0.9$. Thus in the middle of the band there is a finite-energy window with exactly $\mathcal{M}=M$ open modes. Rings of length $L=500$ with $M=10$ modes has been considered. In our reprocessed Fig. 2 the default cutoff is $\varrho_{\rm E}\omega_c\approx 7$ as in Ref. 12 but as the disorder becomes weaker it is adjusted such that the dc condition $\varrho_{\rm E}\omega_c\lesssim b$ is always satisfied.

For white (uncorrelated) disorder the Hamiltonian is given by Eq. (9) with the isotropic scattering term

$$|U_{\boldsymbol{nm}}|^2\approx\frac{a}{\mathcal{M}L}W^2. \tag{B1}$$

The eigenstates of the Hamiltonian can be found numerically. The degree of ergodicity is characterized by the participation number $\mathrm{PN}\equiv[\Sigma\rho^2]^{-1}$, which is calculated in various representations: in position space $\rho_{r_x,r_y}=|\langle r_x,r_y|\Psi\rangle|^2$, in position-mode space $\rho_{r_x,k_y}=|\langle r_x,k_y|\Psi\rangle|^2$, and in mode space $\rho_{k_y}=\Sigma_{r_x}|\langle r_x,k_y|\Psi\rangle|^2$, where $k_y=[\pi/(\mathcal{M}+1)]\times$integer.

APPENDIX C: THE DRUDE FORMULA

The velocity-velocity correlation function, assuming isotropic scattering, is proportional to the survival probability

$P(t)=e^{-t/t_\ell}$. Ignoring a factor that has to do with the dimensionality $d=2,3$ of the sample the relation is

$$\langle v(t)v(0)\rangle \approx v_{\mathrm{E}}^2 P(t) = v_{\mathrm{E}}^2 e^{-|t|/t_\ell}. \tag{C1}$$

The rate of the scattering can be calculated from the FGR, also know as the Born approximation

$$\frac{1}{t_\ell} = 2\pi\varrho_{\mathrm{E}}|U_{mn}|^2 = \frac{\pi a}{v_{\mathrm{E}}}W^2, \tag{C2}$$

where in the last equality we used Eq. (B1). From here we deduce that the mean-free path (disregarding prefactors of order unity)

$$\ell = v_{\mathrm{E}} t_\ell \approx \frac{1}{a}\left(\frac{v_{\mathrm{E}}}{W}\right)^2 \tag{C3}$$

and the diffusion coefficient in real space

$$\mathcal{D}_0 = \frac{1}{2}\int_{-\infty}^{\infty}\langle v(t)v(0)\rangle \approx v_{\mathrm{E}}\ell. \tag{C4}$$

By the Einstein relation we deduce the Drude formula

$$G_{\mathrm{Ohm}} = \left(\frac{e}{L}\right)^2 \varrho_{\mathrm{E}}\mathcal{D}_0 = \frac{e^2}{2\pi\hbar}\mathcal{M}\frac{\ell}{L}. \tag{C5}$$

A literally equivalent route to derive the Drude formula is to semiclassically deduce $\langle\langle|v_{mn}|^2\rangle\rangle$ from the velocity-velocity correlation function as in Sec. VII and then to substitute in Eq. (19). This has the advantage of allowing easy generalizations of the Drude formula in the ballistic and in the Anderson regimes. In this context it is useful to realize[32] that in the semiclassical picture the integral over the velocity-velocity correlation function is related to the transmission g_0 of the ring (if it were dissected). This leads to the identification in Eq. (24).

In the diffusive regime Mott has demonstrated that it is optionally possible to obtain a direct estimate of the dipole matrix elements, using a random-wave picture. Namely, it is assumed that in the diffusive regime the eigenstates of the Hamiltonian are ergodic in position space and look like random waves with a correlation scale ℓ. Locally the eigenstates are similar to free waves. The total volume L^d is divided into domains of size ℓ^d. Hence we have $(L/\ell)^d$ such domains. Given a domain, the condition to have nonvanishing overlap upon integration is $|\vec{q}_n-\vec{q}_m|\ell<2\pi$, where $\vec{q}$ is the local wave number within this domain. The probability that $\vec{q}_n$ would coincide with $\vec{q}_m$ is $1/(k_E\ell)^{d-1}$. The contributions of the nonzero overlaps add with random signs hence

$$|v_{mn}| = \left[\frac{1}{(k_E\ell)^{d-1}}\times\left(\frac{L}{\ell}\right)^d\right]^{1/2}\times(\overline{\Psi^2}\ell^d)v_{\mathrm{E}}. \tag{C6}$$

Assuming ergodicity $\overline{\Psi^2}\approx 1/L^d$ and we get the same estimate as in the semiclassical procedure.

APPENDIX D: THE LOG-BOX ENSEMBLE

The cumulative distribution function that corresponds to Eq. (28) is

$$\mathrm{Prob}(X<x) = \frac{\ln x - \ln x_0}{\ln(x_1/x_0)}. \tag{D1}$$

The algebraic, geometric, and harmonic averages are

$$\langle\langle x\rangle\rangle_{\mathrm{a}} = \frac{x_1-x_0}{\ln(x_1/x_0)}, \tag{D2}$$

$$\langle\langle x\rangle\rangle_{\mathrm{g}} = \sqrt{x_1 x_0}, \tag{D3}$$

$$\langle\langle x\rangle\rangle_{\mathrm{h}} = \ln(x_1/x_0)\frac{x_1x_0}{x_1-x_0}. \tag{D4}$$

Note that for this distribution the median equals the geometric average. The sparsity parameters are

$$s = 2\tilde{p}\frac{e^{-1/\tilde{p}}-1}{e^{-1/\tilde{p}}+1}, \tag{D5}$$

$$p = -\tilde{p}[\ln\tilde{p} + \ln(1-e^{-1/\tilde{p}})], \tag{D6}$$

$$q = \left(2\tilde{p}\,\sinh\frac{1}{2\tilde{p}}\right)^{-1}, \tag{D7}$$

where we defined $\tilde{p}=(\ln(x_1/x_0))^{-1}$. If the distribution is very stretched reasonable approximations are

$$s \approx 2\tilde{p}, \tag{D8}$$

$$p \approx -\tilde{p}\ln\tilde{p}. \tag{D9}$$

For the VRH calculation

$$x_\omega = x_1\left(\frac{x_0}{x_1}\right)^{1/\varrho_{\mathrm{E}}\omega} \approx \frac{\langle\langle x\rangle\rangle_{\mathrm{a}}}{\tilde{p}}\exp\left(-\frac{1}{\tilde{p}\varrho_{\mathrm{E}}\omega}\right). \tag{D10}$$

For a rectangular $\tilde{F}(\omega)$ the VRH optimization is trivial and gives $\omega\approx x_{\omega_c}$, leading to

$$g_{\mathrm{SLRT}} \approx \frac{1}{\tilde{p}}\exp\left[-\frac{1}{\tilde{p}\varrho_{\mathrm{E}}\omega_c}\right]. \tag{D11}$$

For an exponential $\tilde{F}(\omega)$ the VRH optimization gives

$$g_{\mathrm{SLRT}} \approx \frac{1}{\tilde{p}}\exp\left[-2\left(\frac{1}{\tilde{p}\varrho_{\mathrm{E}}\omega_c}\right)^{1/2}\right], \tag{D12}$$

which is the same as in the traditional VRH optimization.

APPENDIX E: THE LOG-NORMAL ENSEMBLE

The cumulative distribution function that corresponds to Eq. (29) is

$$\mathrm{Prob}(X<x) = \frac{1}{2}+\frac{1}{2}\mathrm{erf}\left[\frac{\ln(x)-\mu}{\sigma\sqrt{2}}\right]. \tag{E1}$$

The algebraic, geometric, and harmonic averages are

$$\langle\langle x\rangle\rangle_{\mathrm{a}} = e^{\mu+\sigma^2/2}, \tag{E2}$$

$$\langle\langle x\rangle\rangle_{\mathrm{g}} = e^{\mu}, \tag{E3}$$

$$\langle\langle x\rangle\rangle_{\mathrm{h}} = e^{\mu-\sigma^2/2}. \tag{E4}$$

The sparsity parameters are

$$s = q^2, \tag{E5}$$

$$p = \frac{1}{2}\mathrm{erfc}\left(\frac{\sigma}{2\sqrt{2}}\right), \tag{E6}$$

$$q = e^{-\sigma^2/2}. \tag{E7}$$

The VRH estimate is

$$x_\omega = \exp\left[\mu + \sigma\sqrt{2}\,\mathrm{erfinv}\left(1 - \frac{2}{\varrho_{\mathrm{E}}\omega}\right)\right] \approx \langle\langle x\rangle\rangle_{\mathrm{g}} \exp\left[\sqrt{\ln\left(\frac{1}{q}\right)^2\left(\ln\frac{\varrho_{\mathrm{E}}^2\omega^2}{2\pi} - \ln\ln\frac{\varrho_{\mathrm{E}}^2\omega^2}{2\pi}\right)}\right]. \tag{E8}$$

For a rectangular $\tilde{F}(\omega)$ the VRH optimization is trivial and gives $\omega \approx x_{\omega_c}$, leading to

$$g_{\mathrm{SLRT}} \approx q\,\exp[2\sqrt{-\ln q\,\ln(\varrho_{\mathrm{E}}\omega_c)}]. \tag{E9}$$

For an exponential $\tilde{F}(\omega)$ the VRH optimization gives

$$g_{\mathrm{SLRT}} \approx q\,\exp\left[\sqrt{-\ln q\,\ln\frac{-\varrho_{\mathrm{E}}^2\omega_c^2\ln q}{\pi}} - \sqrt{\frac{\sqrt{-4\pi\ln q}}{\varrho_{\mathrm{E}}\omega_c}}\right] \approx q\,\exp[\sqrt{-2\ln q\,\ln(\varrho_{\mathrm{E}}\omega_c)}]. \tag{E10}$$

Due to the minority dominance the functional form is more robust compared with the log-box case.

[1] D. Cohen, T. Kottos, and H. Schanz, J. Phys. A **39**, 11755 (2006).
[2] S. Bandopadhyay, Y. Etzioni, and D. Cohen, Europhys. Lett. **76**, 739 (2006).
[3] M. Wilkinson, B. Mehlig, and D. Cohen, Europhys. Lett. **75**, 709 (2006).
[4] N. F. Mott, Philos. Mag. **22**, 7 (1970); N. F. Mott and E. A. Davis, *Electronic Processes in Non-Crystalline Materials*, (Clarendon Press, Oxford, 1971).
[5] A. Miller and E. Abrahams, Phys. Rev. **120**, 745 (1960).
[6] V. Ambegaokar, B. Halperin, and J. S. Langer, Phys. Rev. B **4**, 2612 (1971).
[7] M. Pollak, J. Non-Cryst. Solids **11**, 1 (1972).
[8] B. I. Shklovskii and A. L. Efros, *Electronic Properties of Doped Semiconductors* (Springer-Verlag, Berlin, 1984).
[9] D. Cohen, Phys. Rev. B **75**, 125316 (2007).
[10] E. Wigner, Ann. Math **62**, 548 (1955); **65**, 203 (1957).
[11] O. Bohigas, in *Chaos and Quantum Physics*, Proceedings of the Les-Houches Summer School, Session LII, edited by A. Voros and M.-J. Giannoni (North-Holland, Amsterdam, 1990).
[12] A. Stotland, R. Budoyo, T. Peer, T. Kottos and D. Cohen, J. Phys. A **41**, 262001 (2008).
[13] A. Stotland, D. Cohen, and N. Davidson, EPL **86**, 10004 (2009).
[14] For deviation from Gaussian distributions see: T. Prosen and M. Robnik, J. Phys. A **26**, L319 (1993); E. J. Austin and M. Wilkinson, Europhys. Lett. **20**, 589 (1992); Y. Alhassid and R. D. Levine, Phys. Rev. Lett. **57**, 2879 (1986).
[15] Y. V. Fyodorov, O. A. Chubykalo, F. M. Izrailev, and G. Casati, Phys. Rev. Lett. **76**, 1603 (1996).
[16] The first studies have addressed mainly the Debye regime: M. Büttiker, Y. Imry, and R. Landauer, Phys. Lett. **96A**, 365 (1983); R. Landauer and M. Büttiker, Phys. Rev. Lett. **54**, 2049 (1985); M. Büttiker, Phys. Rev. B **32**, 1846 (1985); Ann. N.Y. Acad. Sci. **480**, 194 (1986).
[17] In the deep adiabatic regime the Landau-Zener mechanism might be of relevance: M. Wilkinson, J. Phys. A **21**, 4021 (1988).
[18] The Kubo formula is applied to diffusive rings in: Y. Imry and N. S. Shiren, Phys. Rev. B **33**, 7992 (1986); N. Trivedi and D. A. Browne, *ibid.* **38**, 9581 (1988).
[19] Weak-localization corrections were studied in: B. Reulet and H. Bouchiat, Phys. Rev. B **50**, 2259 (1994); A. Kamenev, B. Reulet, H. Bouchiat, and Y. Gefen, Europhys. Lett. **28**, 391 (1994).
[20] For a review see A. Kamenev and Y. Gefen, Int. J. Mod. Phys. B **9**, 751 (1995).
[21] Measurements of conductance of closed diffusive rings are described by: B. Reulet, M. Ramin, H. Bouchiat, and D. Mailly, Phys. Rev. Lett. **75**, 124 (1995).
[22] Measurements of susceptibility of individual closed rings using SQUID is described in: N. C. Koshnick, H. Bluhm, M. E. Huber, and K. A. Moler, Science **318**, 1440 (2007).
[23] A new micromechanical cantilevers technique for measuring currents in normal metal rings is described in: A. Bleszynski-Jayich, W. Shanks, R. Ilic, and J. Harris, J. Vac. Sci. Technol. B **26**, 1412 (2008).
[24] E. Ott, T. M. Antonsen, Jr., and J. D. Hanson, Phys. Rev. Lett. **53**, 2187 (1984); D. Cohen, Phys. Rev. A **44**, 2292 (1991).
[25] E. M. Q. Jariwala, P. Mohanty, M. B. Ketchen, and R. A. Webb, Phys. Rev. Lett. **86**, 1594 (2001).
[26] H. Bluhm, N. C. Koshnick, J. A. Bert, M. E. Huber, and K. A. Moler, Phys. Rev. Lett. **102**, 136802 (2009).
[27] L. P. Lévy, G. Dolan, J. Dunsmuir, and H. Bouchiat, Phys. Rev. Lett. **64**, 2074 (1990).
[28] R. Deblock, R. Bel, B. Reulet, H. Bouchiat, and D. Mailly, Phys. Rev. Lett. **89**, 206803 (2002).
[29] D. Mailly, C. Chapelier, and A. Benoit, Phys. Rev. Lett. **70**, 2020 (1993).
[30] B. C. Lee, O. Voskoboynikov, and C. P. Lee, Physica E **24**, 87 (2004).
[31] D. Hurowitz and D. Cohen (unpublished).
[32] D. Cohen and Y. Etzioni, J. Phys. A **38**, 9699 (2005).

3.5 The information entropy of quantum mechanical states

The content of this section is available as

- a journal article: A. Stotland, A.A. Pomeransky, E. Bachmat, D. Cohen, Europhysics Letters **67**, 700 (2004)
- a preprint: arXiv:quant-ph/0401021

EUROPHYSICS LETTERS 1 September 2004

Europhys. Lett., **67** (5), pp. 700–706 (2004)
DOI: 10.1209/epl/i2004-10110-1

The information entropy of quantum-mechanical states

A. Stotland[1], A. A. Pomeransky[2], E. Bachmat[3] and D. Cohen[1]

[1] *Department of Physics, Ben-Gurion University - Beer-Sheva 84105, Israel*
[2] *Laboratoire de Physique Théorique, UMR 5152 du CNRS, Université Paul Sabatier 31062 Toulouse Cedex 4, France*
[3] *Department of Computer Science, Ben-Gurion University - Beer-Sheva 84105, Israel*

(received 19 April 2004; accepted in final form 15 June 2004)

PACS. 03.65.Ta – Foundations of quantum mechanics; measurement theory.
PACS. 03.67.-a – Quantum information.

Abstract. – It is well known that a Shannon-based definition of information entropy leads in the classical case to the Boltzmann entropy. It is tempting to regard the von Neumann entropy as the corresponding quantum-mechanical definition. But the latter is problematic from the quantum information point of view. Consequently, we introduce a new definition of entropy that reflects the inherent uncertainty of quantum-mechanical states. We derive for it an explicit expression, and discuss some of its general properties. We distinguish between the minimum uncertainty entropy of pure states, and the excess statistical entropy of mixtures.

The statistical state of a system (ρ) is specified in classical mechanics using a probability function, while in the quantum-mechanical case it is specified by a probability matrix. The information entropy $S[\rho]$ is a measure for the amount of extra information which is required in order to predict the outcome of a measurement. If no extra information is needed, we say that the system is in a definite statistical state with $S = 0$. A classical system can be in principle prepared in a definite state. But this is not true for a quantum-mechanical system. Even if the system is prepared in a pure state, still there is an inherent *uncertainty* regarding the outcome of a general measurement. Therefore, the minimum information entropy of a quantum-mechanical state is larger than zero.

It is clear that the common von Neumann definition of quantum-mechanical entropy does not reflect the inherent uncertainty which is associated with quantum-mechanical states [1,2]. For a pure state it gives $S = 0$. Let us assume that we prepare two spins in a (pure) singlet state. In such a case the von Neumann entropy of a single spin is $S = \ln(2)$, while the system as a whole has $S = 0$. If it were meaningful to give these results an information theoretic interpretation, it would be implied that the amount of information which is needed to determine the outcome of a measurement of a subsystem is larger than the amount of information which is required in order to determine the outcome of a measurement of the whole system. This does not make sense.

Thus we are faced with the need to give a proper definition for the (information) entropy of a quantum-mechanical state. As in the case of the von Neumann entropy, it can be regarded as a measure for the lack of purity of a general (mixed) state. But unlike the von Neumann entropy it does not give $S = 0$ for pure states, and does not coincide with the thermodynamic entropy in case of a thermal state.

In this letter we introduce a Shannon-based definition of quantum-mechanical information entropy; derive explicit expressions for the calculation of this entropy; and discuss some of its

properties. For further motivations and review of the traditional definition of entropy in the context of quantum computation and quantum information, see [3].

The statistical state of a classical system, that can be found in one of N possible states r, is characterized by the corresponding probabilities p_r, with the normalization $\sum p_r = 1$. The amount of information which is required in order to know what is going to be the outcome of a measurement is given by the Shannon formula: $\mathcal{S} = -\sum_r p_r \ln(p_r)$. Note that $S = 0$ if the system is in a definite state, while $S = \ln(N)$ in the worst case of a uniform distribution. This definition coincides with the Boltzmann definition of entropy if r are regarded as phase space cells.

In the quantum-mechanical case the statistical state of a system is described by a probability matrix ρ. A measurement requires the specification of a basis of (pure) states $|a\rangle$. Without any loss of generality, it is convenient to define a given basis by specifying a Hermitian operator $\mathcal{A}$. We note that in a semiclassical context the basis $\mathcal{A}$ can be regarded as a *partitioning* of phase space into cells. The probability to have a as the outcome of a measurement is $\langle a|\rho|a\rangle$. Therefore the information entropy for such a measurement is

$$S[\rho|\mathcal{A}] = -\sum_a \langle a|\rho|a\rangle \ln(\langle a|\rho|a\rangle). \tag{1}$$

Our notation emphasizes that this is in fact a conditional entropy: one has to specify in advance what is the measurement setup. In particular, there is a basis $\mathcal{H}$ in which ρ is diagonal, $\rho = \mathrm{diag}\{p_r\}$. In this basis $S[\rho|\mathcal{A}]$ attains its *minimum* value,

$$S_{\mathrm{H}}[\rho] = S[\rho|\mathcal{H}] = -\sum_r p_r \ln(p_r) = -\mathrm{trace}(\rho \ln \rho), \tag{2}$$

which is known as the von Neumann entropy. We would like to emphasize that from the *strict* information theory point of view, the quantity $S_{\mathrm{H}}[\rho]$ can be interpreted as information entropy (*à la* Shanon) only if we assume *a priori* knowledge of the preferred basis that makes ρ diagonal. In equilibrium statistical mechanics the interest is in stationary states. This means that ρ is diagonal in the basis that is determined by the Hamiltonian $\mathcal{H}$. Therefore, if we measure the energy of the system, the information entropy is indeed $S_{\mathrm{H}}[\rho]$. In particular, for a canonical state $\rho \propto \exp[-\beta\mathcal{H}]$, it reduces to the thermodynamic definition of entropy.

For a pure quantum-mechanical state $\rho = |\Psi\rangle\langle\Psi|$, the von Neumann definition gives $S_{\mathrm{H}}[\rho] = 0$. This seems to imply that a pure quantum-mechanical state is lacking a statistical nature. This is of course not correct. For a general measurement we have *uncertainty*. An absolute definition of an information entropy of a quantum-mechanical state should not assume any special basis. This implies a *unique* definition of the *absolute* entropy. Using standard information theory argumentation we conclude that([1])

$$S[\rho] = \overline{S[\rho|\mathcal{A}]} = S_0(N) + F(p_1, p_2, \ldots) \equiv S_0(N) + S_{\mathrm{F}}[\rho], \tag{3}$$

where the overline indicates averaging over all possible basis sets with uniform measure (no preferred basis). We would like to emphasize that the averaging procedure is *unique*: A choice of a basis is like a choice of "direction" in a $(2N-1)$-dimensional space (in the case of spin 1/2 this direction can be interpreted as the geometrical orientation of our xyz axes in the physical space). The second equality in eq. (3) gives an explicit expression for the absolute entropy,

([1])If we regard the measurement apparatus as a part of the system, then information theory tells us that the total entropy is $S_{\mathrm{total}} = S[\mathcal{A}] + \sum_{\mathcal{A}} P(\mathcal{A}) S[\rho|\mathcal{A}]$. The probability $P(\mathcal{A})$ describes our lack of knowledge regarding the state of the apparatus, and $S[A]$ is its corresponding entropy. Quantum mechanics assumes that there is no preferred basis.

which we are going to derive below. The result is written as a sum of two terms: The first term is the *minimum uncertainty entropy* of a quantum-mechanical state, achieved by a pure state, while the second term gives the deviation from purity. We shall call the second term excess statistical entropy, and will use for it the notation $S_{\rm F}[\rho]$. Conceptually, it is meaningful to ask to what extent $S_{\rm F}[\rho]$ is correlated with $S_{\rm H}[\rho]$. We shall discuss this issue later on.

Assume that $\rho = \mathrm{diag}\{p_r\}$ is diagonal in some basis $\mathcal{H}$. We can regard all the possible $\mathcal{A}$ basis sets, as unitary "rotations" of $\mathcal{H}$. This means that any $a \in \mathcal{A}$ in the rotated basis is obtained from a state $r \in \mathcal{H}$ in the preferred basis by an operation U. Consequently,

$$S = \overline{\sum_a f\left(\sum_r p_r |\langle r|a\rangle|^2\right)}^{A} = \overline{\sum_s f\left(\sum_r p_r |\langle r|U|s\rangle|^2\right)}^{U} \tag{4}$$

$$= N\overline{f\left(\sum_r p_r |\langle r|\Psi\rangle|^2\right)}^{\Psi} = N\overline{f\left(\sum_r p_r \left(x_r^2 + y_r^2\right)\right)}^{\text{sphere}} = N\int_0^\infty f(s)\ P(s)\mathrm{d}s, \tag{5}$$

where we use the notation $f(s) = -s\ln(s)$. Each averaged $|\langle r|U|s\rangle|^2$ in eq. (4) is equal to $|\langle r|\Psi\rangle|^2$ averaged over all possible Ψ, which leads to eq. (5). It is important to re-emphasize that the quantum-mechanical "democracy" uniquely defines the measure for this Ψ average. This becomes more transparent if we define x_r and y_r as the real and imaginary parts of $\Psi_r = \langle r|\Psi\rangle$. The normalization condition is $\sum_r (x_r^2 + y_r^2) = 1$. Hence in the final expression the average is over all possible directions in a $(2N-1)$-dimensional space. In the final expression we introduce the notation

$$s = \sum_r p_r |\Psi_r|^2 = \sum_r p_r \left(x_r^2 + y_r^2\right) \tag{6}$$

and its probability distribution is denoted $P(s)$. In what follows we discuss the calculation of $P(s)$ and its integral with $f(s)$.

In case of a maximally mixed state $P(s)$ is delta-distributed around $s = 1/N$, and hence $f(s) = \ln(N)/N$. The corresponding information entropy is therefore $S[\rho] = \ln(N)$, as expected. If the state is not maximally mixed, then $P(s)$ becomes non-trivial. In case of a pure state $s = |\Psi_1|^2$ and its distribution is well known [4]:

$$P(s) = (N-1)(1-s)^{N-2}. \tag{7}$$

Thus we get an expression for the *"minimum uncertainty entropy"* which is N-dependent:

$$S_0(N) = \sum_{k=2}^{N} \frac{1}{k} \approx \ln(N) - (1-\gamma) + \frac{1}{2N}\,. \tag{8}$$

Using the asymptotic approximation in the last equality we see that the difference between the S of a maximally mixed state, and that of a pure state, approaches a universal value $(1-\gamma)$, where γ is Euler's constant. Using different phrasing, we see that the excess statistical entropy is universally bounded:

$$S_{\rm F}[\rho] < 1 - \gamma. \tag{9}$$

To get an actual expression for the excess statistical entropy, due to lack of purity, requires some more effort. The first stage is to calculate $P(s)$ leading to (see appendix)

$$P(s) = (N-1) \sum_{(p_r > s)} \left[\prod_{r'(\neq r)} \frac{1}{p_r - p_{r'}}\right] (p_r - s)^{N-2}. \tag{10}$$

The second stage is to calculate the integral of eq. (5) using

$$\int_0^p (p-s)^{N-2} s \ln(s) \mathrm{d}s = \frac{p^N}{N(N-1)} \left[\ln(p) - \sum_{k=2}^{n} \frac{1}{k} \right]$$

and then to use the identity (see appendix)

$$\sum_r p_r^N \prod_{r'(\neq r)} \frac{1}{p_r - p_{r'}} = \sum_r p_r = 1. \tag{11}$$

Hence one obtains

$$F(p_1, p_2, \ldots) = -\sum_r \left[\prod_{r'(\neq r)} \frac{p_r}{p_r - p_{r'}} \right] p_r \ln(p_r). \tag{12}$$

This expression is independent of N. Namely, extra zero eigenvalues do not have any effect on the result. Some particular cases are of interest. For a mixture of two states we get

$$F(p_1, p_2) = -\frac{1}{p_1 - p_2} \big(p_1^2 \ln(p_1) - p_2^2 \ln(p_2) \big). \tag{13}$$

For a uniform mixture of n states we get

$$S_{\mathrm{F}}[\rho] \;=\; \ln(n) - \sum_{k=2}^{n} \frac{1}{k}\,, \tag{14}$$

$$S[\rho] \;=\; \ln(n) + \sum_{n<k\leq N} \frac{1}{k}\,. \tag{15}$$

Either $S_{\mathrm{H}}[\rho]$ or $S_{\mathrm{F}}[\rho]$ can serve as a measure for lack of purity. In fig. 1 we present results of calculation of $S_{\mathrm{F}}[\rho]$ *vs.* $S_{\mathrm{H}}[\rho]$ for a set of representative states, both uniform and non-uniform mixtures. We see that there is a very strong correlation between these two (different) measures of purity.

Our definition of entropy has some interesting mathematical properties. One simple property is concavity: Given $0 < \lambda < 1$ and two sets of probabilities, we have

$$F\big(\lambda p_r + (1-\lambda) q_r\big) \geq \lambda F(p_r) + (1-\lambda) F(q_r). \tag{16}$$

This follows from the concavity of $f(s)$ in eq. (5). Concavity and symmetry with respect to the variables p_i imply that $S[\rho]$ attains its maximum for maximally mixed states and its minimum for pure states. This property is helpful for justifying argumentations that are based on "worst case" calculations. Below we list some less trivial properties which are of physical interest.

Consider a system in a state ρ, and its subsystem which is in some state σ. Technically, the reduced probability matrix σ is obtained from ρ by tracing over the irrelevant indices. From general information theoretic considerations we expect

$$S[\sigma] < S[\rho]. \tag{17}$$

This means that determination of a state of a subsystem requires less information. As explained in the introduction, this inequality is violated by the von Neumann entropy. But

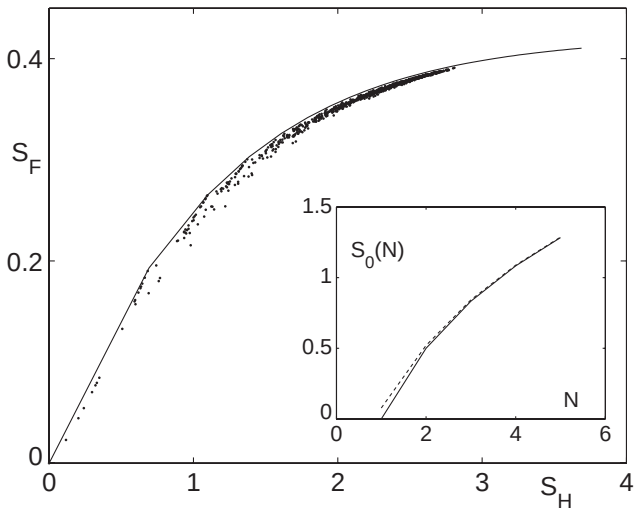

Fig. 1 – The excess information entropy of a mixed quantum-mechanical state $S_{\rm F}$ *vs.* the von Neumann entropy $S_{\rm H}$. The solid line is for uniform mixtures, while the dots are for randomly chosen (non-uniform) mixtures. Inset: The information entropy of a pure quantum-mechanical state as a function of the Hilbert space dimension N. See eq. (8). The dashed line is the asymptotic approximation.

with our definition $S[\rho] \geq S_0(MN) \geq S_0(2N) > \ln(N) > S[\sigma]$, where N and MN are the dimensions of σ and ρ, respectively.

Another common physical situation is having a state $\rho = \sigma_{\rm A} \otimes \sigma_{\rm B}$, where $\sigma_{\rm A}$ and $\sigma_{\rm B}$ are states of subsystems that were prepared independently(!). Obviously, we have the property

$$S[\rho|\mathcal{A} \otimes \mathcal{B}] = S[\sigma_{\rm A}|\mathcal{A}] + S[\sigma_{\rm B}|\mathcal{B}]. \tag{18}$$

But for the absolute information entropy we expect

$$S[\rho] \geq S[\sigma_{\rm A}] + S[\sigma_{\rm B}]. \tag{19}$$

This comes about because there are bases which are not "external tensor product" of $\mathcal{A}$-basis and $\mathcal{B}$-basis. Thus, this inequality reflects the greater uncertainty that we have in the state determination of the combined system. Note that if our world were classical, we would get an equality, which is the case with the Boltzmann entropy, and in fact also with the von Neumann entropy. In order to better establish eq. (19) we can consider a worst case scenario. Let N and M be the dimensions of $\sigma_{\rm A}$ and $\sigma_{\rm B}$, respectively. Assume that these states are uniform mixtures of n and m states, respectively, then ρ is a uniform mixture of nm states in dimension NM. Using eq. (15) and the inequality

$$\begin{aligned}\sum_{k=nm+1}^{NM} \frac{1}{k} &= \sum_{k=nm+1}^{mN} \frac{1}{k} + \sum_{k=mN+1}^{NM} \frac{1}{k} = \\ &= \sum_{k_1=n+1}^{N} \sum_{l_1=0}^{m-1} \frac{1}{k_1 m - l_1} + \sum_{k_2=m+1}^{M} \sum_{l_2=0}^{N-1} \frac{1}{k_2 N - l_2} > \sum_{k=n+1}^{N} \frac{1}{k} + \sum_{k=m+1}^{M} \frac{1}{k},\end{aligned}$$

we confirm that eq. (19) is indeed satisfied. A particular case of the inequality of eq. (19) is that the minimum uncertainty entropy satisfies

$$S_0(NM) > S_0(N) + S_0(M). \tag{20}$$

But what about the excess statistical entropy? Our conjecture is that

$$S_{\mathrm{F}}[\rho] \leq S_{\mathrm{F}}[\sigma_{\mathrm{A}}] + S_{\mathrm{F}}[\sigma_{\mathrm{B}}]. \tag{21}$$

We can again establish this inequality for uniform mixtures of n and m states in dimensions N and M, respectively: Using eq. (14) we observe that

$$S_{\mathrm{F}}[\rho] - S_{\mathrm{F}}[\sigma_{\mathrm{A}}] - S_{\mathrm{F}}[\sigma_{\mathrm{B}}] = S_0(n) + S_0(m) - S_0(nm),$$

which is negative by eq. (20). It is important to realize that eq. (20) overcompensates the inequality eq. (21) leading to eq. (19). It is well known that for the von Neumann entropy we have the general inequality

$$S_{\mathrm{H}}[\rho] \leq S_{\mathrm{H}}[\sigma_{\mathrm{A}}] + S_{\mathrm{H}}[\sigma_{\mathrm{B}}], \tag{22}$$

which holds for any subdivision of a system into two (correlated) subsystems. We already observed (fig. 1) that $S_{\mathrm{F}}[\rho]$ is strongly correlated with $S_{\mathrm{H}}[\rho]$. Moreover, this correlation is *sublinear*. It follows that we expect the easier inequality eq. (21) to hold in general, also in case of correlated subsystems.

The effect of quantum measurements on the entropy is of special interest. Let P_i be a complete orthogonal set of projectors ($\sum_i P_i = 1$). The state after a projective measurement is $\sigma = \sum_i P_i \rho P_i$. Consequently, the state of the system becomes more mixed. This is indeed reflected by an increase in the von Neumann entropy of the systems. Also our entropy is a measure for lack of purity. Therefore, it is reasonable to expect $S[\sigma] \geq S[\rho]$. We were not able to prove this assertion.

Summary. – The von Neumann entropy $S[\rho|\mathcal{H}]$ is useful in the thermodynamic context, where the interest is *a priori* limited to stationary (equilibrium) states. If we want to study the growth of entropy during an ergodization process, we may consider $S[\rho|\mathcal{A}]$, where $\mathcal{A}$ is a basis (or a "partition" of phase space) that does not commute with $\mathcal{H}$. See, for example, ref. [5], where entropy is defined with respect to the position representation. In the latter case the entropy of a pure state is in general non-zero. In the present study we have derived an explicit expression for the minimum uncertainty entropy $S_0(N)$ of pure states. This can be associated with the *average* over the minimum entropic uncertainty [6]. We also have derived an expression for the excess statistical entropy $S_{\mathrm{F}}[\rho]$ of mixtures. The latter can be used as a measure for lack of purity of quantum-mechanical states, and it is strongly correlated with the von Neumann entropy $S_{\mathrm{H}}[\rho]$. It is bounded from above by $(1-\gamma)$, where γ is Euler's constant. The total information entropy $S[\rho]$, unlike the von Neumann entropy, has properties that do make sense from the quantum information point of view.

APPENDIX

Switching to the variables $s_r = x_r^2 + y_r^2$ the definition of $P(s)$ takes the form

$$P(s) = \left\langle \delta\left(s - \sum_r p_r\left(x_r^2 + y_r^2\right)\right)\right\rangle_{\text{sphere}} = (N-1)! \int_0^\infty \mathrm{d}s_1 \ldots \mathrm{d}s_N \; \delta\left(1 - \sum_r s_r\right) \delta\left(s - \sum_r p_r s_r\right)$$

$$= (N-1)! \int_0^\infty \mathrm{d}s_1 \ldots \mathrm{d}s_N \int \frac{\mathrm{d}\omega \, \mathrm{d}\nu}{(2\pi)^2} \mathrm{e}^{(1-\sum_r s_r)(i\nu+0)+i(s-\sum_r p_r s_r)\omega},$$

where the infinitesimal 0 has been introduced to insure convergence once the order of integration is changed. Thus, after the integration over $\mathrm{d}s_1 \ldots \mathrm{d}s_N$, one has

$$P(s) = (N-1)! \int \frac{\mathrm{d}\omega \, \mathrm{d}\nu}{(2\pi)^2} \mathrm{e}^{i\nu + i\omega s} \prod_r \frac{1}{i\omega p_r + i\nu + 0} = \int \frac{\mathrm{d}\omega}{2\pi} \frac{(N-1)!}{(i\omega)^{N-1}} \sum_r \mathrm{e}^{i\omega(s-p_r)} \prod_{r'(\neq r)} \frac{1}{p_{r'} - p_r}.$$

One can show (see below) that there is no singularity in the integral at $\omega = 0$, so one can deform the contour of integration in such a way that it will go slightly above the point $\omega = 0$. Then one can make the integral term by term leading to the final result eq. (10). Namely, if $p_r < s$ the contour is closed in the upper half plane leading to zero, while if $p_r > s$ the contour is closed in the lower half plane leading to a non-zero contribution from the $\omega = 0$ pole.

The above manipulation was based on the observation that the integrand *as a whole* is non-singular: The $1/\omega^{N-1}$ singularity of the individual terms cancel upon summation over r. This cancellation can be established by expanding the exponent in powers of ω, and using the identity

$$\sum_r (s - p_r)^n \prod_{r'(\neq r)} \frac{1}{p_r - p_{r'}} = 0 \quad \text{for } n \leq (N-2).$$

Both this identity and also eq. (11) can be proved by the following procedure:

$$\sum_r g(p_r) \prod_{k(\neq r)} \frac{1}{p_r - p_k} = \oint \frac{\mathrm{d}z}{2\pi i} g(z) \prod_k \frac{1}{z - p_k} = \oint \frac{\mathrm{d}z}{2\pi i} z^{N-2} g(1/z) \prod_k \frac{1}{1 - p_k z}\,,$$

where in the last step one changes $z \mapsto 1/z$.

* * *

DC thanks T. Dittrich (Bogotá) and A. Gersten (Beer Sheva) for a conversation that had motivated this work, and D. Shepelyansky for an exciting visit in Toulouse. We also thank P. Garbaczewski (Zielona Gora) for helpful comments. This research was supported by the Israel Science Foundation (grant No. 11/02). The work of AP was supported by the NSA and ARDA under ARO contract No. DAAD19-01-1-0553.

REFERENCES

[1] Jaynes E. T., *Phys. Rev.*, **108** (1957) 171, end of Sect. 7.
[2] Newton R. G., *Am. J. Phys.*, **72** (2004) 348.
[3] For a detailed review and a full list of references see Nielsen M. A. and Chuang I. L., *Quantum Computation and Quantum Information* (Cambridge) 2000. In particular, Chapt. 11, *Entropy and Information*.
[4] Haake F., *Quantum Signature of Chaos* (Springer) 2000. See, in particular, Sect. 4.8, and eq. (4.8.13).
[5] Garbaczewski P., cond-mat/0301044.
[6] Deutsch D., *Phys. Rev. Lett.*, **50** (1983) 631.

Chapter 4

Summary

In this dissertation we concentrated on the studies of the theory of response of systems to an external driving.

In the first part we were interested in the diffractive energy spreading and its semi-classical limit. We showed that if the conditions for the Bohr quantum-classical correspondence QCC) are unsatisfied, there is a distinction between the restricted and detailed QCC. We demonstrated that the detailed QCC is fragile in three representing problems which are the "worst" for the Bohr QCC because of the strong diffractive effect: particles pulsed by a step potential; particles in a box with a moving wall; particles in a ring driven by an electro-motive force. Along with that we shed new light on the energy spreading process in the case of a EMF-driven ring and solved a long-standing problem of Bloch electrons in a constant electric field. The semiclassical limit in these problems is not perturbative, and in order to derive the LRT the perturbation theory cannot be used - even to the infinite order.

In the second part we analyzed two well-known problems in the new regimes: the heating rate of cold atoms in vibrating traps in the case when the trap is fully chaotic but with a nearly integrable shape; the mesoscopic conductance of disordered rings when the rate of driven transition is larger than the relaxation rate due to the environment. We demonstrated that in such circumstances the analysis should go beyond LRT and should involve a "resistor network" picture of transitions in energy space, somewhat similar to a percolation problem. This is what was called semi-linear response theory (SLRT). In the so-called "quantum-chaos" context Wigner (in the nuclear context) and later Bohigas

(in the mesoscopic context) have motivated the interest in Gaussian ensembles, but there are circumstances when non-Gaussian ensembles are appropriate, which lead to novel physics. SLRT is essential whenever the distribution of matrix elements is wide (sparsity) or if the matrix has texture. We have shown the analysis of log-normal and log-box ensembles corresponding to the weak and strong disorder limits in the mesoscopic ring, and the log-normal ensemble in the nearly integrable optical trap. We have demonstrated that for such ensembles a large SLRT suppression effect is expected, a suppression that could not be anticipated within the LRT framework. Moreover, the generalized variable hopping scheme, from which we could obtain analytical formulas for the diffusion and the conductance, was introduced. In this context Mott's picture of diffusion and localization was revisited. Perhaps, the nicest thing about SLRT is that it consists a natural extension of LRT, that places various results for the conductance / diffusion in different regimes under one roof. For example, in the well-studied diffusive regime the result becomes equivalent to the Drude formula with small weak localization corrections.

In addition, we have introduced actual estimates required in order to observe SLRT in a real experiment. It is important to realize that the experimental procedure allows to distinguish in a non-ambiguous way between SLRT and LRT by playing with the spectral content of the driving source.

Appendix A

Errata:

Phys. Rev. B 81, 115464 (2010)

Typos – After Eq. (22) the reference is to Eq. (19) and not to Eq. (22).

The normalization of $F(\omega)$ is with the measure $d\omega$, Accordingly, in Eq.(4,6) the 2π should be excluded. In this publication $S(\omega) = \epsilon^2 F(\omega)$, where ϵ is the RMS value of the fluctuations. But in other publications we adhere to the common convention with regard to inverse Fourier transform, and define $S(\omega) = 2\pi\epsilon^2 2F(\omega)$, with measure of integration $d\omega/(2\pi)$.

In the definition of the Toy model Eq.(72) the site index has been omitted. It should read

$$w_{i\nu,j\mu} \sim \exp\left[-\frac{|r_i - r_j|}{\ell_\xi} - \frac{|E_{i\nu} - E_{j\mu}|}{\omega_c}\right] \tag{A.1}$$

where the on-site energies are $E_{i\nu} = \alpha_i + \varepsilon_\nu$. Further details on this model and its analysis are presented in the supplementary material (Appendix B).

There are some errors in the numbers that appear in section 13 with regard to the experimental feasibility of witnessing semi-linear response. We clarify the calculation below and add an extra example.

VRH regime of validity – In Section 6 of [P5] we have provided the explicit formulas for calculating the SLRT suppression ratio g for different prototype ensembles. We should note that these formulas are correct only when $b^4 q \lesssim 1$ for the log-normal and $\sqrt{b\tilde{p}}\ln(1/\sqrt{\tilde{p}}) \lesssim 1$ for the log-box ensembles, otherwise $g \sim 1$ (Eqs. (D12),(E8) of [P5]).

See Fig. A.1. Note that in the Fig. 3c of [P5] the actual value of the VRH estimate should be multiplied by a factor of 2 (see the corrected Fig. A.2).

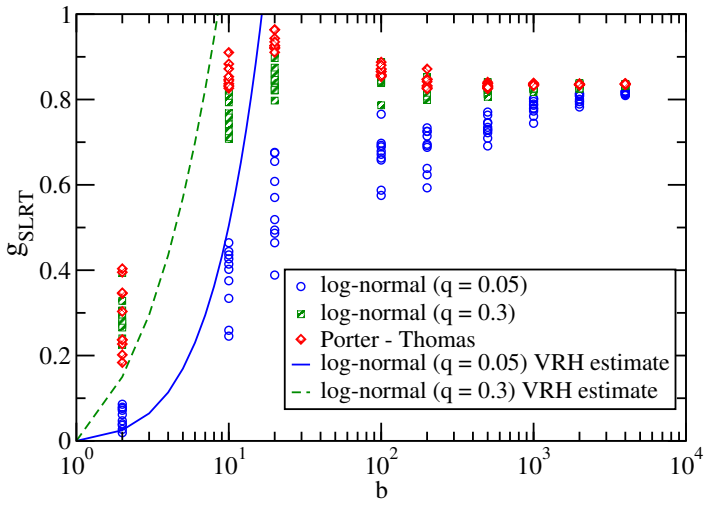

Figure A.1: The suppression SLRT factor g *vs.* the bandwidth b for the log-normal ensemble goes to ~ 1 for $b^4 q \gg 1$. The results for the Porter-Thomas distribution are presented for the sake of comparison.

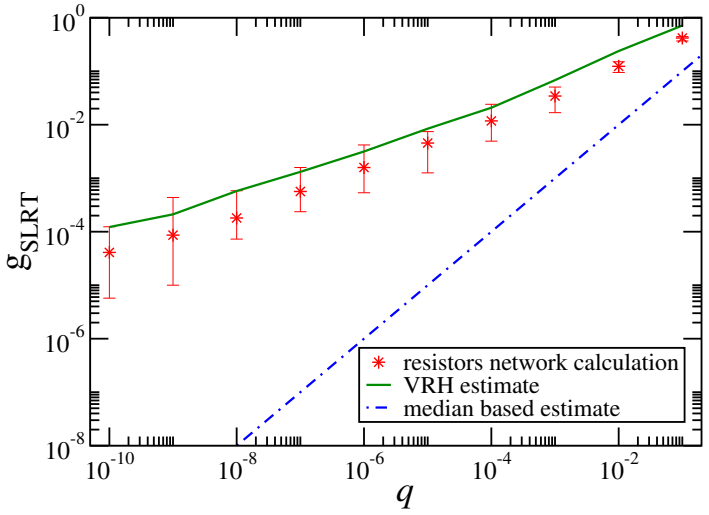

Figure A.2: The corrected version of Fig. 3c of [P5].

Experimental feasibility – In this section we clarify and further explain (with regard to Ref. [P5]) the relevance of LRT/SLRT to experiments with low disorder rings, metallic rings in particular.

The conditions to satisfy LRT / SLRT are [P5]

$$\text{DC driving} \;:\; \omega_0 \ll \omega_c \ll \omega_{\rm L} \tag{A.2}$$

$$\text{FGR condition} \;:\; w_\varepsilon \ll \omega_c \tag{A.3}$$

$$\text{LRT condition} \;:\; w_\varepsilon \ll \gamma \tag{A.4}$$

$$\text{SLRT condition} \;:\; \gamma \ll w_\varepsilon \tag{A.5}$$

where $\omega_{\rm L}$ is the frequency that characterizes the semi-classical motion; $\omega_0 = \varrho_{\rm E}^{-1}$ is the frequency corresponding to the mean level spacing; ω_c and ε are the cut-off frequency and the RMS value of the driving (EMF); w_ε is the FGR transition rate due to the driving; and γ is the rate of the transitions that are induced by the environment (dephasing, relaxation). In the microscopic regime, as in the atomic physics discussion of FGR transitions in a two level system, the FGR condition is $w_\varepsilon < \omega_0$. But in the mesoscopic regime one allows $w_\varepsilon > \omega_0$, which means that the levels form a quasi-continuum.

In order to get the LRT or SLRT behavior the first two conditions must be satisfied. It should be pointed out that if the cut-off frequency of driving becomes smaller than the level spacing ($\omega_c < \omega_0$), i.e. if the first condition of having "quasi-continuum" circumstances is not satisfied, the conductance drops to zero within both LRT and SLRT.

The last two conditions show the difference between the LRT and the SLRT. The LRT to SLRT crossover happens when the driven transition rates become comparable or stronger than the environmentally induced transitions.

In LRT the relevant frequency is the mean level spacing ω_0, whereas in the SLRT analysis the relevant energy scale *might be* the ballistic frequency. This is expected if the scattering is not by white disorder but due to smooth disorder. This issue is discussed with regard to Eq.(60) for the sparsity, and see Fig.4 of [P5]. We also have a new paper regarding a related model [P6] where we verify numerically that indeed sparsity persists beyond the "clean" regime into the genuine "ballistic" regime.

Section 13 of [P5] presents experimental estimates for a possible experiment based on GaAs heterostructure. In the following we show that this effect can *in principle* be observed for a mesoscopic gold ring. The experimental/technical challenge here is to produce tiny ballistic metallic rings, say with the following characteristics:

$$L = 0.5\ \mu m, \quad \mathcal{M} = 100, \quad \ell = 1000\ \mu m, \quad v_{\rm F} = 1.4 \times 10^6\ m/s \tag{A.6}$$

Here L is the length of the ring. The low number of modes $\mathcal{M}$, and the long mean free path ℓ are required in order to be deep in the ballistic regime. Apparently, these values are beyond the current level of technology, but we go on with the analysis to demonstrate the feasibility (in principle) of witnessing an SLRT anomaly.

First of all we note that by the Drude formula of LRT, which is Eq. (23) of [P5] we get

$$G_{\text{Drude}} = \frac{e^2}{2\pi\hbar}\mathcal{M}\frac{\ell}{L} \approx 8\,\Omega^{-1} \tag{A.7}$$

From experimental point of view this is the ratio between the RMS of the induced current and the RMS of the EMF. The LRT to SLRT crossover should be observed as the EMF is increased beyond some threshold that we estimate below. In the SLRT regime the above value of G should be multiplied by an SLRT suppression factor g that we estimate below. In any case it should be re-emphasized that the experimental fingerprint for semi-linear response is not merely the suppression but rather the non-linear dependence on the *spectral content* of the driving.

With the above suggested parameters the mean level spacing is

$$\omega_0 \;=\; \frac{2v_{\text{F}}}{\mathcal{M}L} \;\approx\; 370\ \mu eV \approx 5.6\times 10^{10}\ Hz \tag{A.8}$$

The ballistic time is $t_L = L/v_{\text{F}} \approx 3.6\times 10^{-13}\ s$, hence

$$\omega_{\text{L}} \;=\; \frac{2\pi v_{\text{F}}}{L} \approx 12\ meV \approx 10^{13}\ Hz \tag{A.9}$$

To satisfy the DC driving condition let us choose

$$\omega_c \;=\; 10^{12}\ Hz, \qquad b \;\equiv\; \frac{\omega_c}{\omega_0} \;\approx\; 18 \tag{A.10}$$

The EMF is induced by a time-dependent magnetic field $\varepsilon \approx (\omega_c L^2)B$. The FGR rate is estimated using Eq. (36) of [P5] with $E_n - E_m \sim \omega_0$ and $|v_{nm}|^2 \approx \frac{\ell}{\mathcal{M}L}v_{\text{F}}^2$ as implied by the semiclassical (Drude) formula (Eq. (53) of [P5])

$$w_\varepsilon \;\approx\; \frac{e^2\mathcal{M}\ell}{\pi\hbar^2\omega_c L}\times\varepsilon^2 \;\approx\; \frac{e^2\mathcal{M}\ell L^3\omega_c}{\pi\hbar^2}\times B^2 \tag{A.11}$$

In order to satisfy the FGR condition the magnetic field should be at least $24mG$. The expected crossover between linear to semi-linear response occurs for $w_\varepsilon \sim \gamma$. Assuming $\gamma \sim 10^{12}\ Hz$ we get

$$B_{\text{SLRT threshold}} \;\sim\; 82mG \tag{A.12}$$

Under the above conditions we expect that as the EMF (as determined by B) is increased there will be crossover from linear to semi-linear response. With the above parameters the sparsity is $q = \mathcal{M}L/\ell = 0.05$. Since $b \approx 18$ this would lead to an SLRT suppression factor $g_{\rm SLRT} \approx 0.1$, as implied by Fig. 3 of [P5]. The crossover is of course not sharp because the w_ε are distributed over a wide range. We note that for the above value of B the RMS voltage is $2\mu V$, and hence the induced current is $\sim 0.1mA$, which can be detected.

It is possibly more illuminating to express the FGR condition of Eq. (A.3) using dimensionless quantities. In terms of the dimensionless diffusion coefficient it takes the form

$$\frac{\hbar D_{\rm LRT}}{(\hbar\omega_0)^3} \ll b^{\rm power}, \qquad b \equiv \frac{\omega_c}{\omega_0} \tag{A.13}$$

where power = 2 if w_ε is identified as the nearest neighbors rate (as in Eq. (A.11)), while a self-consistent picture, that assumes an effective w_ε and allows non-perturbative mixing of levels on small energy scales, implies a less restrictive condition with power = 3 [13]. One way to get the former version of FGR is to realize that the diffusion is related to the rate of near-level transitions by the formula $D_{\rm LRT} \approx b \times (\hbar\omega_0)^2 w_\varepsilon$. Another option is simply to substitute the explicit expression for $D_{\rm LRT}$ (see below) and verify the equivalence of Eq. (A.13) with the FGR condition Eq. (A.3). If this dimensionless diffusion is larger than b, then it means that there is a non-perturbative mixing of levels on small scales, which is the typical case in mesoscopic circumstances.

The explicit expression for the dimensionless diffusion coefficient is

$$\frac{\hbar D_{\rm LRT}}{(\hbar\omega_0)^3} = \frac{G_{\rm Drude}\varepsilon^2}{\hbar\omega_0^2} = 2\pi\left(\mathcal{M}\frac{\ell}{L}\right)\left(\frac{\omega_c}{\omega_0}\right)^2\left(\frac{BL^2}{\Phi_0}\right)^2 \tag{A.14}$$

where $\Phi_0 = h/e$. Recall that with the above parameters $b \approx 18$. For the threshold of Eq. (A.12), that corresponds to the assumed γ, we get from Eq. (A.14) the value ~ 100, which is well inside the FGR regime.

For sake of comparison, in the case of GaAs [P5] the numbers are $\mathcal{M} = 5$,$L = 0.1\ \mu m$, $\ell = 50\ \mu m$, $v_{\rm F} = 2.7 \times 10^5\ m/s$, $b = 9$, $\hbar D_{\rm LRT}/(\hbar\omega_0)^3 = 13$. Note that Eq. (87) of [P5] contains a mistake and should be replaced by Eq. (A.11). Therefore, to satisfy the FGR condition the magnetic field should be at least $7G$ and the SLRT threshold occurs at

$13G$. Compared with the rings based on the semiconductors which are relatively easy to fabricate, the Fermi velocity in the metals is about 10 times higher and, therefore, the number of modes is about 100 times higher. In order to see the SLRT effect we need $q \ll 1$ which can be achieved by reducing the number of open modes and/or by increasing the mean free path. Consequently, very thin metals rings with a very long mean free path are required, and that constitutes an experimental / technological challenge.

Appendix B

Supplementary material: Phys. Rev. B 81, 115464 (2010)

In section 11 of [P5] we state that VRH can be obtained from Kubo for an artificial toy model but not for the physical model. We feel that further details should be provided in order to fully explain this point.

The question of whether one can get VRH from LRT is subtle. The details here are important, and can be clarified by the detailed analysis of a toy model. We define below: (1) a non-random lattice model; (2) a random lattice model. We are going to show that for the former both LRT and SLRT give the same VRH result, hence VRH can be regarded as the outcome of the Kubo formula. This is contrasted with the case of the *random* lattice model, where the LRT result, as obtained from the Kubo formula, is not related to VRH. We also discuss this observation in the context of the existing literature.

We consider a one-dimensional lattice. The sites are labeled by i with positions

$$R_i \;=\; i\,a, \qquad i = \ldots -2, -1, 0, 1, 2, \ldots \tag{B.1}$$

where a is a constant. The on-site energies are

$$E_{i\nu} \;=\; (\alpha_i + \nu)\Delta_\xi, \quad \nu = \ldots -2, -1, 0, 1, 2, \ldots \tag{B.2}$$

In the random model the detuning $\alpha_i \in [0, 1]$ is a random number. In the non-random model the detuning is

$$\alpha_i \;=\; \mathrm{mod}(c\,i,\ 1) \;\equiv\; \mathrm{frac}(c\,i) \tag{B.3}$$

such that the difference $\alpha_i - \alpha_j$ is a function of the distance $(R_i - R_j)$. The assumed transition rates are (Eq. (72) of [P5], note the typo due to the omission of the site index):

$$w_{i\nu,j\mu} = w_\varepsilon \exp\left[-\frac{|R_i - R_j|}{\ell_\xi} - \frac{|E_{i\nu} - E_{j\mu}|}{\omega_c}\right] \quad \text{(B.4)}$$

$$= w_\varepsilon \exp\left[-\frac{a|i-j|}{\ell_\xi} - \frac{\Delta_\xi|\alpha_i - \alpha_j + \nu - \mu|}{\omega_c}\right] \quad \text{(B.5)}$$

We use the composite index $n = (i, \nu)$ to label the states. The equivalence of the conventional real-space diffusion picture, and the SLRT energy-space diffusion picture, is discussed in Section 10 of [P5]. For clarity we adopt below the conventional real-space resistor network approach and label by D_n the local diffusion coefficient in real-space. It is defined in complete analogy with its energy space version (see for example Eq. (16) of [7]):

$$D_n = \frac{1}{2}\sum_{j,\mu}(R_j - R_i)^2 \; w_{j\mu,i\nu} \quad \text{(B.6)}$$

$$= \frac{1}{2}a^2 w_\varepsilon \sum_{r=-\infty}^{\infty} r^2 \mathrm{e}^{-\frac{a}{\ell_\xi}|r|} \; (f_r + f'_r) \quad \text{(B.7)}$$

where $f_r + f'_r$ are defined as the two terms in

$$\sum_{\nu=-\infty}^{\infty} \exp\left(-\frac{\Delta_\xi}{\omega_c}|cr - \nu|\right) = \frac{1}{1 - \mathrm{e}^{-\Delta_\xi/\omega_c}}\left[\mathrm{e}^{-\frac{\Delta_\xi}{\omega_c}\mathrm{frac}(cr)} + \mathrm{e}^{-\frac{\Delta_\xi}{\omega_c}(1-\mathrm{frac}(cr))}\right] \quad \text{(B.8)}$$

We assume here low frequency ("DC") driving, hence the prefactor can be approximated by unity, and consequently the expression for D_n can be approximated by the following "VRH" integral:

$$D_n \approx a^2 w_\varepsilon \int_{-\infty}^{\infty} dr \, |r|^2 \, \mathrm{e}^{-(a/\ell_\xi)|r|} \; \mathrm{smoothed}(f_r) \quad \text{(B.9)}$$

$$\approx \frac{2a^2 w_\varepsilon}{R_c} \int_{-\infty}^{\infty} dr \, |r|^2 \, \mathrm{e}^{-(a/\ell_\xi)|r|} \; \mathrm{e}^{-R_c/|r|} \quad \text{(B.10)}$$

where $R_c = \Delta_\xi/\omega_c$. The function f_r is highly fluctuating (Fig. B.1a). The important stage above was based on

$$\mathrm{smoothed}\left[\mathrm{e}^{-R_c \; \mathrm{frac}(\alpha_r)}\right] \approx \frac{2}{R_c}\mathrm{e}^{-R_c/r} \quad \text{(B.11)}$$

which should be contrasted with

$$\mathrm{smoothed}\left[\mathrm{e}^{-R_c \; \mathrm{random}(\alpha_r)}\right] \approx \frac{2}{R_c} \quad \text{(B.12)}$$

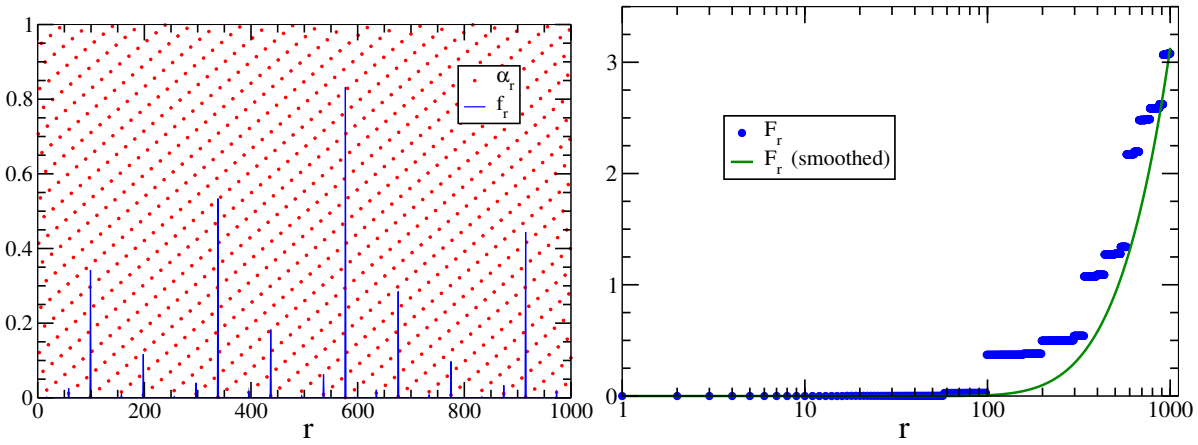

Figure B.1: (a) The plot of $\alpha_r = \mathrm{frac}(cr)$ and $f_r = \mathrm{e}^{-R_c\alpha_r}$, where $c = 1/\sqrt{2}$, and $R_c = 300$. (b) The numerical verification of the smoothing formula. Here $F_r = \sum_{r'=1}^{r} f_{r'}$, where the symbols are calculated with the actual f_r while the line is based on the smoothed expression.

We have verified numerically the above smoothing formula in Fig. B.1b by comparing the commutative sum $F_r = \sum_{r'=1}^{r} f_{r'}$ with the result that is obtained using the smooth expression.

For the toy model all the D_n are identical and are given by the above VRH integral of Eq. (B.10). Therefore, the global D is the same, and there is no difference between LRT and SLRT. For completeness we recall how the saddle-point approximation is used to calculate the VRH integral:

$$D \approx \frac{4a^2 w_\varepsilon}{(\Delta_\xi/\omega_c)} \frac{\partial^2}{\partial(a/\ell_\xi)^2} \left[\int_0^\infty dr\, \mathrm{e}^{-(a/\ell_\xi)r}\ \mathrm{e}^{-(\Delta_\xi/\omega_c)/r} \right] \tag{B.13}$$

$$\approx \frac{4a^2 w_\varepsilon}{(\Delta_\xi/\omega_c)} \frac{\partial^2}{\partial(a/\ell_\xi)^2} \left[\frac{\sqrt{\pi(\Delta_\xi/\omega_c)}}{(a/\ell_\xi)^{3/4}}\, \mathrm{e}^{-2\sqrt{(a/\ell_\xi)(\Delta_\xi/\omega_c)}} \right] \tag{B.14}$$

$$= \frac{8\omega_c w_\varepsilon \ell_\xi^3}{\Delta_\xi a} \times \frac{\sqrt{\pi}}{16(a/\ell_\xi)^{1/4}} \left[21\sqrt{\frac{a\Delta_\xi}{\ell_\xi\omega_c}} + 16\frac{a\Delta_\xi}{\ell_\xi\omega_c}\left(2+\sqrt{\frac{a\Delta_\xi}{\ell_\xi\omega_c}}\right) \right] \mathrm{e}^{-2\sqrt{\frac{a\Delta_\xi}{\ell_\xi\omega_c}}} \tag{B.15}$$

But in the realistic lattice model the detuning α_i is a random number, and therefore we have a *random* resistor network as in [46] (see Section III and the paragraph after Eq.(4.4) at that reference). It is important to realize that in the random model the transition rates are *not* merely a function of the geometrical distance $R_i - R_j$. The SLRT analysis of the random network in [P5] parallels that of [46], leading essentially to the same VRH integral Eq.(B.13). In contrast to that, LRT no longer gives the VRH result.

Using again Eq. (B.9) but with Eq. (B.12) one obtains

$$D_{\rm LRT} \;=\; \frac{8\omega_c w_\varepsilon \ell_\xi^3}{\Delta_\xi a} \;=\; \text{connectivity} \times \text{rate} \times \text{step}^2 \tag{B.16}$$

Consequently, we can define the SLRT suppression factor g such that $D_{\rm SLRT} = g \times D_{\rm LRT}$, and we realize that $g \ll 1$. LRT is a gross over-estimate because it is not based on a semi-linear resistor network calculation (that cares for the majority of small elements), but rather on the algebraic average (which is dominated by the minority of large elements).

The more refined LRT (Kubo) analysis is the so-called Mott resonances picture which we review in section 9 of [P5]. This leads to the "AC Kubo result" that had been introduced by Mott [41]. Note that in the same paper Mott discusses "AC kubo" (which we regard as LRT) and the "DC VRH" (which we regard as SLRT) in different sections.

We hope that we have managed to clarify the reason for the difference between the low frequency result based on Mott's analysis of "AC Kubo", and the "DC VRH" result based on resistor network calculation by placing them under the same umbrella of LRT vs SLRT. The analysis in [P5] has been done for a ring, and adopting a unifying energy-space (rather than real-space) approach. To conclude, we have shown explicitly that

$$D_{\rm LRT} = \quad D_{\rm SLRT} = D_{\rm VRH} \qquad \text{[the non-random toy model]} \tag{B.17}$$

$$D_{\rm LRT} = \qquad D_{\rm Kubo} \qquad \text{[the random model]} \tag{B.18}$$

$$D_{\rm SLRT} = \qquad D_{\rm VRH} \qquad \text{[the random model]} \tag{B.19}$$

The problem of averaging over a random resistor network has a long history (see Section 4.2 of [44]) starting (apparently) with [45]. Irrespective of the above (subtle) discussion it should be clear that a resistor network calculation is semi-linear rather than linear, because $[[A+B]] \neq [[A]] + [[B]]$, whereas $[[\lambda A]] = \lambda [[A]]$.

Appendix C

Numerical routines

The numerical work has been done using MATLAB. The code can be found at the following URL:

`http://physics.bgu.ac.il/SUBMISSIONS/PhD_thesis/Stotland_PhD_thesis_numerics.tar.gz`

Semi-linear response calculations

All the numerical routines are present in the "PROJ" directory in the folders "NUMERICS_KBW" (numerics for [P4]), "NUMERICS_BLD" (numerics for [P3]), "NUMERICS_KBD" (numerics for [P5]). Some of the routines are used for different projects. All the Matlab files contain a short description of their usage in the beginning. In the following the pseudo-code of the main routines is presented.

The code for the "Semilinear response for the heating rate of cold atoms in vibrating traps" used in [P4]

The main routine is *main_real.m*.

$$L_x, L_y, n_x^{\max}, n_y^{\max}, u, \sigma_x, \sigma_y, \omega_c, \text{form}, \text{cuts} \implies G_{\text{SLRT}}, G_{\text{SLRT}}^{\text{non-textured}}, G_{\text{LRT}}, \text{sparsity}$$

1. Input the size of the box L_x, L_y, the strength of the deformation u and its size σ_x, σ_y, maximal quantum numbers for the calculation $n_x^{\max}, n_y^{\max}$, a form of the deformation (s-scatterer / Gaussian) and the numbers of "cuts" for the calculation of the SLRT conductance from the perturbation matrix, and the bandwidth of the power spectrum ω_c.

2. Generate the matrices $\{E_n\}, \{U_{nm}\}, \{V_{nm}\}$

3. Calculate the power spectrum matrix

4. **FOR** different values of u **DO**

   4.1. Diagonalize $\mathcal{H}_0 = \{E_n\} + u\{U_{nm}\}$, sort the eigenvalues $\implies$ the energies D and the diagonalizing matrix V

   4.2. Calculate the perturbation matrix (squared) in the new basis V_{nm}^{new}

   4.3. Find the mean level spacing in the desired region

   4.4. **FOR** different "cuts" of the perturbation matrix in the desired region **DO**

      4.4.1. Calculate the sparsity, median, algebraic and geometric mean of the matrix values

      4.4.2. Calculate the SLRT and the LRT conductance

      4.4.3. Shuffle the matrix elements along the diagonals (remove the texture) and calculate again the SLRT and the LRT conductance

The code for the "Random-matrix modeling of semi-linear response, the generalized variable range hopping picture, and the conductance of mesoscopic rings" used in [P3, P5]

The main routine is *main.m*.

$$\boxed{L, \mathcal{M}, n_x^{\max}, n_y^{\max}, W, \omega_c \implies G_{\mathrm{SLRT}}, G_{\mathrm{SLRT}}^{\text{non-textured}}, G_{\mathrm{LRT}}, \text{sparsity}}$$

1. Input the length of the ring L, the number of open modes $\mathcal{M}$, the disorder parameter W and the bandwidth of the power spectrum ω_c. In addition get the perturbation matrix of velocities (squared) and the energies in the desired energy window.

2. Calculate the sparsity, median, algebraic and geometric mean of the matrix values and find the mean level spacing in the desired region

3. Calculate the power spectrum matrix

4. Calculate the SLRT and the LRT conductance

5. Shuffle the matrix elements along the diagonals (remove the texture) and calculate again the SLRT and the LRT conductance (in *main_shuffle.m*)

6. Given the sparsity and the algebraic mean, generate a random matrix with the desired distribution (log-box, log-normal, bi-modal, etc.)

7. Calculate the SLRT and the LRT conductance from the random matrices

8. Calculate the generalized VRH estimate

The routine *main_RMT.m* goes only over the last 3 steps.

Bibliography

[P1] A. Stotland, A.A. Pomeransky, E. Bachmat, D. Cohen, Europhysics Letters **67**, 700 (2004).

[P2] A. Stotland and D. Cohen, J. Phys. A **39**, 10703 (2006).

[P3] A. Stotland, R. Budoyo, T. Peer, T. Kottos and D. Cohen, J. Phys. A **41**, 262001 (FTC) (2008).

[P4] A. Stotland, D. Cohen and N. Davidson, Europhysics Letters **86**, 10004 (2009).

[P5] A. Stotland, T. Kottos and D. Cohen, Phys. Rev. B **81**, 115464 (2010).

[P6] A. Stotland, L.M. Pecora and D. Cohen, Europhysics Letters **92**, 20009 (2010).

[1] L.D. Landau and E.M. Lifshitz, *Statistical physics*, (Buttrworth Heinemann 2000).

[2] Y. Imry, *Introduction to Mesoscopic Physics* (Oxford Univ. Press 1997), and references therein.

[3] A. Kamenev and Y. Gefen, Int. J. Mod. Phys. **B9**, 751 (1995).

[4] D. Cohen, quant-ph/0403061, published in "Dynamics of Dissipation", Proceedings of the 38th Karpacz Winter School of Theoretical Physics, Edited by P. Garbaczewski and R. Olkiewicz (Springer, 2002).

[5] D. Cohen, Phys. Rev. Lett. **82**, 4951 (1999).

[6] D. Cohen and T. Kottos, Phys. Rev. Lett. **85**, 4839 (2000).

[7] M. Wilkinson, B. Mehlig and D. Cohen, Europhysics Letters **75**, 709 (2006).

[8] D. Cohen, J. von Delft, F. Marquardt and Y. Imry, Phys. Rev. B **80**, 245410 (2009).

[9] D. Cohen and Y. Etzioni, J. Phys. A **38**, 9699 (2005).

[10] D. Cohen, Phys. Rev. B **75**, 125316 (2007).

[11] M. Wilkinson, J. Phys. A **21**, 4021 (1988).

[12] M. Wilkinson, J. Phys. A **20**, 2415 (1987).

[13] D. Cohen, Annals of Physics **283**, 175 (2000); cond-mat/9902168.

[14] E. Ott, Phys. Rev. Lett. **42**, 1628 (1979).

[15] R. Brown, E. Ott and C. Grebogi, Phys. Rev. Lett. **59**, 1173 (1987)

[16] R. Brown, E. Ott and C. Grebogi, J. Stat. Phys. **49**, 511 (1987).

[17] M. Wilkinson and E. J. Austin, J. Phys. A **28** 2277 (1995).

[18] J.M. Robbins and M.V. Berry, J. Phys. A **25**, L961 (1992).

[19] Y. Imry and N.S. Shiren, Phys. Rev. B **33**, 7992 (1986).

[20] N. Trivedi and D. A. Browne, Phys. Rev. B **38**, 9581 (1988).

[21] D. Lubin, Y. Gefen and I. Goldhirsch, Phys. Rev. B **41**, 4441 (1990).

[22] I. Goldhirsch, D. Lubin and Y. Gefen, Phys. Rev. Lett. **67**, 3582 (1991).

[23] D. Cohen, T. Kottos and H. Schanz, J. Phys. A **39**, 11755 (2006).

[24] S. Bandopadhyay, Y. Etzioni and D. Cohen, Europhysics Letters **76**, 739 (2006).

[25] S. Datta, *Electronic Transport in Mesoscopic Systems* (Cambridge University Press 1995).

[26] B. Reulet M. Ramin, H. Bouchiat and D. Mailly, Phys. Rev. Lett. **75**, 124 (1995).

[27] M. Buttiker, Y. Imry and R. Landauer, Phys. Lett. **96A**, 365 (1983).

[28] Y. Imry and N.S. Shiren, Phys. Rev. B **33**, 7992 (1986).

[29] Y. Gefen and D. J. Thouless, Phys. Rev. Lett. **59**, 1752 (1987).

[30] D. Cohen, Phys. Rev. B **68**, 155303 (2003).

[31] M. Moskalets and M. Büttiker, Phys. Rev. B **68** (2003) 161311(R).

[32] D. Cohen, Phys. Rev. B **68**, 201303(R) (2003).

[33] M. Büttiker, Y. Imry and R. Landauer, Phys. Lett. **96A**, 365 (1983).

[34] R. Landauer and M. Büttiker, Phys. Rev. Lett. **54**, 2049 (1985).

[35] M. Büttiker, Phys. Rev. B **32**, 1846 (1985).

[36] M. Büttiker, Annals of the New York Academy of Sciences, **480**, 194 (1986).

[37] B. Reulet, H. Bouchiat, Phys. Rev. B **50**, 2259 (1994).

[38] A. Kamenev, B. Reulet, H. Bouchiat, Y. Gefen, Europhys. Lett. **28**, 391 (1994).

[39] N.C. Koshnick, H. Bluhm, M.E. Huber, K.A. Moler, Science **318**, 1440 (2007).

[40] A.C. Bleszynski-Jayich, W.E. Shanks, R. Ilic, J.G.E. Harris, J. Vac. Sci. Technol. B **26**, 1412 (2008) .

[41] N.F. Mott, Phil. Mag. **22**, 7 (1970).

[42] N.F. Mott and E.A. Davis, Electronic processes in non-crystalline materials, (Clarendon Press, Oxford, 1971).

[43] B.I. Shklovskii and A.L. Efros, Electronic properties of doped semiconductors, (Springer-Verlag Berlin Heidelberg 1984).

[44] Bottger and Bryksin, Phys. Stat. Sol. **78**, 9 (1976).

[45] A. Miller and E. Abrahams, Phys. Rev. **120**, 745 (1960).

[46] V. Ambegaokar, B. Halperin, J.S. Langer, Phys. Rev. B **4**, 2612 (1971).

[47] M. Pollak, J. Non-Cryst. Solids **11**, 1 (1972).

[48] J. Blocki, Y. Boneh, J.R. Nix, J. Randrup, M. Robel, A.J. Sierk and W.J. Swiatecki, Ann. Phys. **113**, 330 (1978).

[49] S.E. Koonin, R.L. Hatch and J. Randrup, Nucl. Phys. A **283**, 87 (1977).

[50] S.E. Koonin and J. Randrup, Nucl. Phys. A **289**, 475 (1977).

[51] N. Friedman, A. Kaplan, D. Carasso, and N. Davidson, Phys. Rev. Lett. **86**, 1518 (2001).

[52] A. Kaplan, N. Friedman, M. F. Andersen, and N. Davidson, Phys. Rev. Lett. **87**, 274101 (2001).

[53] M. Andersen, A. Kaplan, T. Grunzweig and N. Davidson, Phys. Rev. Lett. **97**, 104102 (2006).

[54] A. Barnett, D. Cohen and E.J. Heller, Phys. Rev. Lett. **85**, 1412 (2000).

[55] A. Barnett, D. Cohen and E.J. Heller, J. Phys. A **34**, 413 (2001).

[56] S.W. Doescher and M.H. Rice, Am. J. Phys. **37**, 1246 (1969).

[57] A.J. Makovski and S.T. Demebinski, Phys. Rev. Lett. **56**, 290 (1986).

[58] D.Cohen, A. Barnett and E.J. Heller, Phys. Rev. E **63**, 46207 (2001).

[59] G. H. Wannier, Phys. Rev. **117**, 432 (1960).

[60] J. Zak, Phys. Rev. Lett. **20**, 1477 (1968).

[61] J. Zak, Phys. Rev. **168**, 686 (1968).

[62] J. Zak, J. Phys.: Condens. Matter **8**, 8265 (1996).

[63] A. Rabinovitch and J. Zak, Phys. Lett. **40A**, 189 (1972).

[64] A. Rabinovitch, Phys. Lett. **59A**, 475 (1977).

[65] D. Emin and C.F. Hart, Phys. Rev. B **36**, 7353 (1987).

[66] C.F. Hart, Phys. Rev. B **38**, 2158 (1988).

[67] C.F. Hart and D. Emin, Phys. Rev. B **37**, 6100 (1988).

[68] J. Zak, Phys. Rev. B **43**, 4519 (1991).

[69] J. Leo and A. MacKinnon, Phys. Rev. B **43**, 5166 (1991).

[70] E.E. Mendez, F. Agullo-Rueda, and J.M. Hong, Phys. Rev. Lett. **60**, 2426 (1988).

[71] R. Jozsa, D. Robb, and W. K. Wootters, Phys. Rev. A **49**, 668 (1994).

תקציר

ניקח מערכת המתוארת ע״י המילטוניאן התלוי בזמן. במערכת כזאת האנרגיה איננה קבוע התנועה, יתרה מזאת, הנעת המערכת משרה התפשטות האנרגיה. ניתן לשאול כיצד תלויה התפלגות האנרגיה בזמן. ככלל, פונקציה זו תהיה שונה במערכות קלאסיות וקוונטיות. התפלגות זו יכולה להיות מאופיינת ע״י המומנטים שלה. המשמעות של התאמה קוונטית-קלאסית (QCC) היא שהמומנטים של התפלגות האנרגיה הקלאסית זהים למומנטים הקוונטיים. השאלה היא באלו תנאים מתקיימת ההתאמה הנ״ל ומהם גבולותיה. ה-QCC המוכרת ביותר היא ה-QCC של בוהר הקובעת כי במקרה שחבילות הגלים גאוסיאניות והפוטנציאלים חלקים, המומנטים יהיו זהים בזמנים קצרים. אך לא תמיד חבילות גלים הן גאוסיאניות או הפוטנציאלים חלקים. נוסף על כך, לא ניתן לסמוך על QCC בזמנים ארוכים. כיצד עניין ה-QCC קשור לתורת התגובה? בעוד אנו מצפים שה-QCC תתקיים בזמנים קצרים, בתורת התגובה אנו מעוניינים בהתנהגות המערכת בזמנים ארוכים. אנו מתחילים בחקירת התפשטות אנרגיה עקיפתית (דיפרקטיבית) וגבולה הקלאסי למחצה. אנו דנים בשלוש מערכות מונעות שבהן ההנעה משרה קפיצות במרחב האנרגיה: (1) חלקיקים המונעים באמצעות פוטנציאל מדרגה; (2) חלקיקים בקופסה בעלת קיר נע; (3) חלקיקים בטבעת המונעים באמצעות כוח אלקטרו-מניע (כא״מ). בכל המקרים האלה הדרך להתאמה קוונטית-קלאסית איננה פשוטה. כל הבעיות הנ״ל חולקות אותה תכונה: בתיאור הקלאסי שלהן בליעת האנרגיה קשורה לקפיצות פתאומיות במרחב הפאזה. בתיאור הקוונטי קפיצות אלה גורמות לתופעת עקיפה חזקה שהיא המקרה הגרוע ביותר ל-QCC של בוהר. ניתן לקבל הבנה מסוימת ע״י הבחנה כי הדינמיקה במרחב האנרגיה, שבו n היא מספר הרמה, זהה למעשה לזו של האלקטרונים של בלוך במודל הקשר ההדוק, שבו n היא מספר האתר. המרחק הממוצע בין הרמות הינו כמו שדה חשמלי קבוע, וההנעה משרה דילוג רחוק טווח. בכל המקרים הנ״ל מתקיימת QCC מוגבלת (רק לשני המומנטים הראשונים של ההתפלגות), בעוד QCC פרטנית (למומנטים גבוהים יותר) נשברת.

במסגרת תורת התגובה הלינארית (LRT) בליעת האנרגיה של מערכת קוונטית נקבעת ע״י פונקצית קורלציה של איבר ההפרעה. במסגרת הנחות מגבילות מאוד ניתן לטעון כי קיימת התאמה קוונטית-קלאסית טובה מאוד לפונקצית הקורלציה, ולכן ניתן לצפות ל-QCC מוגבלת בתהליך בליעת האנרגיה. הלכה למעשה, מעניין מאוד לבחון את גבולות התורה הלינארית ולקבל תורת התגובה כללית יותר.

מערכות ביליארד ״אופטי-אטומי״ מערכות מזוסקופיות סגורות הן מערכות אידאליות לבחינת התגלמות של תופעות קוונטיות. אנו מראים כי חישוב קצב החימום של אטומים קרים במלכודות אופטיות רוטטות וחישוב של מוליכות של טבעות מזוסקופיות בעלות אי סדר דורשים תורה שהולכת מעבר למסגרת הסטנדרטית של תגובה לינארית. ניתוח המעברים בין רמות האנרגיה דומה מאוד לבעיית החלחול (פרקולציה) במרחב האנרגיה, אם ההנחה של ״כאוס קוונטי״ חזק לא תקפה בבעיה הראשונה או אם מניחים תנאים ״מזוסקופיים״ בבעיה השנייה. אנו מראים כי המבניות והדלילות של מטריצת ההפרעה (שנקבעות ע״י הגאומטריה של המלכודת או מידת אי הסדר) מכתיבות את התוצאה. אנו משתמשים בתורת התגובה הלינארית למחצה (SLRT) על מנת לחשב את מקדם הבליעה של מערכת מונעת באמצעות חישוב של רשת הנגדים: כל רמת אנרגיה (לא מופרעת) של חלקיק במלכודת או של אלקטרון בטבעת המזוסקופית היא כמו צומת של הרשת; קצבי המעברים בין הרמות הם כמו אלמנטים של מטריצה אקראית שמתארת את הרשת. אם ההתפלגות של אלמנטים אלה רחבה (לוג-נורמלית, למשל, ולא גאוסית), אזי התוצאה עבור מקדם הבליעה שונה בצורה ניכרת מניבוי התורה הלינארית הרגילה. אנו משתמשים במודל משופר של מטריצות אקראיות שתופס את המרכיבים החיוניים של הבעיות ומובילה לתמונת ״הדילוגים לטווח משתנה״ (VRH) מוכללת שנותנת תוצאה אנליטית. בפרט, אנו משתמשים בגישה זו כדי לקבל קירובים מעשיים למוליכות של טבעות מזוסקופיות.

העבודה נעשתה בהדרכת

פרופ׳ דורון כהן

במחלקה לפיסיקה

בפקולטה למדעי הטבע

מאפיינים לא הפרעתיים של אבולוציה קוונטית
והשלכותיהם על תורת התגובה הלינארית

מחקר לשם מילוי חלקי של הדרישות לקבלת תואר "דוקטור לפילוסופיה"

מאת

אלכסנדר סטוטלנד

הוגש לסינאט אוניברסיטת בן גוריון בנגב

אישור המנחה _____

אישור דיקן בית הספר ללימודי מחקר מתקדמים ע"ש קרייטמן _____

כ"ו בטבת תש"ע **12 ינואר 2010**

באר שבע

מאפיינים לא הפרעתיים של אבולוציה קוונטית
והשלכותיהם על תורת התגובה הלינארית

מחקר לשם מילוי חלקי של הדרישות לקבלת תואר "דוקטור לפילוסופיה"

מאת

אלכסנדר סטוטלנד

הוגש לסינאט אוניברסיטת בן גוריון בנגב

כ"ו בטבת תש"ע **12 ינואר 2010**

באר שבע